ON THREE-DIMENSIONAL ASYMPTOTIC STRESS FIELDS IN THE NEIGHBORHOOD OF HOMOGENEOUS AND BIMATERIAL WEDGE FRONTS

by

Minsheng Xie

A dissertation submitted to the faculty of
The University of Utah
in partial fulfillment of the requirements for the degree of

Doctor of Philosophy

Department of Civil Engineering

The University of Utah

August 1994

THE UNIVERSITY OF UTAH GRADUATE SCHOOL

SUPERVISORY COMMITTEE APPROVAL

of a dissertation submitted by

Minsheng Xie

This dissertation has been read by each member of the following supervisory committee and by majority vote has been found to be satisfactory.

Oct. 15, 1993 — Chair: Reaz A. Chaudhuri

oct 15, 1993 — E. S. Folias

Oct 15, 1993 — K. L. DeVries

Oct. 15, 1993 — Frank Stenger

Oct 15, 1993 — Douglas S. Cairns

THE UNIVERSITY OF UTAH GRADUATE SCHOOL

FINAL READING APPROVAL

To the Graduate Council of the University of Utah:

I have read the dissertation of Minsheng Xie in its final form and have found that (1) its format, citations and bibliographic style are consistent and acceptable; (2) its illustrative materials including figures, tables, and charts are in place; and (3) the final manuscript is satisfactory to the supervisory committee and is ready for submission to The Graduate School.

11-16-93
Date

Reaz A. Chaudhuri
Chair, Supervisory Committee

Approved for the Major Department

Lawrence Reaveley
Chair/Dean

Approved for the Graduate Council

Ann W. Hart
Dean of The Graduate School

ABSTRACT

A new eigenfunction expansion method is developed to obtain three-dimensional asymptotic stress fields in the vicinity of (a) an interior point and (b) the surface corner point located at the front of a (i) homogeneous and (ii) bimaterial wedge, subjected to three combinations of wedge-side boundary conditions — clamped-clamped, clamped-free and free-free. In comparison with the existing method, the present method is much easier to implement, and is also computationally more efficient in the sense that it does not need to resort to iterative schemes to solve the three partial differential equations, which limits the former's applicability to more complex geometric shapes, such as a wedge. Expressions for singular stress fields in the neighborhood of an interior point and the surface corner point located at the front of a semiinfinite crack — a special case of a homogeneous wedge — are also presented. Likewise, expressions for singular stress fields in the neighborhood of these points located at the front of a semiinfinite crack along the interface— a special case of a bimaterial wedge — are also presented.

Additionally, heretofore unavailable numerical results, especially for three-dimensional stress fields in the vicinity of the surface corner point at the front of a (i) homogeneous and (ii) bimaterial wedge subjected to the aforementioned wedge-side boundary conditions, and their comparisons with their two-dimensional (i.e., plane stress) counterparts are also presented. Relative dominance of the computed eigenvalues (i.e., order of singularity) for different types of loading, such as extension/bending and antiplane shear is also studied in this investigation. The relationship between the strain energy release rate and the stress intensity factor is investigated from a three-dimensional standpoint. Furthermore, numerical results pertaining to development of plastic yield zone

at the front of a semiinfinite crack are also obtained. Finally, derivation of the general stress intensity factor (for $\theta \neq \pm\pi$) and the corresponding expressions of singular stresses for homogeneous wedges also form a part of this dissertation research.

TABLE OF CONTENTS

LIST Of FIGURES

ACKNOWLEDGEMENTS

The author wishes to express sincere gratitude to his adviser, Dr. R. A. Chaudhuri, for his guidance, advice, and support throughout this work. As well, I would like to acknowledge the financial aid received from the Office of Naval Scientific Research and the University of Utah Research Committee.

Sincere thanks are also extended to my committee members, Drs. E. S. Folias, K. L. DeVries, Frank Stenger, Douglas S. Cairns for many fruitful discussions during the completion of this work. The author also wishes to thank Dr. Y. Rajapakshe of Naval Research, Dr. J.Corrado, Dr. B. Douglas and Mr. H. j. Garala of Naval Surface Warfare Center, Caderock Division, for financial support of this research.

Finally, special thanks are given to his wife, Xihong Chen, for her help, understanding and encouragement throughout the work. Very sincere thanks are also due to his parents for their support throughout his life.

CHAPTER 1

INTRODUCTION

1.1 Motivation

The primary motivation of the present research stems from the need of understanding the stress field in a wedge-shaped kink band zone, which causes premature failure in thick composite cylinders subjected to hydrostatic compression (see, e.g., Garala [1,2], Chaudhuri [3], Chaudhuri and Garala [4], Garala and Chaudhuri [5]). Prior investigations into the hydrostatic strength of thick-section graphite/epoxy cylinders have resulted in failures that are significantly lower (50 to 70% of design pressure) than anticipated [1, 2]. The formation and propagation of fiber kink bands at the microscopic level, triggered by the fiber misalignment defects formed during the manufacturing process, leading to a shear crippling failure at the macroscopic level is one of the principal compressive failure modes [3]. It has been hypothesized that one way to improve compressive strength is through the use of a hybrid fiber system. Commingling glass fibers with graphite fibers is expected to prevent the propagation of kink bands of the graphite fibers and provide stability to the graphite fibers [4,5]. A parallel study is currently being conducted to obtain two dimensional Williams type asymptotic results for a kink wedge bimaterial interface in order to understand the relative kink toughness of glass and carbon fibers. These investigations are expected to lead to a more defect tolerant design of the thick section composite cylinders, subjected to hydrostatic compression.

As the following literature review will reveal, not a single analytical study on the nature of singularity of the three-dimensional stress field in the vicinity of a wedge front

has been found in literature. If a plate is very thick (so that the thickness can be assumed to be infinity), for some case (such as, extension problem), the two-dimensional (plane strain) solution can serve as a reasonably good approximation to the three-dimensional singular stresses in the interior of the plate. It is worthwhile to mention here that the two-dimensional solution cannot give a good approximation to the three-dimensional singular stresses in the interior of the plate for bending problem, even though the plate is very thick. Besides, in many practical applications, such as in the aforementioned kink band zone, cracks and bimaterial interface cracks the stress fields in the neighborhood of the plate surface corner point at the wedge front may exhibit a different behavior from the interior, in which case the plane strain assumption becomes invalid. In such situations, a three-dimensional elasticity approach is the only option left.

1.2 Literature Review on Two-Dimensional Wedge/Crack Solutions

A detailed review of the literature suggests that analytical investigations pertaining to the two-dimensional linear elastic wedge problem have derived their original practical importance from the stress analysis of swept aircraft and missile wings. With the missile wing idealized as a swept plate with reentrant corners, the study has led naturally to research into the singular stress state at angular corners. The nature of the stress singularity has been first investigated by Williams[6]. He has assumed the Airy stress function, using the method of separation of variables, in the form,

$$F(r,\theta) = r^{s+1} f(\theta).$$

Substituting the Airy stress function into the governing biharmonic equation,

$$\nabla^4 F(r,\theta) = 0.$$

Williams[6] has obtained the singular stresses in the form,

$$\sigma_{ij} \sim 0\left(r^{s-1}\right).$$

For various boundary conditions, the order of stress singularity depends on the eigenvalue λ, which is evaluated for different boundary conditions at the wedge side surfaces ($\theta = \pm\theta_0$) in a manner shown below:

(1) Free-Free

$$\sin 2s\theta_0 = \pm s \sin 2\theta_0,$$

(2) Clamped-Clamped

$$\sin 2s\theta_0 = \pm \frac{s \sin 2\theta_0}{(3-4\sigma)};$$

(3) Free-Clamped

$$\sin^2 2s\theta_0 = \left(\frac{4(1-\sigma)^2}{3-4\sigma}\right) - \left(\frac{\sin^2 2\theta_0}{(3-4\sigma)(2\theta_0)^2}\right)(2s\theta_0)^2;$$

and $\sigma=\nu/(\nu+1)$, ν is Poisson's ratio. Williams [6] has found that for $\theta_0=\pm\pi$ (i. e., the case of crack surfaces), the order of singularity is the most severe. He has also found that for the free-free and clamped-clamped boundary conditions, the value of $\sigma_{ij} \sim 0(r^{-0.5})$ in the vicinity of the crack tip, and for free-clamped boundary condition, $\sigma_{ij} \sim 0(r^{-0.75})$. In a subsequent study [7], he has succeeded in establishing the relationship between the unknown constants arising from the solution of the partial differential equations and the stress intensity factors.

Williams [8] has also applied the same method to solve the problem of two-dimensional interface crack, and has thus become the first to find that the stress in the neighborhood of the crack tip has an oscillatory character of the type σ_{ij}-$0(r^{-0.5})$ sin (or) cos of the argument $\varepsilon\log(r)$. The problem of bending of plates of dissimilar materials has first been addressed by Sih and Rice [9, 10]. From the two-dimensional point of view, the bending fields of singular stresses at the crack tip are different from the extensional one. Additionally, they have found through the use of Boussinesq's solution that the constant coefficients a_n,b_n, etc. in William's [8] interface crack solution under extension, are related to the stress intensity factors. This behavior has, later on, been verified by Erdogan [11,12]. England [13] has shown that the oscillatory displacement field that implies interpenetration of the materials across the crack discontinuity is physically inadmissible. He has also noted that this interpenetration is confined to a very small region near the crack tip. Elimination of this unrealistic interpenetration in the displacement field solution has been studied by Comninou [14], Comninou and Schmueser[15], Achenbach et al.[16], Knowles and Sternberg [17], and Gautesen and Dundurs [18].

It is noteworthy that homogeneous and bimaterial wedge type solutions can serve as general prototypes for a variety of geometrical shapes, that engineers have to grapple with. For example, Zak and Williams [19] have investigated the extensional stress field around the tip of a crack, which is oriented perpendicular to the dividing line between two dissimilar media. Dempsey and Sinclair [20, 21] have found that the singular term log(r) may also occur in two-dimensional solutions pertaining to bimaterial as well as composite wedges.

Mellin transform is another powerful tool that has been frequently used to solve two-dimensional wedge problem. For example, Bogy [22, 23] has used this technique for analyzing the singular stress behavior of two edge-bonded elastic wedges made of

different materials. Hein and Erdogan [24] have also employed the same method to study a similar problem.

Sih [25] has employed an eigenfunction expansion method and has obtained the eigenvalue, which is related to the order of singularity, pertaining to the two-dimensional antiplane shear problem. For the 'free-free' boundary condition, the eigenvalue is found to be

$$s=\frac{\pi}{2\theta_0}.$$

Ma and Hour [26] have used the Mellin transform method and have found that the order of stress singularity is always real for isotropic and anisotropic bimaterial wedges under antiplane shear.

Sih et al. [27] were the first to investigate the problem of a crack in an anisotropic material. They have used Lekhnitskii's approach and have shown that the singular parts of stresses are the same as their isotropic counterparts, i.e., $\sigma_{ij}\sim 0(r^{-0.5})$, when $\theta_0=\pm\pi$. Bogy [28], and Kuo and Bogy [29] have employed a complex function representation of the solution in conjunction with a generalized Mellin transform to analyze stress singularity in an anisotropic wedge, and have come to the same conclusion for $\theta_0=\pm\pi$. Gotoh [30], Willis [31], Clements [32], Delale and Erdogan [33], Hoenig [34], and Wang and Choi [35,36] have studied the problems of interface crack and edge-bonded wedge made of anisotropic materials, and have found that the singular stresses are also similar to their isotropic counterparts and that $\sigma ij\sim 0(r^{-.5\pm\lambda})$. The oscillatory phenomenon also exists in this case in a manner similar to the aforementioned case of isotropic materials. In recent years, the elegant and powerful Stroh formalism [37] for two-dimensional anisotropic elasticity has rekindled interest in the subject. Many studies have appeared in the literature from a number of investigators, such as Ting [38-41], Bassani and Qu [42-43],Tewary et al. [44], Suo[45], Li and Nemat-Nasser[46] and others.

1.3 Literature Review on Three-Dimensional Wedge/Crack Solutions

The mathematical difficulties posed by the three-dimensional wedge problems are substantially greater than their two-dimensional counterparts. Only the special case of a semiinfinite crack, i. e., when $\theta_0=\pm\pi$, has been attempted. Hartranft and Sih [47] have used an eigenfunction asymptotic expansion method to solve the three-dimensional semiinfinite crack problem, and have come to the conclusion that the singular stresses in the interior of a thick plate is $\sigma_{ij} \sim 0(r^{-0.5})$. The stress field at crack front is given by

$$\sigma_r = r^{-\frac{1}{2}} A_1(z)\left(\frac{1}{2}\cos\left(\frac{3\theta}{2}\right)-\frac{5}{2}\cos\left(\frac{\theta}{2}\right)\right)+ r^{-\frac{1}{2}} A_2(z)\left(\frac{1}{2}\sin\left(\frac{3\theta}{2}\right)-\frac{5}{6}\sin\left(\frac{\theta}{2}\right)\right)$$

$$\sigma_\theta = -r^{-\frac{1}{2}} A_1(z)\left(\frac{1}{2}\cos\left(\frac{3\theta}{2}\right)+\frac{3}{2}\cos\left(\frac{\theta}{2}\right)\right)-r^{-\frac{1}{2}} A_2(z)\left(\frac{1}{2}\sin\left(\frac{3\theta}{2}\right)+\frac{1}{2}\sin\left(\frac{\theta}{2}\right)\right)$$

$$\tau_{r\theta} = -r^{-\frac{1}{2}} A_1(z)\left(\frac{1}{2}\sin\left(\frac{3\theta}{2}\right)+\frac{1}{2}\sin\left(\frac{\theta}{2}\right)\right)+ r^{-\frac{1}{2}} A_2(z)\left(\frac{1}{2}\cos\left(\frac{3\theta}{2}\right)+\frac{1}{6}\cos\left(\frac{\theta}{2}\right)\right)$$

$$\sigma_z = -r^{-\frac{1}{2}} 4\nu A_1(z)\cos\left(\frac{\theta}{2}\right)-\frac{4\nu}{3} r^{-\frac{1}{2}} A_2(z)\sin\left(\frac{\theta}{2}\right)$$

$$\tau_{rz} = r^{-\frac{1}{2}} A_3(z)\frac{1}{4}\sin\left(\theta/2\right)$$

$$\tau_{\theta z} = r^{-\frac{1}{2}} A_3(z)\frac{1}{4}\cos(\theta/2).$$

The stress free conditions on the faces of a plate is given by

$$\sigma_{zz} = \tau_{\theta z} = \tau_{zr} = 0 \qquad \text{for} \quad z = \pm h.$$

Hartranft and Sih have found that the boundary conditions on plate faces ($z=\pm h$) are satisfied, only if the coefficients $A_j(z)$ ($j=1,2,3$) vanish. Unfortunately, this would result in zero displacements and vanishing singular stresses on the plate faces near the corner point at the crack front, a result that is suspect on physical grounds. Their solution satisfies the plane strain relationship

$$\sigma_{zz} = \nu(\sigma_{rr} + \sigma_{\theta\theta}),$$

which means that their solution is only valid in the interior region. On the surface, the state of stress is expected to be entirely different from that resulting from aforementioned plane strain type solution. Therefore, it can be concluded that the singular stress field in the vicinity of the surface corner point located at the front of a semiinfinite crack has so far remained an open question.

Benthem [48], using the method of separation of variables, has attempted to determine the singular stress distribution in the neighborhood of the corner point of a quarter plane crack. The stress fields that he has obtained satisfy the differential equation, but does not satisfy the free surface boundary condition. He has, therefore, been forced to apply approximate weighted residual operators as shown below:

$$\text{on} \quad \sigma_{xz}, \quad \int_0^{2\pi} \cdots \cos(n-1)\phi d\phi$$

$$\text{on} \quad \sigma_{yz}, \quad \int_0^{2\pi} \cdots \sin n\phi d\phi$$

$$\text{on} \quad \sigma_{zz}, \quad \int_0^{2\pi} \cdots \cos(n-1)\phi d\phi.$$

$$n=1,2,3,.....$$

The above operation leads to a system of algebraic equations of infinite order, which must be truncated to obtain numerical results. Unfortunately, however, he has not succeeded in achieving convergence. Therefore he has assumed that the half space surface (z=0) is " struck" by an arbitrary load

$$\sigma_{xz} = 0$$

$$\sigma_{yz} = 0$$

$$\sigma_{zz} = r^{\lambda}.$$

His results, thus obtained, show that the stresses at the corner point behave like r^{-a}, where $o \leq a \leq 1/2$. In order to obtain the order of singularity, Benthem has to assume some loading distribution on the surface. It is very clear that Benthem's results do not exactly satisfy free surface boundary conditions, and that the solution thus obtained is only valid for a particular loading applied on the surface.

Folias has been the first to solve the problem of a center crack of finite length. He [49-51] has extended the Lur'e symbolic method [52], originally developed by Lur'e for a simply connected domain, to solve the aforementioned doubly connected problem. The method he has used in his pioneer work is able to solve three-dimensional Navier's equations as applied to the center crack problem in an elastic layer $-\infty<x, y<\infty$, $|z|\leq h$. His method has reproduced the stress field at crack front in the interior region. For surface corner point, he has used an asymptotic method to infer that the stresses are proportional to $\rho^{-(1/2+2\nu)} f_{ij}(\theta, \phi)$ and displacements are proportional to $\rho^{1/2-2\nu}$, ρ, θ, ϕ being the spherical coordinate system. Later on, he has used the same method in successfully solving three-dimensional hole and inclusion problems.

Bapu Rao [53-54] and Iyengar et al. [55] have studied the same problem as Folias. They have also used the Lur'e symbolic method of solution. The primary difference is that they have used polar coordinates, whereas Folias has used Cartesian coordinates; however, their conclusions are different. The explicit displacement expression is not found in their papers. The displacements are, therefore, derived here (see Appendix). It appears that the solution technique used by Iyengar et al [55] can not keep the displacement components at the crack front finite, unless $M_{3/2}$ and $f(d_{k-.5})$ vanish. Nonvanishing $M_{3/2}$ and $f(d_{k-.5})$ will lead to infinite energy, which, in turn, will lead to nonuniqueness.

The previously cited literature review suggests that the three-dimensional stress singularity problems can be classified in two broad categories:

(i) Center crack of finite length, investigated by Folias [49-51], Bapu Rao[53-54] and Iyengar et al. [55] ;

(ii) Wedge and its special case, i.e., semiinfinite crack studied by Hartranft and Sih [47] and Benthem [48].

The present dissertation research will address the latter category.

1.4 Comments on Two-Dimensional Solutions

It is well known that the two-dimensional assumption can accurately represent the plane strain situation. However, the same can not be said for the plane stress case. For a generalized plane stress problem, which does not involve stress singularity, the two-dimensional assumption can still yield acceptable (in the engineering sense) results. However, the issue of adequacy of the two-dimensional assumption in the case of plane stress problems with stress singularity has not been addressed in the literature.

Timoshenko and Goodier in their discussion on plane stress problem [57] have pointed out that under the assumptions of vanishing transverse stresses, and the inplane stresses being independent of the thickness coordinate, a two-dimensional approach

does not ensure satisfaction of all the compatibility conditions. From the three-dimensional equations, they have obtained the plane stress solution in the form:

$$\phi = \phi_0 - \frac{1}{2}\frac{\nu}{\nu+1}\theta_0 z^2,$$

where

$$\nabla_1^2 \phi_0 = \theta_0$$

$$\nabla_1^4 \phi_0 = 0;$$

and

$$\sigma_r = \frac{1}{r}\frac{\partial \phi}{\partial r} + \frac{1}{r^2}\frac{\partial^2 \phi}{\partial^2 \theta}$$

$$\sigma_\theta = \frac{\partial^2 \phi}{\partial r^2}$$

$$\tau_{r\theta} = \frac{1}{r^2}\frac{\partial \phi}{\partial \theta} - \frac{1}{r}\frac{\partial^2 \phi}{\partial \theta \partial r}.$$

The Williams type solution will yield the following:

$$\phi_0 = r^{s+1} f_1(\theta)$$

$$f_1(\theta) = A_1 \sin(s+1)\theta + A_2 \cos(s+1)\theta + A_3 \sin(s-1)\theta + A_4 \cos(s-1)\theta$$

$$\theta_0 = r^{s-1} f_2(\theta)$$

$$f_2(\theta) = 4s\big(A_3 \sin(s-1)\theta + A_4 \cos(s-1)\theta\big).$$

Therefore, the final solution is of the form:

$$\sigma_\theta = \sigma_{\theta 1} + \sigma_{\theta 2}$$

$$\sigma_r = \sigma_{r1} + \sigma_{r2}$$

$$\tau_{r\theta} = \tau_{r\theta 1} + \tau_{r\theta 2},$$

where

$$\sigma_{r1} = r^{s-1}\left(\frac{\partial^2 f_1(\theta)}{\partial^2 \theta} + (s+1)f_1(\theta)\right)$$

$$\sigma_{r2} = r^{s-3}\frac{(s-1)(s-2)\nu}{2(1+\nu)}z^2 f_2(\theta)$$

$$\sigma_{\theta 1} = r^{s-1}s(s+1)f_1(\theta)$$

$$\sigma_{\theta 2} = -r^{s-3}\frac{(s-1)(s-2)\nu}{2(1+\nu)}z^2 f_2(\theta)$$

$$\tau_{r\theta 1} = -r^{s-1}s\frac{\partial f_1(\theta)}{\partial \theta}$$

$$\tau_{r\theta 2} = r^{s-3}\frac{(s-2)\nu}{2(1+\nu)}z^2\frac{\partial f_2(\theta)}{\partial \theta}.$$

$\sigma_{r1}, \sigma_{\theta 1}, \tau_{r\theta 1}$ represent approximate plane stress solutions for nonsingular elasticity problems. If the plate is very thin, then z^2 is very small, so that $\sigma_{r2}, \sigma_{\theta 2}, \tau_{r\theta 2}$ can be ignored. However, for singular plane stress problems, $\sigma_{r2}, \sigma_{\theta 2}, \tau_{r\theta 2}$ are no longer

negligible. For example, the crack surface is free of stresses. By Williams' two-dimensional solution, s=1/2 is obtained. The singular stress field then takes the form

$$\sigma_{ij} \sim 0\left(r^{-1/2}\right) + z^2 \cdot 0\left(r^{-5/2}\right).$$

Therefore, even though z is very small, σ_{ij2} cannot still be neglected, because this is the dominant term in this case. The solution does not satisfy the boundary condition of wedge surface. At present, however, the first term of the solution is still used to represent the singular plane stress fields. This type of discrepancy can be resolved only through the use of a three-dimensional approach.

1.5 Objectives and Outline of the Present Investigation

Since Williams[6] obtained the two-dimensional stress field at the crack front, the three-dimensional wedge problem has remained a challenge to researchers in the field. Because of its general geometric form, it has wide applications for many practical problems, such as for semiinfinite cracks, interface cracks and edge bonded wedges. Although these problems have been thoroughly studied under the premises of two-dimensionality, their three-dimensional counterparts continue to pose an insurmountable challenge to the researchers. The following questions must be answered for understanding the singular stress behavior in the vicinity of the front of a homogeneous as well as a bimaterial wedge.

1. What is the order of stress singularity at the wedge front in the interior region? Also, is it possible to derive the expressions of stresses and displacements in this region at the wedge front ?

2. What is the order of stress singularity at the surface corner region at the wedge front ? Also, is it possible to derive the expressions of stresses and displacements in the neighborhoodof this point at the wedge front?

The following main numerical results are presented in the dissertation:

(i) Computation of the order of stress singularity for different wedge angles (including the semiinfinite crack as a special case) and various wedge side boundary conditions, for the case of a homogeneous wedge;

(ii) Computation of the order of stress singularity for different wedge angles (including the semiinfinite crack as a special case) and various wedge side boundary conditions, for the case of for a bimaterial wedge;

(iii) The effect of material property on the singular stress fields in the neighborhood of the homogeneous and bimaterial wedge fronts;

(iv)The study of the dominance of the computed eigenvalues (i.e., order of singularity) for different types of loading, such as extension/bending, and antiplane shear;

(v) The development of plastic yield zone at the front of a semiinfinite crack;

(vi) The study of boundary-layer effects in bonded orthogonal plate made of dissimilar materials.

CHAPTER 2

THREE-DIMENSIONAL WEDGE PROBLEM

2.1 Statement of the Problem

The cylindrical polar coordinate system (r,θ, z), is convenient to describe the deformation behavior of an infinite wedge. Here, the z-axis is placed along the straight wedge front, and the coordinates r, θ, are used to define the position of an element in the plane of the plate. See Figure 2.1. The components of the displacements in the radial and tangential directions are represented by U_r, U_θ, and the component in the z-direction is denoted by Uz.

In the absence of body forces, the coupled partial differential equations in terms of the displacement functions U_r, U_θ , and U_Z are given as follows:

$$(\lambda+2G)\frac{\partial^2 U_r}{\partial r^2}+\frac{(\lambda+2G)}{r}\frac{\partial U_r}{\partial r}-(\lambda+2G)\frac{U_r}{r^2}+\frac{G}{r^2}\frac{\partial^2 U_r}{\partial\theta^2}+\frac{(\lambda+G)}{r}\frac{\partial^2 U_\theta}{\partial r\partial\theta}-\frac{(\lambda+3G)}{r^2}\frac{\partial U_\theta}{\partial\theta}$$

$$+G\frac{\partial^2 U_r}{\partial z^2}+(\lambda+G)\frac{\partial^2 U_z}{\partial r\partial z}=0$$

$$\frac{(\lambda+G)}{r}\frac{\partial^2 U_r}{\partial\theta\partial r}+\frac{(\lambda+3G)}{r^2}\frac{\partial U_r}{\partial\theta}+G\frac{\partial^2 U_\theta}{\partial r^2}+G\frac{\partial U_\theta}{r\partial r}-G\frac{U_\theta}{r^2}+(\lambda+2G)\frac{\partial^2 U_\theta}{r^2\partial\theta^2}$$

$$+G\frac{\partial^2 U_\theta}{\partial z^2}+\frac{(\lambda+G)}{r}\frac{\partial^2 U_z}{\partial\theta\partial z}=0$$

$$(\lambda+G)\frac{\partial^2 U_r}{\partial r\partial z}+\frac{(\lambda+G)}{r}\frac{\partial U_r}{\partial z}+\frac{(\lambda+G)}{r}\frac{\partial^2 U_\theta}{\partial\theta\partial z}+(\lambda+2G)\frac{\partial^2 U_z}{\partial z^2}+G\frac{\partial^2 U_z}{\partial r^2}$$

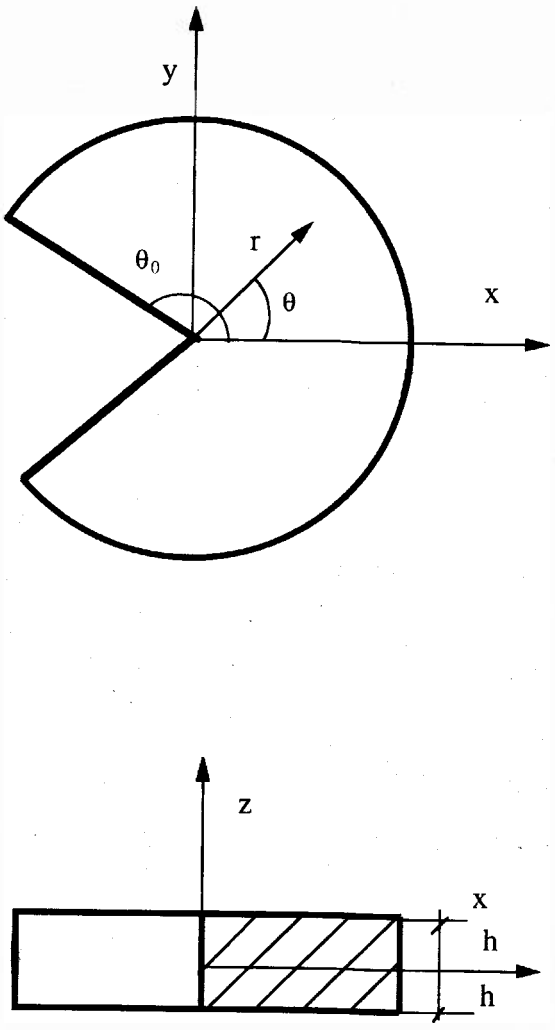

Figure 2.1 A homogeneous wedge

$$+G\frac{\partial U_z}{r\partial r}+\frac{G}{r^2}\frac{\partial^2 U_z}{\partial\theta^2}=0, \tag{2.1}$$

where λ and G are known as Lame's coefficients. The assumed displacement functions for the three-dimensional wedge problem under consideration are selected on the basis of separation of variables in a manner similar to their two-dimensional counterparts first investigated by Williams[6] . These are as given below:

$$U_r = e^{ikz}\phi_r(\theta)R_r = e^{ikz+p\theta}R_r$$

$$U_\theta = e^{ikz}\phi_\theta(\theta)R_\theta = e^{ikz+p\theta}R_\theta$$

$$U_z = e^{ikz}\phi_z(\theta)R_z = e^{ikz+p\theta}R_z. \tag{2.2}$$

It may be noted that since the z-dependent term is nonsingular and at most admits discontinuity, it can be best represented represented by Fourier series, wherein the presence of such discontinuities (with measure zero) can be handled by means of the Lebesgue integration theory [79]. Substitution of equation (2.2) into equation (2.1) yields the following:

$$(\lambda+2G)\frac{d^2R_r}{dr_1^2}+\frac{(\lambda+2G)}{r_1}\frac{dR_r}{dr_1}-(\lambda+2G)\frac{R_r}{r_1^2}+\frac{G}{r_1^2}p^2R_r+\frac{(\lambda+G)}{r_1}p\frac{dR_\theta}{dr_1}$$

$$\frac{-(\lambda+3G)}{r_1^2}pR_\theta+GR_r+(\lambda+G)\frac{dR_z}{dr_1}=0$$

$$\frac{(\lambda+G)}{r_1}p\frac{dR_r}{dr_1}+\frac{(\lambda+3G)}{r_1^2}pR_r+G\frac{d^2R_\theta}{dr_1^2}+\frac{G}{r_1}\frac{dR_\theta}{dr_1}-\frac{G}{r_1^2}R_\theta+\frac{(\lambda+2G)}{r_1^2}p^2R_\theta$$

$$+GR_\theta+\frac{(\lambda+G)}{r_1}pR_z=0$$

$$(\lambda+G)\frac{dRr}{dr_1}+\frac{(\lambda+G)}{r_1}R_r+\frac{(\lambda+G)}{r_1}pR_\theta+(\lambda+2G)R_z+G\frac{d^2R_z}{dr_1^2}$$

$$+\frac{G}{r_1}\frac{dR_z}{dr_1}+\frac{G}{r_1^2}p^2R_z=0, \tag{2.3}$$

where

$$r_1=ikr.$$

The correct solution must satisfy the governing equations and boundary conditions. The boundary conditions include those at the plate faces and wedge-side surface. The boundary condition of plate faces, $z=\pm h$, are given by

$$\sigma_z=\tau_{\theta z}=\tau_{rz}=0. \tag{2.4}$$

The boundary conditions at the wedge-side surface consist of three types,

$$\theta=\pm\theta_0,$$

1. Free-Free

$$\sigma_\theta=\tau_{r\theta}=\tau_{\theta z}=0; \tag{2.5}$$

2. Clamped-Clamped

$$U_r = U_\theta = U_z = 0; \tag{2.6}$$

3. Clamped-Free

$$\theta = -\theta_0$$

$$U_r = U_\theta = U_z = 0$$

$$\theta = \theta_0$$

$$\sigma_\theta = \tau_{r\theta} = \tau_{\theta z} = 0. \tag{2.7}$$

2.2 Singular Stress Fields at the Front of a Wedge Subjected to Antiplane Shear Loading

The system of coupled differential equations (2.3) can be solved in the form:

$$R_r = \sum_{n=0}^{\infty} a_{s+2n}\, r_1^{s+2n+1}$$

$$R_\theta = \sum_{n=0}^{\infty} b_{s+2n}\, r_1^{s+2n+1}$$

$$R_z = \sum_{n=0}^{\infty} c_{s+2n}\, r_1^{s+2n}. \tag{2.8}$$

Substitution of equations (2.8) into equations (2.3) yield a recurrent relationship, which, for n=0, supply the following the characteristic equation for the coupled differential equations:

$$s^2 + p^2 = 0$$

$$p_{1,2} = \pm is.$$

This permits the θ-dependent term to be written in the form:

$$\phi_z(\theta) = \left(\overline{\overline{A}}_1 \sin(s\theta) + \overline{\overline{A}}_2 \cos(s\theta)\right)$$

$$\phi_r(\theta) = \left(\overline{\overline{A}}_1 \sin(s\theta) + \overline{\overline{A}}_2 \cos(s\theta)\right)$$

$$\phi_\theta(\theta) = \left(\overline{\overline{A}}_1 \cos(s\theta) - \overline{\overline{A}}_2 \sin(s\theta)\right). \tag{2.9}$$

In addition, since z-dependent term is, as mentioned earlier, assumed in the form of Fourier series, the assumed displacement functions can be written as follows:

$$U_Z = I_{1s}\left(\overline{D}_1 \cos(kz) + \overline{D}_2\, i \sin(kz)\right)\left(\overline{\overline{A}}_1 \sin(s\theta) + \overline{\overline{A}}_2 \cos(s\theta)\right)$$

$$U_r = -I_{2s+1}\left(\overline{D}_1\, i \sin(kz) + \overline{D}_2 \cos(kz)\right)\left(\overline{\overline{A}}_1 \sin(s\theta) + \overline{\overline{A}}_2 \cos(s\theta)\right)$$

$$U_\theta = I_{3s+1}\left(\overline{D}_1 i \sin(kz) + \overline{D}_2 \cos(kz)\right)\left(\overline{\overline{A}}_1 \cos(s\theta) - \overline{\overline{A}}_2 \sin(s\theta)\right), \tag{2.10}$$

where

$$I_{1s} = \sum_{n=0}^{\infty} c_{s+2n} r_1^{s+2n}$$

$$I_{2s+1} = \sum_{n=0}^{\infty} a_{s+2n} r_1^{s+2n+1}$$

$$I_{3s+1} = \sum_{n=0}^{\infty} b_{s+2n} r_1^{s+2n+1}. \tag{2.11}$$

The general recurrent relationship for the coefficients is given by

$$a_{s+2n}\left[-(\lambda+2G)(s+2n+2)(s+2n)+Gs^2\right]+b_{s+2n}s\left[-(\lambda+G)(s+2n+1)+(\lambda+3G)\right]$$

$$-a_{s+2n-2}G+c_{s+2n}(\lambda+G)(s+2n)=0 \qquad (2.12)$$

$$-a_{s+2n}s\left[(\lambda+G)(s+2n+1)+(\lambda+3G)\right]+b_{s+2n}\left[G(s+2n+2)(s+2n)-(\lambda+2G)s^2\right]$$

$$+Gb_{s+2n-2}+c_{s+2n}s(\lambda+G)=0 \qquad (2.13)$$

$$-a_{s+2n-2}(\lambda+G)(s+2n)-b_{s+2n-2}(\lambda+G)s+c_{s+2n-2}(\lambda+2G)$$

$$+c_{s+2n}G\left((s+2n)^2-s^2\right)=0. \qquad (2.14)$$

When n=0, both equations (2.12) and (2.13) reduce to equation (2.15), as shown below:

$$a_s\left[(\lambda+G)s+2(\lambda+2G)\right]+b_s\left[(\lambda+G)(s+1)-(\lambda+3G)\right]=(\lambda+G)c_s. \qquad (2.15)$$

The general asymptotic form can be written as follows:

$$U_z=\frac{r^sB_b(z)}{G}\left(A_1\sin(s\theta)+A_2\cos(s\theta)\right)+0\left(r^{s+2}\right)$$

$$Ur=0\left(r^{s+1}\right),\quad U_\theta=0\left(r^{s+1}\right), \qquad (2.16)$$

where

$$\overline{\overline{A}}_{1,2}=\frac{A_{1,2}}{Gc_s}$$

$$D_1 = -(ik)^s \overline{D}_1, \qquad D_2 = i(ik)^s \overline{D}_2$$

$$B_b(z) = -D_1 \cos(kz) + D_2 \sin(kz). \tag{2.17}$$

wherein k is the arbitrary unknown constant. The fields of singular stresses can be obtained from (2.16):

$$\tau_{\theta z} = r^{s-1} B_b(z) s\left(A_1 \cos(s\theta) - A_2 \sin(s\theta)\right) + 0\left(r^{s+1}\right) \tag{2.18}$$

$$\tau_{rz} = r^{s-1} B_b(z) s\left(A_1 \sin(s\theta) + A_2 \cos(s\theta)\right) + 0\left(r^{s+1}\right) \tag{2.19}$$

$$\tau_{r\theta} = 0\left(r^s\right), \quad \sigma_r = 0\left(r^s\right)$$

$$\sigma_\theta = 0\left(r^s\right), \quad \sigma_z = 0\left(r^s\right).$$

Satisfaction of stress-free condition, given by equation (2.4), on the plate faces results in:

$$B_b(\pm h) = B_{bs}(\pm h) + B_{ba}(\pm h) = 0, \tag{2.20}$$

where

$$B_{bs}(\pm h) = -D_1 \cos(\pm kh)$$

$$B_{ba}(\pm h) = D_2 \sin(\pm kh).$$

The special case of symmetric deformation is obtained as follows:

$$k_i = \frac{(2i+1)}{2h}\pi \qquad i = 0, \pm 1, \pm 2, \cdots\cdots$$

$$B_{bs}(z) = \sum_{i=0}^{\pm\infty} -D_{1i} \cos\left(\frac{(2i+1)}{2h}\pi z\right). \tag{2.21}$$

The antisymmetric deformation case can also be obtained in a similar manner:

$$k_i = \frac{i\pi}{h} \qquad i = 0, \pm 1, \pm 2, \cdots\cdots$$

$$B_{ba}(z) = \sum_{i=0}^{\pm\infty} D_{2i} \sin\left(\frac{i}{h}\pi z\right). \tag{2.22}$$

The expressions for stresses and displacements also need to satisfy the boundary condition on the wedge side surfaces. The following three combinations are considered:

2.2.1 Clamped-Clamped

Substitution of equation (2.16) into equation (2.6), the following characteristic equation is obtained:

$$\sin(2s\theta_0) = 0. \tag{2.23}$$

The minimum root (eigenvalue) contributing to the singular stresses is

$$s = \frac{\pi}{2\theta_0}. \tag{2.24}$$

It may be noted that when $\theta_0 \leq |\pm\pi/2|$, the stresses at the wedge front are nonsingular. The special case of $\theta_0 = |\pm\pi/2|$ represents the half space, which yields s=1. However, when $\theta_0 > |\pm\pi/2|$, the wedge front has singular stresses. Another special case is given by $\theta_0 = \pm\pi$, which yields s=1/2.

2.2.2 Clamped-Free

Substitution of equations (2.16) and equation (2.18) into equation (2.7) yields the following characteristic equation:

$$\cos(2s\theta_0)=0. \tag{2.25}$$

The minimum roots (eigenvalue) contributing to the singular stresses are:

$$s_1=\frac{\pi}{4\theta_0} \tag{2.26}$$

$$s_2=\frac{3\pi}{4\theta_0}. \tag{2.27}$$

For $\theta_0 > |\pm\pi / 4|$, the wedge has the singular stresses. $\theta_0 > |\pm 3\pi / 4|$, τ_{rz} and $\tau_{\theta z}$ possess two singular values. In the special case $\theta_0=\pm\pi$, the singular parts of τ_{rz} and $\tau_{\theta z}$ are given by

$$\tau_{rz},\ \tau_{\theta z} \sim 0\left(r^{-3/4}\right)+0\left(r^{-1/4}\right). \tag{2.28}$$

2.2.3 Free-Free

Substitution of equation (2.18) into equation (2.5) supplies the following characteristic equation:

$$\sin(2s\theta_0)=0. \tag{2.29}$$

The minimum root (eigenvalue) contributing to the singular stresses is

$$s=\frac{\pi}{2\theta_0}. \tag{2.30}$$

The above eigenvalue is the same as that obtained by Sih [25] for the special case of a semiinfinite crack, $\theta_0=\pm\pi$, s=1/2.

It must be stressed that the singularity of stresses remains unchanged throughout the plate thickness. The stress distribution in the vicinity of a semiinfinite crack ($\theta_0=\pm\pi$) front, i.e., r<<1, and for the case of free-free edge, can be expressed as follows:

$$\tau_{rz}=\frac{K_{III}}{\sqrt{2\pi r}}\sin\left(\theta/2\right) \tag{2.31}$$

$$\tau_{\theta z}=\frac{K_{III}}{\sqrt{2\pi r}}\cos(\theta/2) \tag{2.32}$$

$$U_z=\frac{2K_{III}}{G}\sqrt{\frac{r}{2\pi}}\sin\left(\frac{\theta}{2}\right), \tag{2.33}$$

where

$$K_{III}(z)=K_{III\,s}(z)+K_{III\,a}(z) \tag{2.34}$$

$$K_{IIIs}=\sqrt{\frac{\pi}{2}}\,A_1B_{bs}(z)$$

$$K_{IIIa}=\sqrt{\frac{\pi}{2}}\,A_1B_{ba}(z).$$

Thus, the stress intensity factor for mode III can be separated into symmetric (K_{IIIs}) and antisymmetric (K_{IIIa}) parts. It is clear that

$$\int_{-h}^{h} K_{III\,a}\,dz=0. \tag{2.35}$$

K_{IIIa} thus obtained represents the self-equilibrating stress intensity factor for a semiinfinite crack, resulting in the residual stresses in the material. It must be noted that K_{IIIa} cannot be determined by a two-dimensional approximation, which yields constant K_{IIIs}, while both K_{IIIa} and K_{IIIs}, obtained by the above three-dimensional approach, are functions of z.

2.3 Singular Stress Fields in the Interior Region of a Wedge under Extension/Bending

The system of coupled differential equations (2.3) can also be solved using the following infinite series:

$$R_r = \sum_{n=0}^{\infty} a_{s+n}\, r_1^{s+2n}$$

$$R_\theta = \sum_{n=0}^{\infty} b_{s+n}\, r_1^{s+2n}$$

$$R_z = \sum_{n=0}^{\infty} c_{s+n}\, r_1^{s+2n+1}. \tag{2.36}$$

On substitution of equations (2.36) into equation (2.3), a set of recurrent relationships can be derived. When n=0, the characteristic equations for the coupled differential equations are given by

$$a_s\left[(\lambda+2G)\left(s^2-1\right)+Gp^2\right]+b_s\, p\left[(\lambda+G)s-(\lambda+3G)\right]=0$$

$$a_s\, p\left[s(\lambda+G)+(\lambda+3G)\ \right]+b_s\left[G\left(s^2-1\right)+(\lambda+2G)p^2\right]=0. \tag{2.37}$$

The above equations are found to have four imaginary root:

$$p_{1,2}=\pm i(s+1), \qquad p_{3,4}=\pm i(s-1). \tag{2.38}$$

The final results that satisfy the equilibrium equations (2.1) can be expressed in the following form:

$$U_r = U_{r1} + U_{r2}$$

$$U_\theta = U_{\theta 1} + U_{\theta 2}$$

$$U_z = U_{z1} + U_{z2}, \tag{2.39}$$

where

$$U_{r1} = I_s\left(\overline{\overline{D}}_1 i\sin(kz) + \overline{\overline{D}}_2\cos(kz)\right)\left(\overline{A}_1\sin(s+1)\theta + \overline{A}_2\cos(s+1)\theta\right)$$

$$U_{\theta 1} = I_s\left(\overline{\overline{D}}_1 i\sin(kz) + \overline{\overline{D}}_2\cos(kz)\right)\left(\overline{A}_1\cos(s+1)\theta - \overline{A}_2\sin(s+1)\theta\right)$$

$$U_{z1} = I_{s+1}\left(\overline{\overline{D}}_1\cos(kz) + \overline{\overline{D}}_2 i\sin(kz)\right)\left(\overline{A}_1\sin(s+1)\theta + \overline{A}_2\cos(s+1)\theta\right); \tag{2.40}$$

$$U_{r2} = I_{s1}\left(\overline{\overline{D}}_1 i\sin(kz) + \overline{\overline{D}}_2\cos(kz)\right)\left(\overline{A}_3\sin(s-1)\theta + \overline{A}_4\cos(s-1)\theta\right)$$

$$U_{\theta 2} = I_{s1}\left(\overline{\overline{D}}_1 i\sin(kz) + \overline{\overline{D}}_2\cos(kz)\right)\left(\overline{A}_3\cos(s-1)\theta - \overline{A}_4\sin(s-1)\theta\right)$$

$$U_{z2} = I_{s3}\left(\overline{\overline{D}}_1\cos(kz) + \overline{\overline{D}}_2 i\sin(kz)\right)\left(\overline{A}_3\sin(s-1)\theta + \overline{A}_4\cos(s-1)\theta\right). \tag{2.41}$$

I_S and I_{S+1} are modified Bessel functions. I_{S1}, I_{S2}, and I_{S3} are in the form as follows:

$$I_{s1} = \sum_{i=0}^{\infty} a_{s+2n} r_1^{s+2n}$$

$$I_{s2} = \sum_{i=0}^{\infty} b_{s+2n} r_1^{s+2n}$$

$$I_{s3} = \sum_{i=0}^{\infty} c_{s+2n} r_1^{s+2n+1} \tag{2.42}$$

Their coefficients can be determined by the following equations

$$a_{s+2n}\left[(\lambda+2G)(s+2n+1)(s+2n-1)-G(s-1)^2\right]-b_{s+2n}(s-1)$$

$$\left[(\lambda+G)(s+2n)-(\lambda+3G)\right]+a_{s+2n-2}G+c_{s+2n-2}(\lambda+G)(s+2n-1)=0$$

$$a_{s+2n}(s-1)\left[(\lambda+G)(s+2n)+(\lambda+3G)\right]+b_{s+2n}$$

$$\left[G(s+2n+1)(s+2n-1)-(\lambda+2G)(s-1)^2\right]$$

$$+b_{s+2n-2}G+c_{s+2n-2}(\lambda+G)(s-1)=0$$

$$a_{s+2n}(\lambda+G)(s+2n+1)-b_{s+2n}(\lambda+G)(s-1)+c_{s+2n-2}(\lambda+2G)$$

$$+c_{s+2n}G\left[(s+2n+1)^2-(s-1)^2\right]=0. \tag{2.43}$$

The asymptotic form of equations (2.39) is

$$U_r = r_1^s B_1(z)\left[\frac{2^{-s}}{\Gamma(s+1)}\left(\overline{A}_1\sin(s+1)\theta+\overline{A}_2\cos(s+1)\theta\right)+\right.$$

$$\left.a_s\left(\overline{A}_3\sin(s-1)\theta+\overline{A}_4\cos(s-1)\theta\right)\right]+0\left(r^{s+2}\right)$$

$$U_\theta = r_1^s B_1(z)\left[\frac{2^{-s}}{\Gamma(s+1)}\left(\overline{A}_1\cos(s+1)\theta - \overline{A}_2\sin(s+1)\theta\right) + \right.$$

$$\left. f_1 a_s\left(\overline{A}_3\cos(s-1)\theta - \overline{A}_4\sin(s-1)\theta\right)\right] + 0\left(r^{s+2}\right)$$

$$U_z = 0\left(r^{s+1}\right), \tag{2.44}$$

where

$$f_1 = \frac{(\lambda+G)s + (\lambda+3G)}{(\lambda+G)s - (\lambda+3G)}$$

$$B_1(z) = D_1\sin(kz) + D_2\cos(kz) \tag{2.45}$$

$$D_1 = i\overline{\overline{D}}_1, \qquad D_2 = \overline{\overline{D}}_2;$$

in which k is the arbitrary constants. Expressing

$$\overline{A}_{1,2} = \frac{1}{2Gs}A_{1,2}\frac{\Gamma(s+1)2^s}{(ik)^s}$$

$$\overline{A}_{3,4} = \frac{(\lambda+G)s - (\lambda+3G)}{2sG(\lambda+G)a_s(ik)^s}A_{3,4}.$$

The displacement fields and stresses can be written down in the form

$$U_r = \frac{r^s}{2Gs}\left[B_1(z)\left(A_1\sin(s+1)\theta + A_2\cos(s+1)\theta\right) + (s-3+4\nu)\right.$$

$$\left. B_1(z)\left(A_3\sin(s-1)\theta + A_4\cos(s-1)\theta\right)\right] + 0\left(r^{s+2}\right) \tag{2.46}$$

$$U_\theta = \frac{r^s}{2Gs}\left[B_1(z)\left(A_1\cos(s+1)\theta - A_2\sin(s+1)\theta\right) + (s+3-4\nu)\right.$$

$$\left.B_1(z)\left(A_3\cos(s-1)\theta - A_4\sin(s-1)\theta\right)\right] + 0\left(r^{s+2}\right) \qquad (2.47)$$

$$\sigma_r = r^{s-1}\left[B_1(z)\left(A_1\sin(s+1)\theta + A_2\cos(s+1)\theta\right) + (s-3)\right.$$

$$\left.B_1(z)\left(A_3\sin(s-1)\theta + A_4\cos(s-1)\theta\right)\right] + 0\left(r^{s+1}\right) \qquad (2.48)$$

$$\sigma_\theta = -r^{s-1}\left[B_1(z)\left(A_1\sin(s+1)\theta + A_2\cos(s+1)\theta\right) + (s+1)\right.$$

$$\left.B_1(z)\left(A_3\sin(s-1)\theta + A_4\cos(s-1)\theta\right)\right] + 0\left(r^{s+1}\right) \qquad (2.49)$$

$$\tau_{r\theta} = r^{s-1}\left[B_1(z)\left(A_1\cos(s+1)\theta - A_2\sin(s+1)\theta\right) + (s-1)\right.$$

$$\left.B_1(z)\left(A_3\cos(s-1)\theta - A_4\sin(s-1)\theta\right)\right] + 0\left(r^{s+1}\right) \qquad (2.50)$$

$$\sigma_z = -4\nu r^{s-1}B_1(z)\left(A_3\sin(s-1)\theta + A_4\cos(s-1)\theta\right) + 0\left(r^{s+1}\right) \qquad (2.51)$$

$$U_z = 0\left(r^{s+1}\right), \quad \tau_{rz} = 0\left(r^s\right), \quad \tau_{\theta z} = 0\left(r^s\right). \qquad (2.52)$$

On substitution of equations (2.46-2.51) into the boundary conditions on the wedge-side surface given by equations (2.5-2.7), the eigenvalues for different boundary conditions can be obtained.

2.3.1 Clamped-Clamped

The equation of root is

$$\sin(2s\theta_0) = \pm \frac{s}{(3-4\nu)} \sin(2\theta_0), \tag{2.53}$$

when $\theta_0 = \pm\pi$, s = 1/2.

2.3.2 Clamped-Free

The equation of root is

$$\cos(4s\theta_o) = \frac{1}{D_2}\left[2\left(C_1C_2 + s^2 - 1\right) - D_1\cos(4\theta_o)\right], \tag{2.54}$$

where

$$C_1 = s - 3 + 4\nu, \qquad C_2 = s + 3 - 4\nu$$

$$D_1 = 4s^2, \qquad D_2 = 12 - 16\nu.$$

where $\theta_O = \pm\pi$, equation (2.54) has two roots contributing to singular stresses

$$s = \lambda_1 + i\lambda_2$$

a. $\lambda_1 = \frac{1}{4}, \quad \lambda_2 = \pm\frac{1}{4\pi}\cosh^{-1}\left(\frac{C^2+1}{2C}\right)$

b. $\lambda_1 = \frac{3}{4}, \quad \lambda_2 = \pm\frac{1}{4\pi}\cosh^{-1}\left(\frac{C^2+1}{2C}\right),$

where C = 3-4v.

2.3.3 Free-Free

The equation of root is

$$\sin(2s\theta_o)=\pm s\sin(2\theta_o). \tag{2.56}$$

when $\theta_O=\pm\pi$, s= 1/2. The stress distribution in the vicinity of a semiinfinite crack ($\theta_O=\pm\pi$) front, i.e., r<<1, and for the case of free-free edge, can be expressed as follows:

$$\sigma_r=\frac{K_I}{\sqrt{2\pi r}}\left(-\frac{1}{4}\cos\left(\frac{3\theta}{2}\right)+\frac{5}{4}\cos\left(\frac{\theta}{2}\right)\right)+\frac{K_{II}}{\sqrt{2\pi r}}\left(\frac{3}{4}\sin\left(\frac{3\theta}{2}\right)-\frac{5}{4}\sin\left(\frac{\theta}{2}\right)\right)$$

$$\sigma_\theta=\frac{K_I}{\sqrt{2\pi r}}\left(\frac{1}{4}\cos\left(\frac{3\theta}{2}\right)+\frac{3}{4}\cos\left(\frac{\theta}{2}\right)\right)-\frac{K_{II}}{\sqrt{2\pi r}}\left(\frac{3}{4}\sin\left(\frac{3\theta}{2}\right)+\frac{3}{4}\sin\left(\frac{\theta}{2}\right)\right)$$

$$\tau_{r\theta}=\frac{K_I}{\sqrt{2\pi r}}\left(\frac{1}{4}\sin\left(\frac{3\theta}{2}\right)+\frac{1}{4}\sin\left(\frac{\theta}{2}\right)\right)+\frac{K_{II}}{\sqrt{2\pi r}}\left(\frac{3}{4}\cos\left(\frac{3\theta}{2}\right)+\frac{1}{4}\cos\left(\frac{\theta}{2}\right)\right)$$

$$\sigma_z=\frac{2\nu K_I}{\sqrt{2\pi r}}\cos\left(\frac{\theta}{2}\right)-\frac{2\nu K_{II}}{\sqrt{2\pi r}}\sin\left(\frac{\theta}{2}\right), \tag{2.57}$$

$$U_r=-\frac{K_I}{G}\sqrt{\frac{r}{2\pi}}\left(\frac{1}{4}\cos\left(\frac{3}{2}\theta\right)+\frac{-5+8\nu}{4}\cos\left(\frac{\theta}{2}\right)\right)+\frac{K_{II}}{G}$$

$$\sqrt{\frac{r}{2\pi}}\left(\frac{3}{4}\sin\left(\frac{3\theta}{2}\right)+\frac{-5+8\nu}{4}\sin\left(\frac{\theta}{2}\right)\right)$$

$$U_\theta=\frac{K_I}{G}\sqrt{\frac{r}{2\pi}}\left(\frac{1}{4}\sin\left(\frac{3}{2}\theta\right)+\frac{-7+8\nu}{4}\sin\left(\frac{\theta}{2}\right)\right)+\frac{K_{II}}{G}\sqrt{\frac{r}{2\pi}}$$

$$\left(\frac{3}{4}\cos\left(\frac{3\theta}{2}\right)+\frac{-7+8\nu}{4}\cos\left(\frac{\theta}{2}\right)\right); \tag{2.58}$$

where

$$K_I = -2\sqrt{2\pi}\ A_4 B_1(z)$$

$$K_{II} = -2\sqrt{2\pi}\ A_3 B_1(z) \tag{2.59}$$

The stress field in the vicinity of the front of a semiinfinite crack under in-plane extension can be recovered if

$$B_1(z) = B_{1s}(z) = D_2 \cos(kz). \tag{2.60}$$

By using the boundary condition of free plate surface, the general form of B_{1s} can be obtained

$$B_{1s}(z) = \sum_{i=0}^{\pm\infty} D_{2i} \cos\left(\frac{(2i+1)}{2h}\pi z\right). \tag{2.61}$$

Hence, $K_I = K_{Is}$ and $K_{II} = K_{IIs}$ represent symmetric stress intensity factors. If the odd functions are selected from $B_1(z)$, it can yield the out-of-plane bending case given by.

$$B_1(z) = B_{1a}(z) = D_1 \sin(kz). \tag{2.62}$$

B_{1a} that satisfies free plate surface is given by

$$B_{1a}(z) = \sum_{i=0}^{\pm\infty} D_{1i} \sin\left(\frac{i\pi}{h} z\right). \tag{2.63}$$

Here $K_I = K_{Ia}$ and $K_{II} = K_{IIa}$ are antisymmetric stress intensity factors. If the boundary conditions on the free plate faces are satisfied, all the stresses and displacements on the plate faces in the vicinity of the front of a semiinfinite crack and a wedge vanishes. It is contrary to the experimental results except for $\nu=0$ [75]. Sih [56] has, therefore, predicted another solution on the surface.

2.4 Singular Stress Fields on the Surface Region of a Wedge under Extension/Bending

The singular stress field in the vicinity of the surface corner point is different from its interior region counterpart on account of the contribution from the singular transverse normal strain, ε_z. If the transverse normal strain is not singular, the solution obtained always satisfies the plane strain condition, which is valid only in the interior region. Therefore, the singular stress field in the vicinity of the surface corner point must account for the contribution from the transverse normal strain, ε_z, which forms the basis of the present investigation in this section.

The three-dimensional asymptotic solution for displacements and singular stresses in the vicinity of the surface corner point at the front of an infinite wedge under extension and bending can be derived directly as follows: first, s in equation (2.10) is replaced by (s-1); the resulting intermediate solution is superimposed upon that given by equation (2.40) to produce the following final solution:

$$U_r = I_s\left(\overline{\overline{D}}_1 i\sin(kz) + \overline{\overline{D}}_2\cos(kz)\right)\left(\overline{A}_1\sin(s+1)\theta + \overline{A}_2\cos(s+1)\theta\right) -$$

$$I_{2s}\left(\overline{D}_1 i\sin(kz) + \overline{D}_2\cos(kz)\right)\left(\overline{\overline{A}}_1\sin(s-1)\theta + \overline{\overline{A}}_2\cos(s-1)\theta\right)$$

$$U_\theta = I_s\left(\overline{\overline{D}}_1 i\sin(kz) + \overline{\overline{D}}_2\cos(kz)\right)\left(\overline{A}_1\cos(s+1)\theta - \overline{A}_2\sin(s+1)\theta\right) +$$

$$I_{3s}\left(\overline{D}_1 i\sin(kz) + \overline{D}_2\cos(kz)\right)\left(\overline{\overline{A}}_1\cos(s-1)\theta - \overline{\overline{A}}_2\sin(s-1)\theta\right)$$

$$U_z = I_{s+1}\left(\overline{\overline{D}}_1\cos(kz) + \overline{\overline{D}}_2 i\sin(kz)\right)\left(\overline{A}_1\sin(s+1)\theta + \overline{A}_2\cos(s+1)\theta\right) +$$

$$I_{1s-1}\left(\overline{D}_1\cos(kz) + \overline{D}_2 i\sin(kz)\right)\left(\overline{\overline{A}}_1\sin(s-1)\theta + \overline{\overline{A}}_2\cos(s-1)\theta\right). \qquad (2.64)$$

The corresponding asymptotic expression for displacements and stresses in the vicinity of the wedge front is given by

$$U_z = r^{s-1}B_3(z)c_{s-1}\left(\overline{\overline{A}}_1 \sin(s-1)\theta + \overline{\overline{A}}_2 \cos(s-1)\theta\right) + 0\left(r^{s+1}\right)$$

$$U_r = r^s B_2(z)\left[\left(\overline{A}_1 \sin(s+1)\theta + \overline{A}_2 \cos(s+1)\theta\right)\right.$$

$$\left. -a_{s-1}\left(\overline{\overline{A}}_1 \sin(s-1)\theta + \overline{\overline{A}}_2 \cos(s-1)\theta\right)\right] + 0\left(r^{s+2}\right)$$

$$U_\theta = r^s B_2(z)\left[\left(\overline{A}_1 \cos(s+1)\theta - \overline{A}_2 \sin(s+1)\theta\right)\right.$$

$$\left. +b_{s-1}\left(\overline{\overline{A}}_1 \cos(s-1)\theta - \overline{\overline{A}}_2 \sin(s-1)\theta\right)\right] + 0\left(r^{s+2}\right)$$

$$\sigma_r = r^{s-1}B_2(z)G\left[2s\left(\overline{A}_1 \sin(s+1)\theta + \overline{A}_2 \cos(s+1)\theta\right) + \right.$$

$$\left(\overline{\overline{A}}_1 \sin(s-1)\theta + \overline{\overline{A}}_2 \cos(s-1)\theta\right)\left(-a_{s-1}(\lambda(s+1) + 2Gs)\right.$$

$$\left. -\lambda b_{s-1}(s-1) + \lambda c_{s-1}\right)\ ] + 0\left(r^{s+1}\right)$$

$$\sigma_\theta = -\,r^{s-1}B_2(z)G\left[2s\left(\overline{A}_1 \sin(s+1)\theta + \overline{A}_2 \cos(s+1)\theta\right) + \right.$$

$$\left(\overline{\overline{A}}_1 \sin(s-1)\theta + \overline{\overline{A}}_2 \cos(s-1)\theta\right)\left(a_{s-1}(\lambda(s+1) + 2G) + \right.$$

$$\left. b_{s-1}(s-1)(\lambda + 2G) - \lambda c_{s-1}\ \right)\ ] + 0\left(r^{s+1}\right)$$

$$\tau_{r\theta} = r^{s-1}B_2(z)G\left[2s\left(\overline{A}_1 \cos(s+1)\theta - \overline{A}_2 \sin(s+1)\theta\right) + \right.$$

$$\left(\overline{\overline{A}}_1 \cos(s-1)\theta - \overline{\overline{A}}_2 \sin(s-1)\theta\right)(s-1)(b_{s-1} - a_{s-1}) \;] + 0\left(r^{s+1}\right)$$

$$\tau_{\theta z} = r^{s-2} B_3(z) G(s-1) c_{s-1}\left(\overline{\overline{A}}_1 \cos(s-1)\theta - \overline{\overline{A}}_2 \sin(s-1)\theta\right) + \left(r^s\right)$$

$$\tau_{rz} = r^{s-2} B_3(z) G(s-1) c_{s-1}\left(\overline{\overline{A}}_1 \sin(s-1)\theta + \overline{\overline{A}}_2 \cos(s-1)\theta\right) + \left(r^s\right)$$

$$\sigma_z = r^{s-1} B_2(z)\left(\overline{\overline{A}}_1 \sin(s-1)\theta + \overline{\overline{A}}_2 \cos(s-1)\theta\right)\left(-a_{s-1}\lambda(s+1) -\right.$$

$$\left. b_{s-1}\lambda(s-1) + c_{s-1}(\lambda + 2G) \;) \;] + 0\left(r^{s+1}\right), \right. \tag{2.65}$$

where

$$B_2(z) = D_3 \sin(kz) + D_4 \cos(kz) \tag{2.66}$$

$$B_3(z) = k^{-1}(\; -D_3 \cos(kz) + D_4 \sin(kz) \;) \tag{2.67}$$

$$D_3 = -(ik)^{s-1} k\overline{D}_1 = \frac{i\left(ik2^{-1}\right)^s}{\Gamma(s+1)}\overline{\overline{D}}_1$$

$$D_4 = (ik)^s \overline{D}_2 = \frac{\left(ik2^{-1}\right)^s}{\Gamma(s+1)}\overline{\overline{D}}_2.$$

The transverse normal stress, σ_z vanishes over the plate surface ($z = \pm h$), which can be satisfied if $B_2(\pm h)$ is equal to zero. This condition, however, results in the vanishing of all the singular stresses in the vicinity of corner point at the wedge front on the plate surface — a result unacceptable on physical grounds. The only physical alternative is then that the coefficient of σ_z must be forced to vanish as shown below:

$$a_{s-1}\lambda(s+1) + b_{s-1}\lambda(s-1) - c_{s-1}(\lambda + 2G) = 0. \tag{2.68}$$

It is noteworthy that equation (2.68) is a homogeneous algebraic equation in terms of three unknown constant coefficients. Additionally, substitution of (s-1) for s in equation (2.15), yields the second homogeneous algebraic equation as written below:

$$a_{s-1}\left[(\lambda+G)s+(\lambda+3G)\right]+b_{s-1}\left[(\lambda+G)s-(\lambda+3G)\right]=(\lambda+G)c_{s-1}. \tag{2.69}$$

Combining (2.68) and (2.69), two of the three unknown coefficients can be expressed in term of the third as shown below:

$$a_{s-1}=\frac{(3-2\nu)-s}{(3-2\nu)+s}b_{s-1}$$

$$c_{s-1}=\frac{4\nu s}{(3-2\nu)+s}b_{s-1}. \tag{2.70}$$

For the boundary condition of free plate surface, τ_{rz} and $\tau_{\theta z}$ must also be equal to zero. The singular stresses on the surface of a wedge under in-plane extension can be obtained, if

$$B_2(z)=B_{2s}(z)=D_4\cos(kz) \tag{2.71}$$

$$B_3(z)=B_{3a}(z)=k^{-1}D_4\sin(kz), \tag{2.72}$$

which, in conjunction with the free plate surface condition, yields

$$B_{3a}(\pm h)=k^{-1}D_4\sin(\pm kh)=0;$$

which, in turn, leads to

$$k=\frac{\pi i}{h}. \qquad i=0,\pm1,\pm2,\cdots\cdots$$

Substitution of the expression of k into equation (2.71) yields

$$B_{2s}(\pm h) = \sum_{i=0}^{\pm\infty} D_{4i} \cos(\pi i) \neq 0. \tag{2.73}$$

In the same way, the singular stresses of out-of-bending on the plate surface can be obtained if

$$B_{3s}(\pm h) = -k^{-1} D_3 \cos(\pm kh) = 0,$$

which, in turn, leads to

$$k = \frac{2i+1}{2h}\pi. \qquad i = 0, \pm 1, \pm 2, \cdots\cdots$$

$B_{2a}(\pm h)$ can be obtained as follows:

$$B_{2a}(\pm h) = \pm \sum_{i=0}^{\pm\infty} D_{3i} \sin\frac{(2i+1)}{2}\pi \neq 0. \tag{2.74}$$

The fields of displacements and stresses on the surface are in the form

$$U_r = \frac{r^s}{2Gs} B_1(\pm h)\left[\left(A_1 \sin(s+1)\theta + A_2 \cos(s+1)\theta\right) + (s - 3 + 2\nu)\right.$$

$$\left.\left(A_3 \sin(s-1)\theta + A_4 \cos(s-1)\theta\right)\right] \tag{2.75}$$

$$U_\theta = \frac{r^s}{2Gs} B_1(\pm h)\left[\left(A_1 \cos(s+1)\theta - A_2 \sin(s+1)\theta\right) + (s + 3 - 2\nu)\right.$$

$$\left.\left(A_3 \cos(s-1)\theta - A_4 \sin(s-1)\theta\right)\right] \tag{2.76}$$

$$\sigma_r = r^{s-1}B_1(\pm h)\Big[\big(A_1\sin(s+1)\theta + A_2\cos(s+1)\theta\big) + (s-3-2\nu)$$

$$\big(A_3\sin(s-1)\theta + A_4\cos(s-1)\theta\big)\Big] \qquad (2.77)$$

$$\sigma_\theta = -r^{s-1}B_1(\pm h)\Big[\big(A_1\sin(s+1)\theta + A_2\cos(s+1)\theta\big) + (s+1+2\nu)$$

$$\big(A_3\sin(s-1)\theta + A_4\cos(s-1)\theta\big)\Big] \qquad (2.78)$$

$$\tau_{r\theta} = r^{s-1}B_1(\pm h)\Big[\big(A_1\cos(s+1)\theta - A_2\sin(s+1)\theta\big) + (s-1)$$

$$\big(A_3\cos(s-1)\theta - A_4\sin(s-1)\theta\big)\Big] \qquad (2.79)$$

$$U_z = 0\big(r^{s+1}\big), \qquad \sigma_z = 0\big(r^{s+1}\big), \qquad \tau_{rz} = 0\big(r^s\big), \qquad \tau_{\theta z} = 0\big(r^s\big),$$

where

$$\overline{A}_{1,2} = \frac{A_{1,2}}{2Gs}$$

$$\overline{\overline{A}}_{3,4} = \frac{(3-2\nu)+s}{2Gsb_{s-1}}A_{3,4}.$$

The eigenvalue, s, can be determined by the boundary condition on the wedge side surfaces.

2.4.1 Clamped-Clamped

The equation of root is

$$\sin(2s\theta_0) = \pm \frac{s}{(3-2\nu)} \sin(2\theta_0), \tag{2.80}$$

when $\theta_0 = \pm\pi/2$, $s = 1$, $\theta_0 = \pm\pi$, $s = 1/2$

2.4.2 Clamped-Free

The equation of root is

$$\cos(4s\theta_0) = \frac{1}{D_2}\left[2\left(2s^2 + 2\nu(s-1) - (3-2\nu)^2\right) - D_1\cos(4\theta_0)\right], \tag{2.81}$$

where

$$D_1 = 4s(s+\nu), \qquad D_2 = 4(3-2\nu)(1+\nu);$$

when $\theta_0 = \pm\pi$, equation (2.82) has two roots contributing to singular stresses:

$$s = \lambda_1 + i\lambda_2$$

a. $$\lambda_1 = \frac{1}{4}, \qquad \lambda_2 = \pm\frac{1}{4\pi}\cosh^{-1}\left(\frac{5-5\nu+2\nu^2}{(1+\nu)(3-2\nu)}\right)$$

b. $$\lambda_1 = \frac{3}{4}, \qquad \lambda_2 = \pm\frac{1}{4\pi}\cosh^{-1}\left(\frac{5-5\nu+2\nu^2}{(1+\nu)(3-2\nu)}\right).$$

2.4.3 Free-Free

The equation of root is

$$\sin(2s\theta_0) = \pm\frac{s+\nu}{1+\nu}\sin(2\theta_0). \tag{2.82}$$

when $\theta_0 = \pm\pi/2$, s= 1, $\theta_0 = \pm\pi$, s= 1/2. The stress distribution in the vicinity of a semiinfinite crack ($\theta_0 = \pm\pi$) front, i. e., r<<1, and for the case of free-free edge, can be expressed as follows:

$$\sigma_r = \frac{K_I}{\sqrt{2\pi r}}\left(-\frac{1}{4+4\nu}\cos\left(\frac{3\theta}{2}\right)+\frac{5+4\nu}{4+4\nu}\cos\left(\frac{\theta}{2}\right)\right)+\frac{K_{II}}{\sqrt{2\pi r}}\left(\frac{3+4\nu}{4+4\nu}\sin\left(\frac{3\theta}{2}\right)-\frac{5+4\nu}{4+4\nu}\sin\left(\frac{\theta}{2}\right)\right)$$

$$\sigma_\theta = \frac{K_I}{\sqrt{2\pi r}}\left(\frac{1}{4+4\nu}\cos\left(\frac{3\theta}{2}\right)+\frac{3+4\nu}{4+4\nu}\cos\left(\frac{\theta}{2}\right)\right)-\frac{K_{II}}{\sqrt{2\pi r}}\left(\frac{3+4\nu}{4+4\nu}\right)\left(\sin\left(\frac{3\theta}{2}\right)+\sin\left(\frac{\theta}{2}\right)\right)$$

$$\tau_{r\theta} = \frac{K_I}{\sqrt{2\pi r}}\frac{1}{4+4\nu}\left(\sin\left(\frac{3\theta}{2}\right)+\sin\left(\frac{\theta}{2}\right)\right)+\frac{K_{II}}{\sqrt{2\pi r}}\left(\frac{3+4\nu}{4+4\nu}\cos\left(\frac{3\theta}{2}\right)+\frac{1}{4+4\nu}\cos\left(\frac{\theta}{2}\right)\right), \tag{2.83}$$

$$U_r = -\frac{K_I}{G}\sqrt{\frac{r}{2\pi}}\left(\frac{1}{4+4\nu}\cos\left(\frac{3}{2}\theta\right)+\frac{-5+4\nu}{4+4\nu}\cos\left(\frac{\theta}{2}\right)\right)+$$

$$\frac{K_{II}}{G}\sqrt{\frac{r}{2\pi}}\left(\frac{3+4\nu}{4+4\nu}\sin\left(\frac{3}{2}\theta\right)+\frac{-5+4\nu}{4+4\nu}\sin\left(\frac{\theta}{2}\right)\right)$$

$$U_\theta = \frac{K_I}{G}\sqrt{\frac{r}{2\pi}}\left(\frac{1}{4+4\nu}\sin\left(\frac{3}{2}\theta\right)+\frac{-7+4\nu}{4+4\nu}\sin\left(\frac{\theta}{2}\right)\right)+$$

$$\frac{K_{II}}{G}\sqrt{\frac{r}{2\pi}}\left(\frac{3+4\nu}{4+4\nu}\cos\left(\frac{3\theta}{2}\right)+\frac{-7+4\nu}{4+4\nu}\cos\left(\frac{\theta}{2}\right)\right); \tag{2.84}$$

where

$$K_I = K_{Is} + K_{Ia} = -2\sqrt{2\pi}(1+\nu)A_4\left(B_{2s}(\pm h) + B_{2a}(\pm h)\right) \tag{2.85}$$

$$K_{II} = K_{IIs} + K_{IIa} = -2\sqrt{2\pi}(1+\nu)A_3\left(B_{2s}(\pm h) + B_{2a}(\pm h)\right). \tag{2.86}$$

where K_{Is} and K_{IIs} are symmetric stress intensity factors, which correspond to the problem of in-plane extension. On the other hand, K_{Ia} and K_{IIa} are antisymmetric stress intensity factors belonging to the out-of-plane bending problem.

2.5 Numerical Results and Discussions

In what follows, numerical results pertaining to three dimensional stress fields in the vicinity of the surface corner region at the front of a homogeneous wedge subjected to three different wedge-side boundary conditions. Additionally, comparisons of these results with their two-dimensional approximate (i.e., plane stress) counterparts are also presented.

2.5.1 Clamped-Clamped

Figure 2.2 shows the comparisons of the variation of the lowest eigenvalue computed for four different conditions — (i) antiplane shear loading, (ii) interior region under bending/extension, (iii) surface region under bending/extension and (iv) two-dimensional (plane stress) condition under bending/extension — with respect to the included angle, θ_0, with ν=0.3. It is interesting to observe that the lowest eigenvalue for the interior region is the smallest in the entire range of the included angle beyond the case of a half-space ($\theta_0 = \pm 90^o$), implying thereby the most severe stress singularity in the vicinity of the wedge front, whereas its antiplane shear counterpart is the largest. Among the remaining two cases, the eigenvalue for the two-dimensional (plane stress) approximation is slightly larger than that of the surface region. It is further noteworthy that the case of antiplane shear loading has only one eigenvalue, which is independent of the Poisson's ratio, whereas exactly the reverse order is true in the case of the second eigenvalue (shown in Figure 2.3 for ν=0.3) for the three remaining conditions. The smallest second eigenvalue is given for the surface region computed using the three-dimensional analysis, while its counterpart for the interior region yields the largest eigenvalue. Furthermore, for the case of the antisymmetric loading (θ direction) acting alone, the first eigenvalue

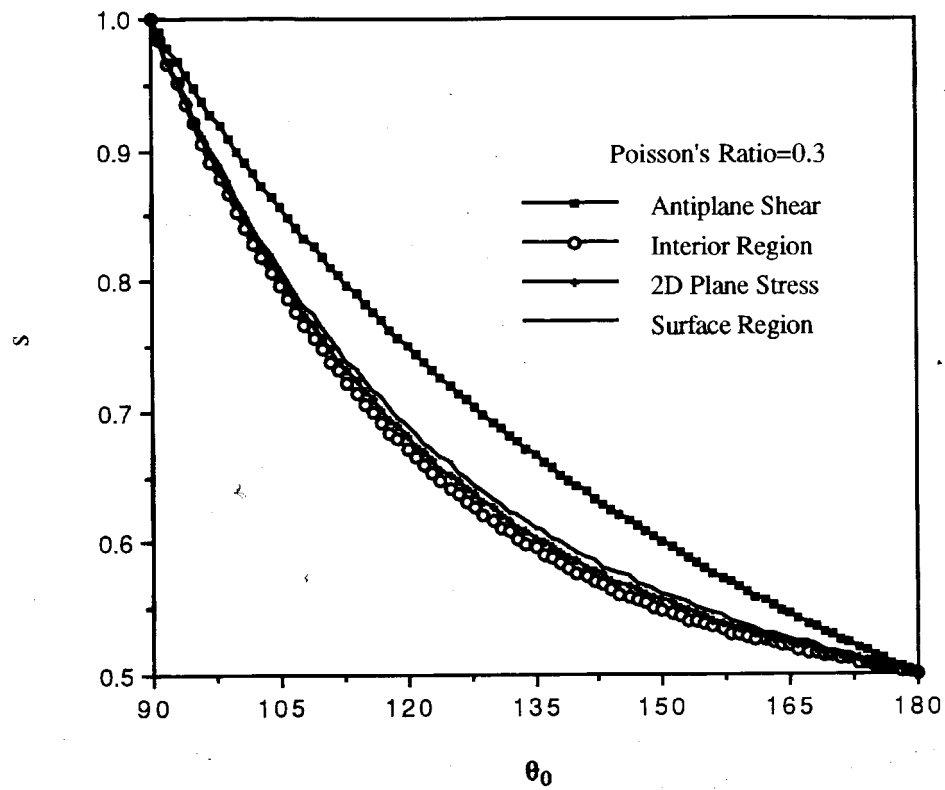

Figure 2.2 Variation of the lowest eigenvalue with respect to wedge angle, for a clamped-clamped wedge with ν=0.3.

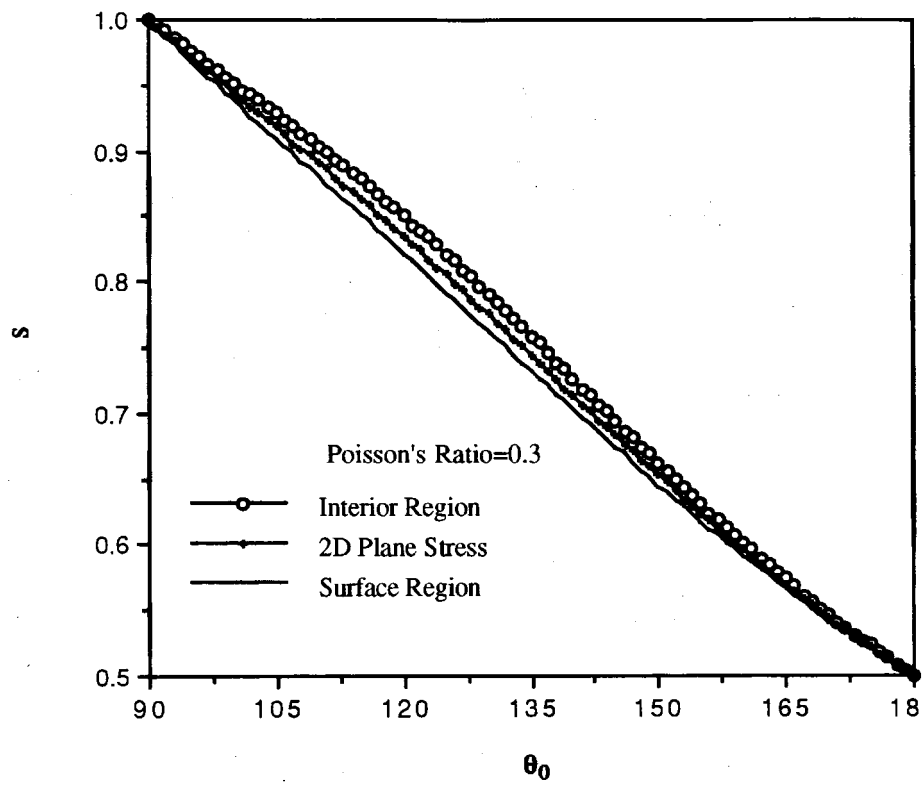

Figure 2.3 Variation of the second eigenvalue with respect to wedge angle, for a clamped-clamped wedge with ν=0.3.

disappears leaving the second eigenvalue to be the only one to produce a singular stress field.

Comparisons of the variation of the lowest and second eigenvalues, computed for the aforementioned four cases for a homogeneous wedge with Poisson's ratio, ν=0.5, with respect to the included angle, θ_0 , are displayed in Figures 2.4 and 2.5. Trends similar to those for ν=0.3 are observed here, the only exception being that the second eigenvalue for the interior region does not begin at $\theta_0 = \pm 90^0$, but at $\pm 129^0$. It is further interesting to observe from inspection of Figures 2.2 - 2.5 that the lowest eigenvalue decreases, while the second eigenvalue increases with the increase of Poisson's ratio for all the conditions under consideration except for antiplane shear loading. Furthermore, the lowest eigenvalue computed from the two-dimensional (plane stress) condition is closest to that for the case of surface region among all the cases.

2.5.2 Free-Clamped

Figure 2.6 shows the comparisons of the variation of the lowest real part of the eigenvalue computed for the aforementioned four different conditions with respect to the included angle, θ_0, with ν=0.3. It is interesting to observe that the lowest real part of the eigenvalue for the interior region is the smallest for the included angle ranging from $\pm 27^0$ to $\pm 65^0$, implying thereby the most severe stress singularity in the vicinity of the wedge front, whereas its antiplane shear counterpart is the largest in this range. The lowest real part of the eigenvalue in the range of the angle, $\theta_0 = \pm 75^0 - \pm 180^0$, for all the four cases are almost the same. It is further interesting to observe that unlike the case of clamped-clamped boundary condition, the lowest real part of the eigenvalue yielding singular stresses, commences at an angle, θ_{0crit}, smaller than $\pm 90^0$. The computed θ_{0crit} depends on the loading condition, and the Poisson's ratio, e. g., $\theta_{0crit} = \pm 45^0, \pm 28.2^0, \pm 31^0, \pm 31.2^0$ for the (i) antiplane shear loading condition, (ii) interior region computed using the present three-dimensional analysis, (iii) the two-dimensional (plane stress) approximation, and

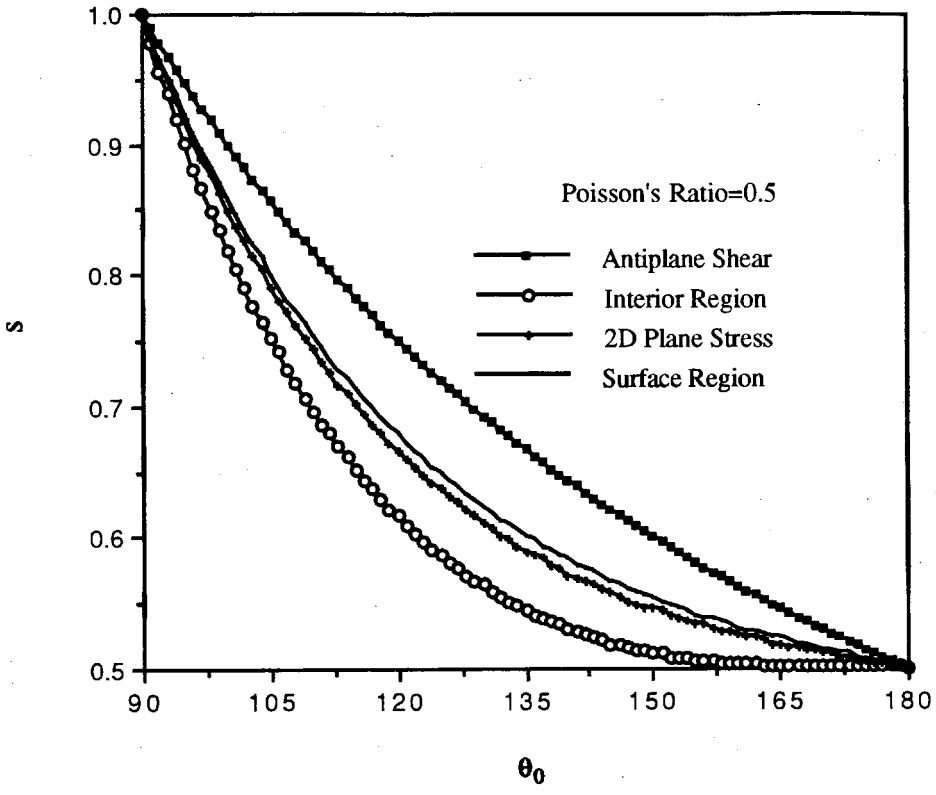

Figure 2.4 Variation of the lowest eigenvalue with respect to wedge angle, for a clamped-clamped wedge with ν=0.5.

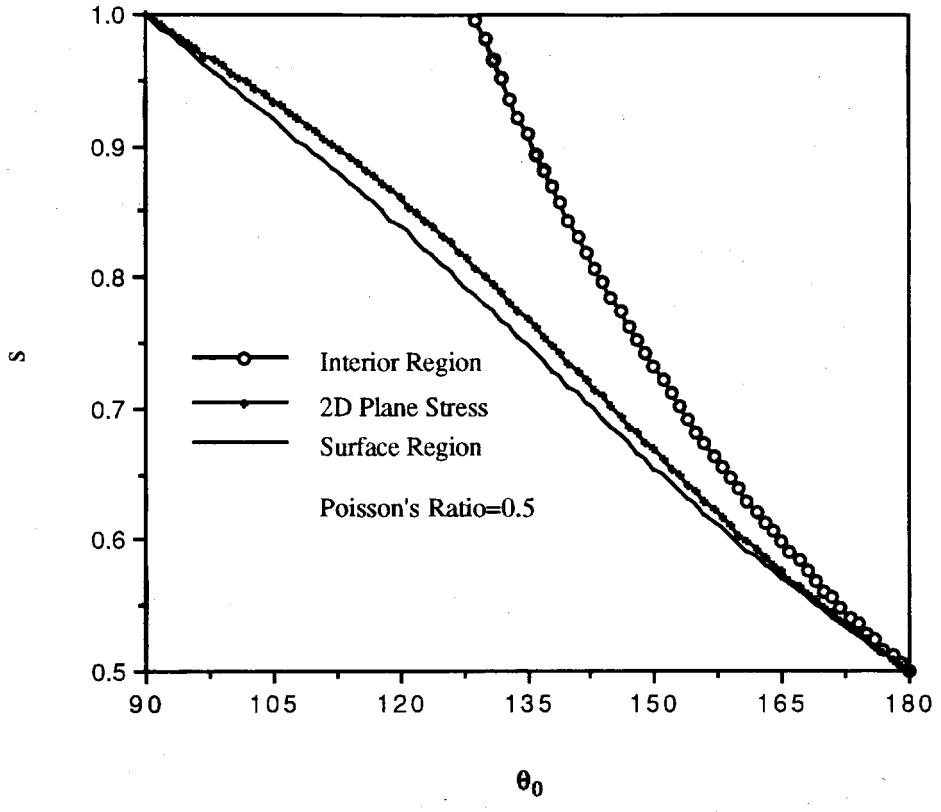

Figure 2.5 Variation of the second eigenvalue with respect to wedge angle, for a clamped-clamped wedge with ν=0.5.

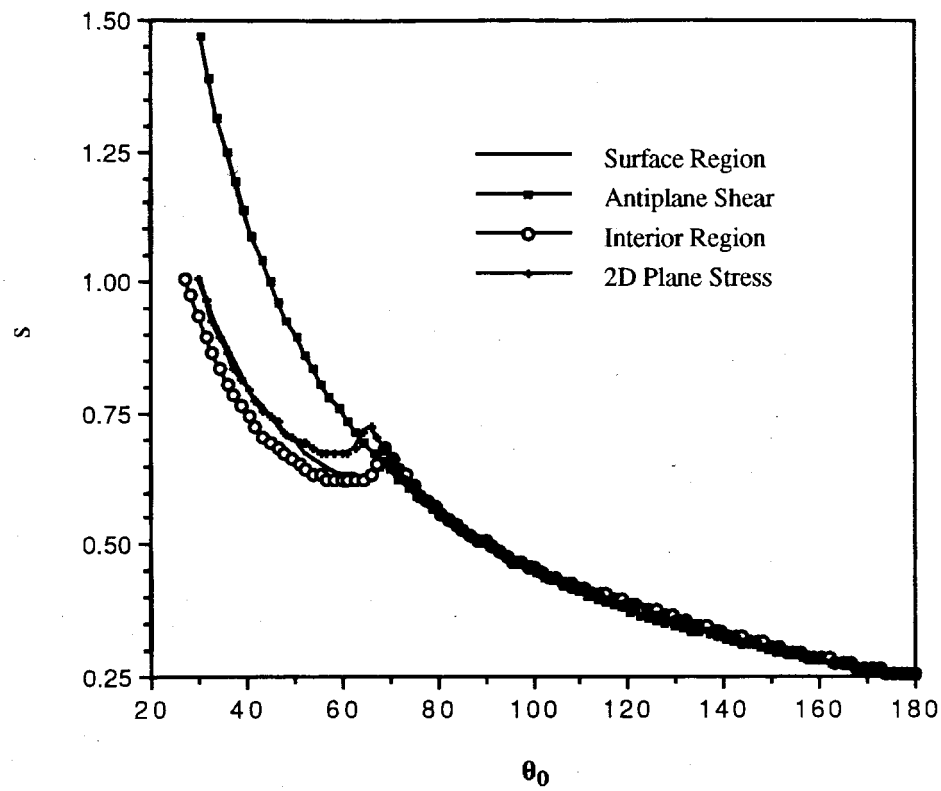

Figure 2.6 Variation of the lowest eigenvalue with respect to wedge angle, for a free-clamped wedge with ν=0.3.

(iv) surface region computed using the present three-dimensional analysis, respectively. It is interesting to notice from Figure 2.7 that unlike the case of clamped-clamped and free-free (see below) boundary conditions, the eigenvalue yielding singular stresses consists of real and imaginary parts for a certain range of the included angle, It is further noteworthy that the occurrence of the nonvanishing imaginary part starting at $\theta_0 = \pm 69^0$ is accompanied by the appearance of a clearly visible cusp in the real part at the same θ_0. Furthermore, the lowest eigenvalue decreases monotonically with the increase of included angle, θ_0, for the antiplane shear loading condition, because the computed eigenvalue is always real. For the remaining three cases, this monotonicity of the real part is disturbed by the appearance of the imaginary part.

Comparisons of the variation of the lowest real part of the eigenvalue computed for the aforementioned four different conditions are plotted in Figure 2.8 with ν=0.5. For the included angle, θ_0, ranging from $\pm 22.05^0$ to $\pm 63^0$, the lowest real part of the eigenvalue for the interior region is the smallest, whereas its antiplane shear counterpart is the largest in this range, and is also independent of the Poisson's ratio. For the angle ranging from $\pm 63^0$ to $\pm 180^0$, the lowest real part of the eigenvalue is on the surface region. The computed values of θ_{0crit} are $\pm 45^0$, $\pm 23^0$, $\pm 26.75^0$, $\pm 27^0$ for the (i) antiplane shear loading condition, (ii) interior region computed using the present three-dimensional analysis, (iii) the two-dimensional (plane stress) approximation, and (iv) surface region using the present three-dimensional analysis, respectively. Like the clamped-clamped edge, the lowest real part of the eigenvalue decreases with the increase of Poisson's ratio for all the conditions under consideration except for antiplane shear loading. The lowest real part of the eigenvalue computed from two-dimensional (plane stress) condition, like clamped-clamped boundary condition, is closest to that of surface region among all the cases.

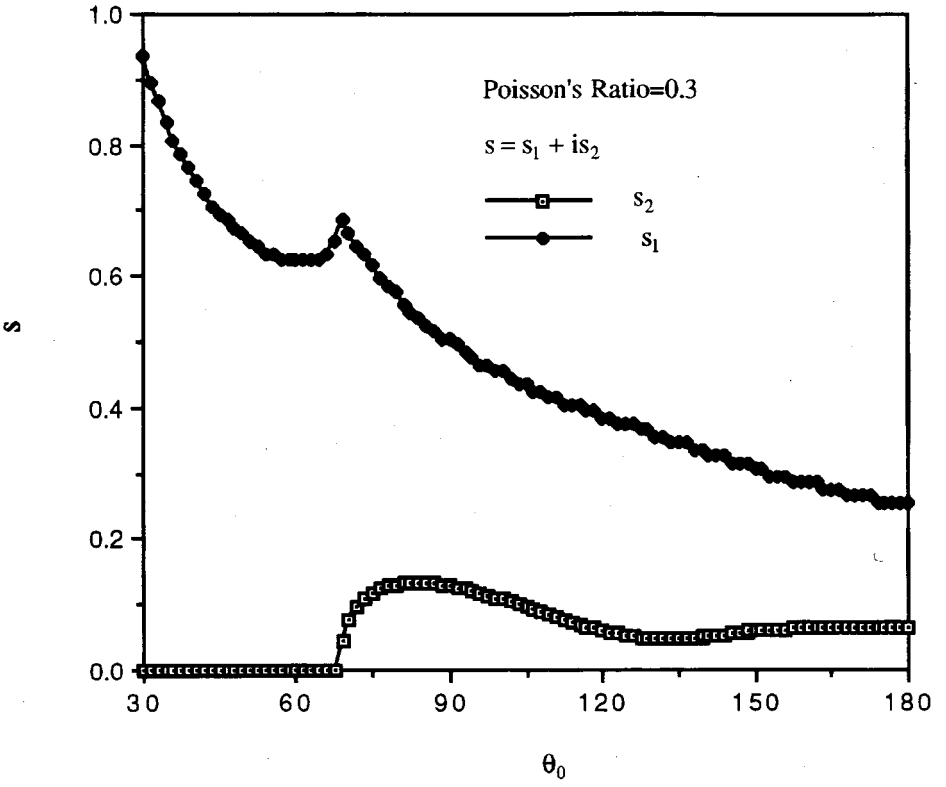

Figure 2.7 Variation of the imaginary and the lowest real parts of the eigenvalue in the interior region of a clamped-clamped wedge with respect to wedge angle.

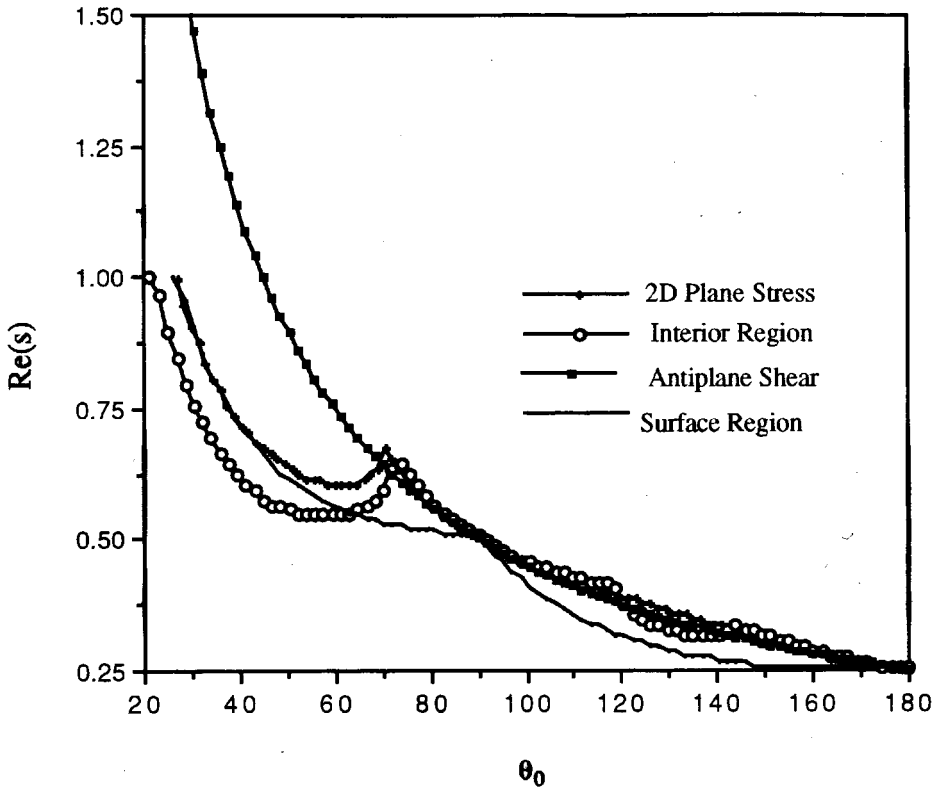

Figure 2.8 Variation of the lowest eigenvalue with respect to wedge angle, for a free-clamped wedge with ν=0.5.

2.5.3 Free-Free

Due to the lack of displacement boundary condition, the deformable body is not fixed in space. This causes occurrence of the rigid body mode eigenvalue on the surface region for free-free edge (see Figure 2.9). This eigenvalue has no physical meaning in regards to the singular stress field in the vicinity of the wedge front. Only those eigenvalues that yield physically meaningfull singular stress fields are discussed below.

The lowest eigenvalue computed for the aforementioned four different conditions with ν=0.3 is shown in Figure 2.10. As in the case of the other two boundary conditions discussed above, the eigenvalue for antiplane shear loading is independent of Poisson's ratio. The eigenvalue for two-dimensional (plane stress) condition is the same as its interior region counterpart, and is, as expected, independent of Poisson's ratio. The lowest eigenvalue for the surface region is the smallest in the entire range of the included angle beyond the case of a half space ($\theta_0 = \pm 90^o$). It implies that the most severe stress singularity occurs in the vicinity of the surface corner point at the wedge front, whereas its antiplane shear counterpart, which is the largest, causes the least severe stress singularity. It is further noteworthy that s=0.5, corresponding to $\theta_0=\pm 180^0$ (i.e., the case of a semi-infinite crack) is not the smallest eigenvalue for the surface region, which is contrary to what has been observed in the case of the clamped-clamped boundary condition discussed above. The smallest eigenvalue, s=0.492, occurs at $\theta_0=\pm 157.5^0$. The variation of the second eigenvalue with respect to the included angle, θ_0, is shown in Figure 2.11 for ν=0.3. The second eigenvalue, in contrast to the case of the lowest eigenvalue, computed for the interior region is smaller than its surface counterpart. It is also contrary to the results for the clamped-clamped boundary condition. It is further interesting to observe that the second eigenvalue yielding singular stresses, commences at an included angle, θ_{0crit}, larger than 180^0— the computed values of θ_{0crit} are $\pm 128.5^0$, $\pm 129^0$ for the (i) interior region, and (ii) surface region, respectively.

Comparisons of the variation of the lowest and second eigenvalues, for three

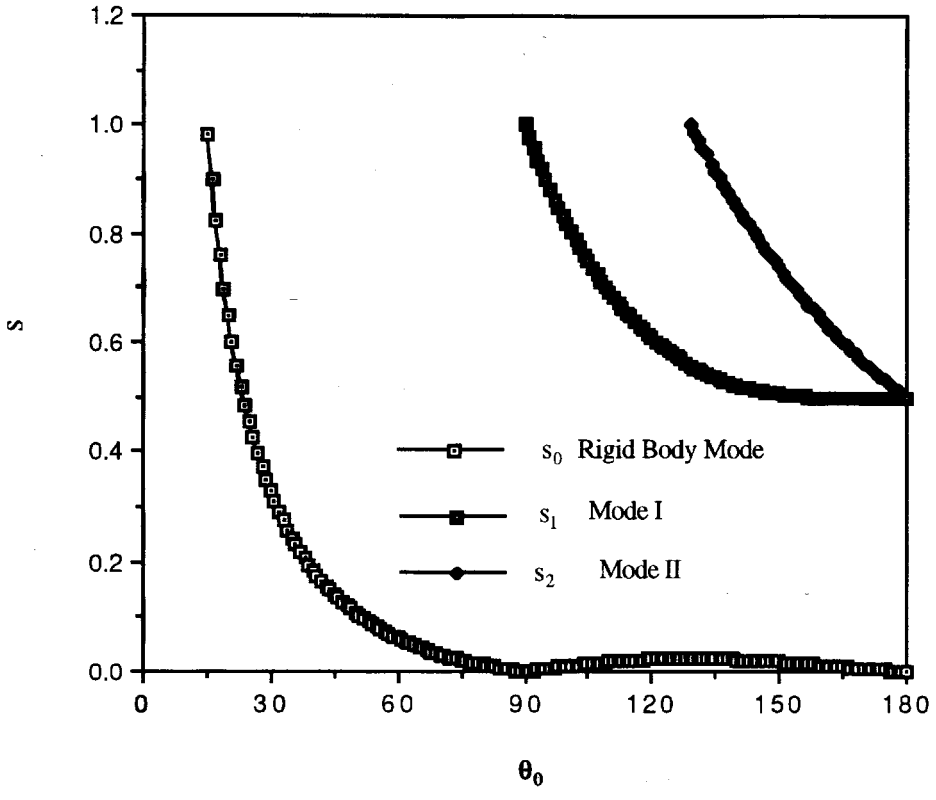

Figure 2.9 Variation of eigenvalues corresponding to rigid body Mode, Mode I & Mode II for free-free wedge with ν=0.1.

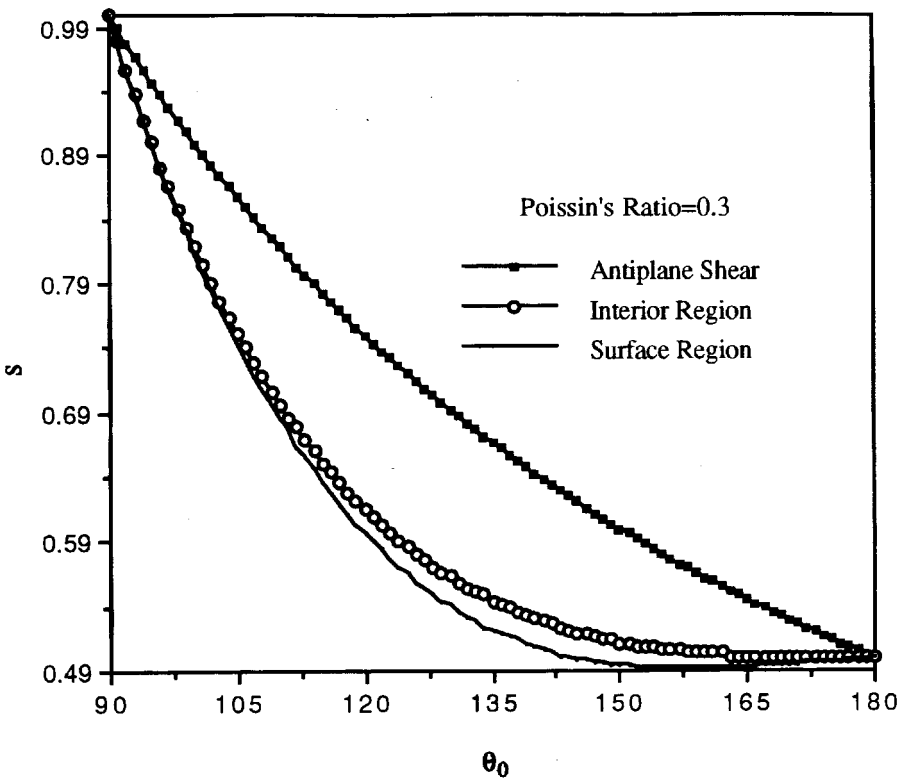

Figure 2.10 Variation of the lowest eigenvalue with respect to wedge angle, for a free-free wedge with ν=0.3.

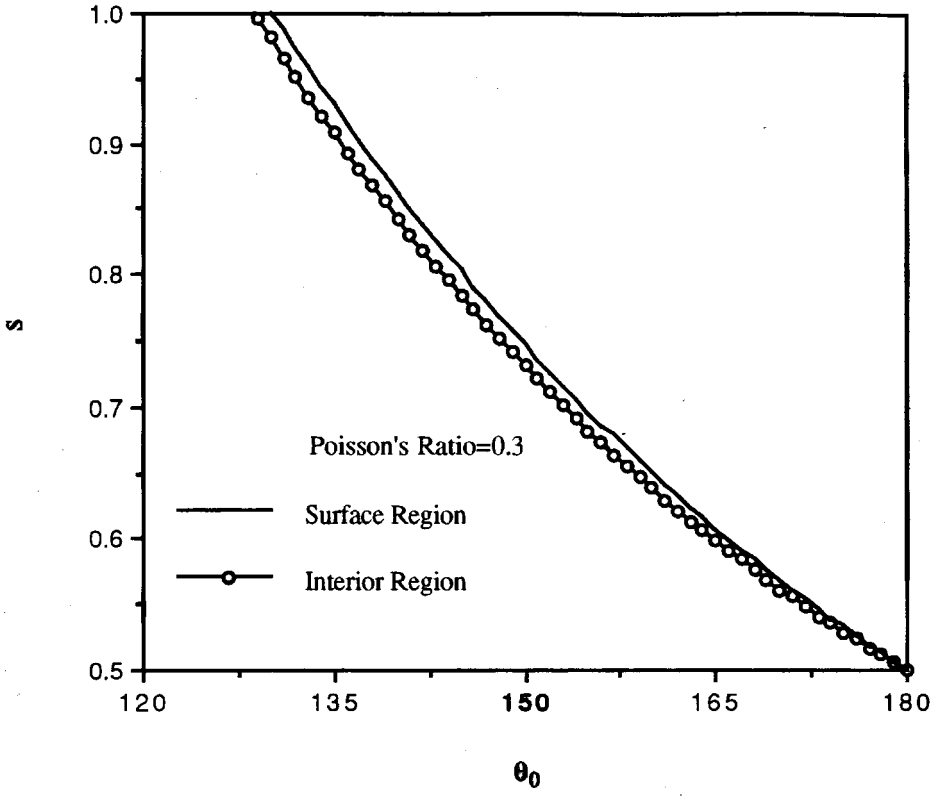

Figure 2.11 Variation of the second eigenvalue with respect to wedge angle, for a free-free wedge with ν=0.3.

conditions — (i) interior region, (ii) surface region and (iii) antiplane shear — with Poisson's ratio, ν=0.5, with respect to the included angle, θ_0 , are displayed in Figures. 2.12 and 2.13. Trends similar to those for ν=0.3 are also observed here. It is further interesting to observe from inspection of Figures 2.10 - 2.13 that, on the surface region, the lowest eigenvalue decreases, whereas the second eigenvalue increases with the increase of Poisson's ratio.

2.6 General Stress Intensity Factors and the General Singular Stresses Fields

It is quite clear that a semiinfinite crack is only a particular case of an infinite wedge. The concept of stress intensity factors prevalent in LEFM (Linear Elastic Fracture Mechanics) is, therefore, not only limited to the problem of a crack, but can easily be extended to a general reentrant wedge or a notch. The general stress intensity factors for such a reentrant wedge are therefore defined in a manner similar to their counterparts for a semiinfinite crack as follows:

$$K_I = \lim_{r\to 0} \sqrt{2\pi} r^{-s_1+1} \sigma_\theta(r,0)$$

$$K_{II} = \lim_{r\to 0} \sqrt{2\pi} r^{-s_2+1} \tau_{r\theta}(r,0)$$

$$K_{III} = \lim_{r\to 0} \sqrt{2\pi} r^{-s_3+1} \tau_{Z\theta}(r,0). \qquad (2.87)$$

The following three specific cases are considered:

2.6.1 Interior Region

The general asymptotic singular stress fields in the vicinity of wedge front and valid in the interior region of a wedge under extension and bending are expressed in the following forms

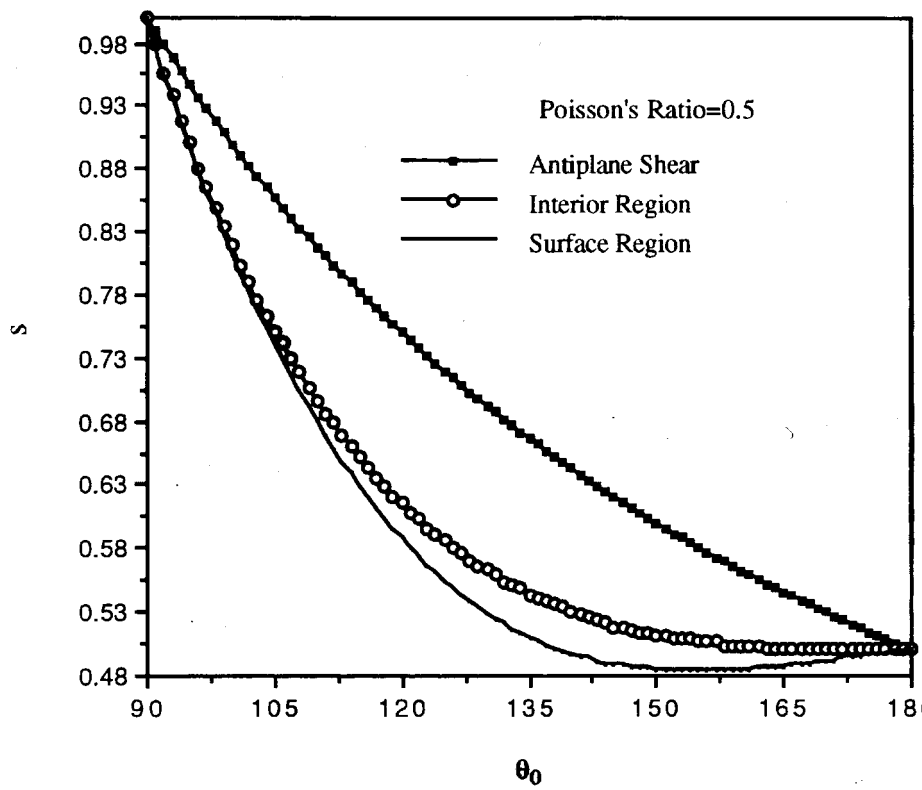

Figure 2.12 Variation of the lowest eigenvalue with respect to wedge angle, for a free-free wedge with ν=0.5.

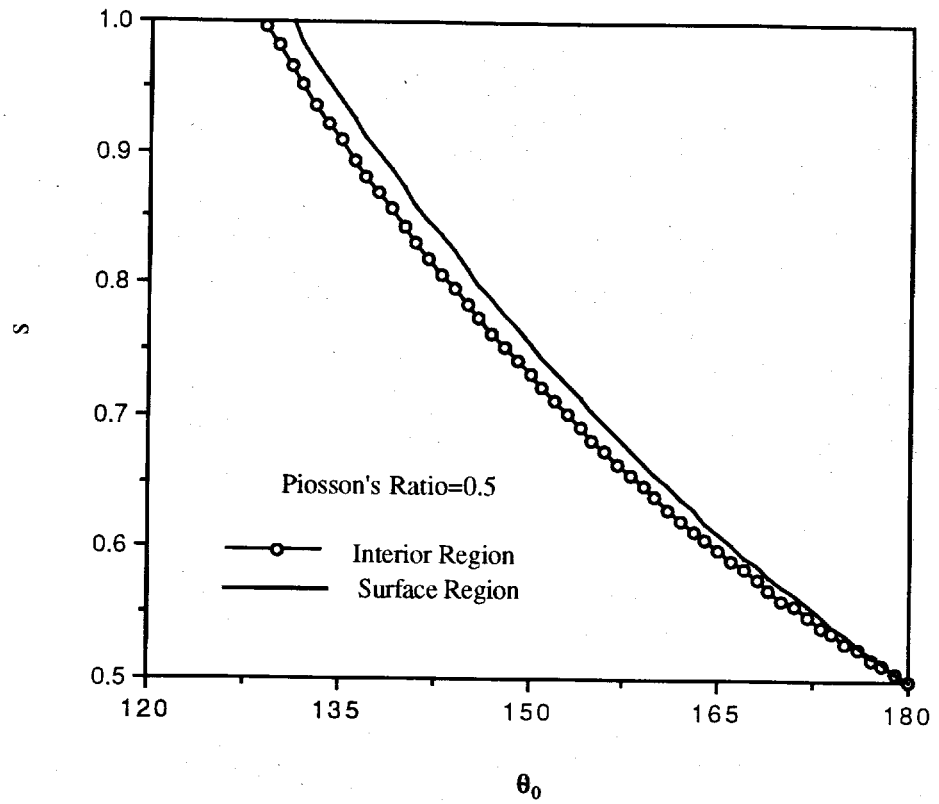

Figure 2.13 Variation of the second eigenvalue with respect to wedge angle, for a free-free wedge with ν=0.5.

$$\sigma_r = \frac{r^{s_1-1}K_I}{\sqrt{2\pi}}\left(\frac{(s_1-1)\sin(s_1-1)\theta_0\cos(s_1+1)\theta}{-(s_1-1)\sin(s_1-1)\theta_0+(s_1+1)\sin(s_1+1)\theta_0}-\frac{(s_1-3)\sin(s_1+1)\theta_0\cos(s_1-1)\theta}{-(s_1-1)\sin(s_1-1)\theta_0+(s_1+1)\sin(s_1+1)\theta_0}\right)$$

$$\sigma_\theta = \frac{r^{s_1-1}K_I}{\sqrt{2\pi}}\left(\frac{-(s_1-1)\sin(s_1-1)\theta_0\cos(s_1+1)\theta}{-(s_1-1)\sin(s_1-1)\theta_0+(s_1+1)\sin(s_1+1)\theta_0}+\frac{(s_1+1)\sin(s_1+1)\theta_0\cos(s_1-1)\theta}{-(s_1-1)\sin(s_1-1)\theta_0+(s_1+1)\sin(s_1+1)\theta_0}\right)$$

$$\tau_{r\theta} = \frac{r^{s_1-1}K_I}{\sqrt{2\pi}}\left(\frac{-(s_1-1)\sin(s_1-1)\theta_0\sin(s_1+1)\theta}{-(s_1-1)\sin(s_1-1)\theta_0+(s_1+1)\sin(s_1+1)\theta_0}+\frac{(s_1-1)\sin(s_1+1)\theta_0\sin(s_1-1)\theta}{-(s_1-1)\sin(s_1-1)\theta_0+(s_1+1)\sin(s_1+1)\theta_0}\right)$$

(2.88)

$$\sigma_r = \frac{r^{s_2-1}K_{II}}{\sqrt{2\pi}}\left(\frac{-(s_2+1)\sin(s_2-1)\theta_0\sin(s_2+1)\theta}{(s_2-1)\sin(s_2+1)\theta_0-(s_2+1)\sin(s_2-1)\theta_0}+\frac{(s_2-3)\sin(s_2+1)\theta_0\sin(s_2-1)\theta}{(s_2-1)\sin(s_2+1)\theta_0-(s_2+1)\sin(s_2-1)\theta_0}\right)$$

$$\sigma_\theta = \frac{r^{s_2-1}K_{II}}{\sqrt{2\pi}}\left(\frac{(s_2+1)\sin(s_2-1)\theta_0\sin(s_2+1)\theta}{(s_2-1)\sin(s_2+1)\theta_0-(s_2+1)\sin(s_2-1)\theta_0}-\frac{(s_2+1)\sin(s_2+1)\theta_0\sin(s_2-1)\theta}{(s_2-1)\sin(s_2+1)\theta_0-(s_2+1)\sin(s_2-1)\theta_0}\right)$$

$$\tau_{\theta r} = \frac{r^{s_2-1}K_{II}}{\sqrt{2\pi}}\left(\frac{-(s_2+1)\sin(s_2-1)\theta_0\cos(s_2+1)\theta}{(s_2-1)\sin(s_2+1)\theta_0-(s_2+1)\sin(s_2-1)\theta_0}+\frac{(s_2-1)\sin(s_2+1)\theta_0\cos(s_2-1)\theta}{(s_2-1)\sin(s_2+1)\theta_0-(s_2+1)\sin(s_2-1)\theta_0}\right),$$

(2.89)

where

$$K_I = \sqrt{2\pi}\left(\frac{(s_1-1)\sin(s_1-1)\theta_0-(s_1+1)\sin(s_1+1)\theta_0}{\sin(s_1+1)\theta_0}\right)A_4B_1(z) \tag{2.90}$$

$$K_{II} = \sqrt{2\pi}\left(\frac{(s_2-1)\sin(s_2+1)\theta_0-(s_2+1)\sin(s_2-1)\theta_0}{\sin(s_2+1)\theta_0}\right)A_3B_1(z). \tag{2.91}$$

Substitution of $\theta_0=\pm\pi$ into equations (2.88 - 2.91) reduce them to their semiinfinite crack counterparts, given by equations (2.57, 2.59).

2.6.2 Surface Corner Region

The general singular stress fields in the vicinity of the surface corner region at the wedge front are in the forms:

$$\sigma_r = \frac{r^{s_1-1}K_I}{\sqrt{2\pi}}\left(\frac{(s_1-1)\sin(s_1-1)\theta_0 \cos(s_1+1)\theta}{-(s_1-1)\sin(s_1-1)\theta_0 + (s_1+1+2\nu)\sin(s_1+1)\theta_0} \right.$$

$$\left. - \frac{(s_1-3-2\nu)\sin(s_1+1)\theta_0 \cos(s_1-1)\theta}{-(s_1-1)\sin(s_1-1)\theta_0 + (s_1+1+2\nu)\sin(s_1+1)\theta_0} \right)$$

$$\sigma_\theta = \frac{r^{s_1-1}K_I}{\sqrt{2\pi}}\left(\frac{-(s_1-1)\sin(s_1-1)\theta_0 \cos(s_1+1)\theta}{-(s_1-1)\sin(s_1-1)\theta_0 + (s_1+1+2\nu)\sin(s_1+1)\theta_0} \right.$$

$$\left. + \frac{(s_1+1+2\nu)\sin(s_1+1)\theta_0 \cos(s_1-1)\theta}{-(s_1-1)\sin(s_1-1)\theta_0 + (s_1+1+2\nu)\sin(s_1+1)\theta_0} \right)$$

$$\tau_{r\theta} = \frac{r^{s_1-1}K_I}{\sqrt{2\pi}}\left(\frac{-(s_1-1)\sin(s_1-1)\theta_0 \sin(s_1+1)\theta}{-(s_1-1)\sin(s_1-1)\theta_0 + (s_1+1+2\nu)\sin(s_1+1)\theta_0} \right.$$

$$\left. + \frac{(s_1-1)\sin(s_1+1)\theta_0 \sin(s_1-1)\theta}{-(s_1-1)\sin(s_1-1)\theta_0 + (s_1+1+2\nu)\sin(s_1+1)\theta_0} \right) \qquad (2.92)$$

$$\sigma_r = \frac{r^{s_2-1}K_{II}}{\sqrt{2\pi}}\left(\frac{-(s_2+1+2\nu)\sin(s_2-1)\theta_0 \sin(s_2+1)\theta}{(s_2-1)\sin(s_2+1)\theta_0 - (s_2+1+2\nu)\sin(s_2-1)\theta_0} \right.$$

$$\left. + \frac{(s_2-3-2\nu)\sin(s_2+1)\theta_0 \sin(s_2-1)\theta}{(s_2-1)\sin(s_2+1)\theta_0 - (s_2+1+2\nu)\sin(s_2-1)\theta_0} \right)$$

$$\sigma_\theta = \frac{r^{s_2-1}K_{II}}{\sqrt{2\pi}}\left(\frac{(s_2+1+2\nu)\sin(s_2-1)\theta_0 \sin(s_2+1)\theta}{(s_2-1)\sin(s_2+1)\theta_0 - (s_2+1+2\nu)\sin(s_2-1)\theta_0} \right.$$

$$\left. - \frac{(s_2+1+2\nu)\sin(s_2+1)\theta_0 \sin(s_2-1)\theta}{(s_2-1)\sin(s_2+1)\theta_0 - (s_2+1+2\nu)\sin(s_2-1)\theta_0} \right)$$

$$\tau_{\theta r} = \frac{r^{s_2-1}K_{II}}{\sqrt{2\pi}}\left(\frac{-(s_2+1+2\nu)\sin(s_2-1)\theta_0 \cos(s_2+1)\theta}{(s_2-1)\sin(s_2+1)\theta_0 - (s_2+1+2\nu)\sin(s_2-1)\theta_0} \right.$$

$$\left. + \frac{(s_2-1)\sin(s_2+1)\theta_0 \cos(s_2-1)\theta}{(s_2-1)\sin(s_2+1)\theta_0 - (s_2+1+2\nu)\sin(s_2-1)\theta_0} \right). \tag{2.93}$$

where

$$K_I = \sqrt{2\pi}\left(\frac{(s_1-1)\sin(s_1-1)\theta_0 - (s_1+1+2\nu)\sin(s_1+1)\theta_0}{\sin(s_1+1)\theta_0} \right) A_4 B_2(\pm h) \tag{2.94}$$

$$K_{II} = \sqrt{2\pi}\left(\frac{(s_2-1)\sin(s_2+1)\theta_0 - (s_2+1+2\nu)\sin(s_2-1)\theta_0}{\sin(s_2+1)\theta_0} \right) A_3 B_2(\pm h). \tag{2.95}$$

It is worthwhile to note here that when Poisson's ratio is equal to zero, equations (2.92-2.95) reduce to their counterparts valid for the interior region and given by equations (2.88-2.91). Furthermore, the corresponding expression for a semiinfinite crack given by equation (2.83) can be recovered on substitution of $\theta_0 = \pm\pi$.

2.6.3 Antiplane Shear

The general singular stress fields in the vicinity of the front of a wedge subjected to antiplane shear loading can be written as follows:

$$\tau_{\theta z} = \frac{K_{III} r^{s_3 - 1}}{\sqrt{2\pi}} \cos(s_3 \theta)$$

$$\tau_{rz} = \frac{K_{III} r^{s_3 - 1}}{\sqrt{2\pi}} \sin(s_3 \theta), \tag{2.96}$$

where

$$K_{III} = \sqrt{2\pi} s_3 A_1 B_b(z). \tag{2.97}$$

On substitution of $\theta_0 = \pm\pi$, the corresponding expressions, given by equations (2.31) and (2.32) for a cracked plate subjected to antiplane shear loading, can be recovered.

It is interesting to report that the computed eigenvalues for a wedge satisfy the following relationship (see Figures 2.14 and 2.15),

$$s_2 \geq s_3 \geq s_1, \tag{2.98}$$

wherein the equality sign is valid for a semiinfinite crack, given by $\theta_0 = \pm\pi$.

2.7 Equivalence between Strain Energy Release Rate and Stress Intensity Factor

The connection between the strain energy release rate, which is a global quantity, and the stress intensity factor, which expresses the strength of the local elastic stress field in the neighborhood of the crack front, is very important in engineering design. For the opening mode case, the work performed at both ends of the crack is defined as follows:

$$G_I = 2 \lim_{\delta \to 0} \frac{1}{\delta} \int_0^{\delta} \frac{1}{2} \sigma_\theta(\delta - r, 0) u_\theta(r, \pi) dr, \tag{2.99}$$

which, together with equations (2.57) and (2.58), finally gives

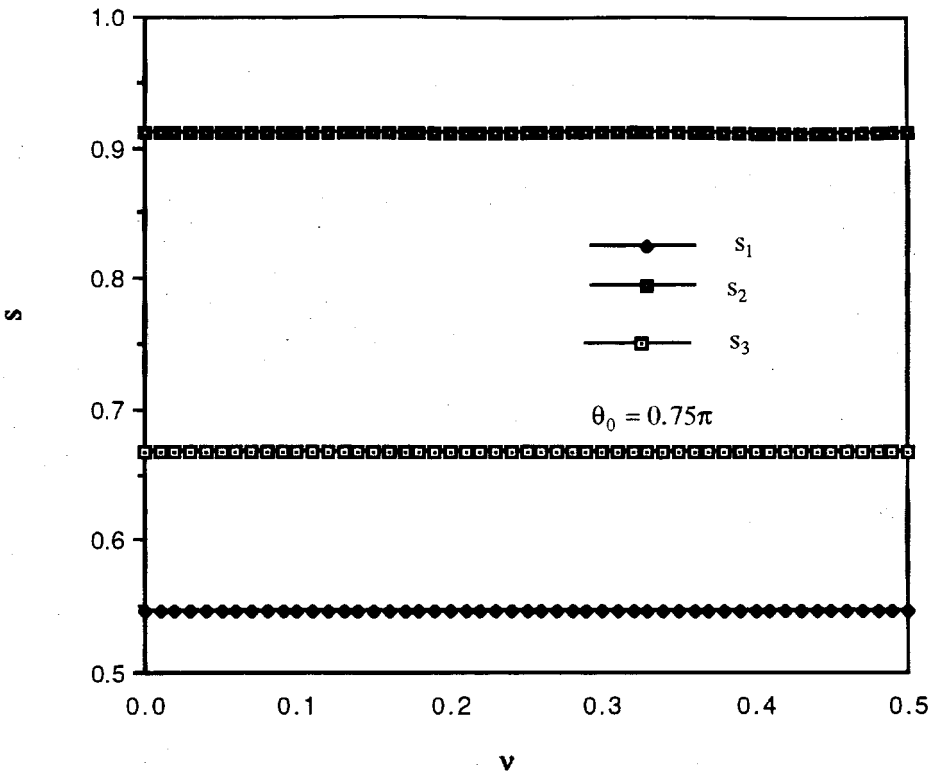

Figure 2.14 Dependence of the interior region eigenvalues on the Poisson's ratio(ν), corresponding to Modes I, II & III with $\theta_0=0.75\pi$.

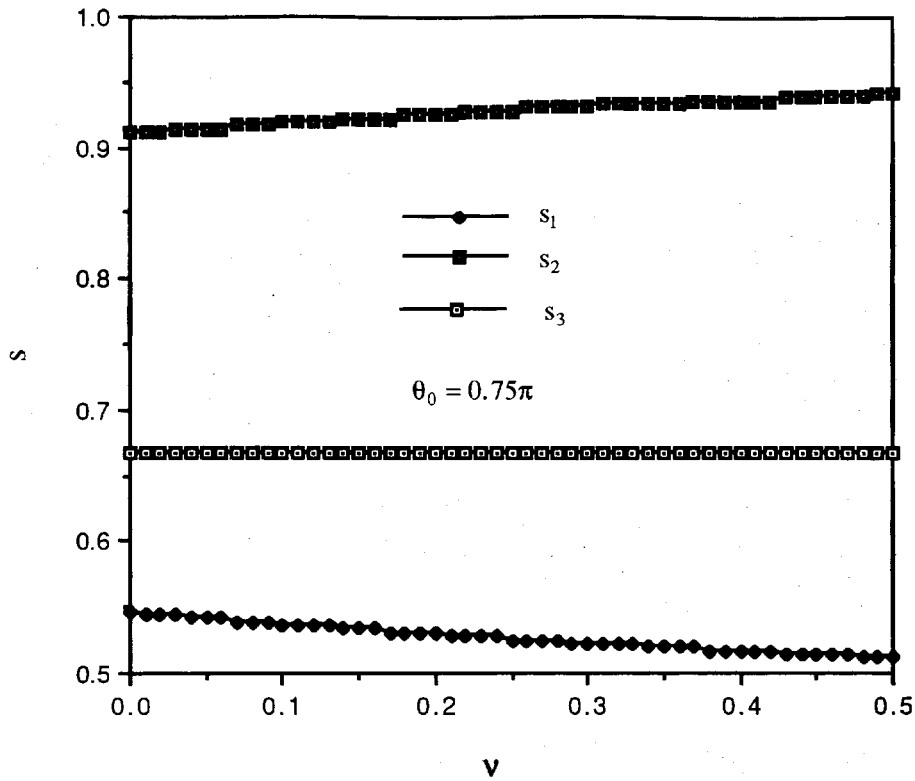

Figure 2.15 Dependence of the surface region eigenvalues on the Poisson's ratio(ν), corresponding to Modes I, II & III, with $\theta_0=0.75\pi$.

$$G_I = G_{Is} + G_{Ia}; \tag{2.100}$$

where

$$G_{Is} = \frac{1-\nu^2}{E} K^2_{Is} \tag{2.101}$$

$$G_{Ia} = \frac{1-\nu^2}{E} K^2_{Ia}. \tag{2.102}$$

for the interior layer region. G_{Is} is the same as that for the corresponding two-dimensional extension loading case, while G_{Ia}, the strain energy release rate for the bending problem, can not be obtained by the two-dimensional approach.

Introducing the expressions for σ_θ and u_θ from equations (2.83) and (2.84), the strain energy release rate for Mode I loading on the surface region can be obtained:

$$G_I = G_{Is} + G_{Ia}, \tag{2.103}$$

where

$$G_{Is} = \frac{1-0.5\nu}{E} K^2_{Is} \tag{2.104}$$

$$G_{Ia} = \frac{1-0.5\nu}{E} K^2_{Ia}. \tag{2.105}$$

The above results are different from those obtained in the case of two-dimensional generalized plane stress approximation. G_{Is} and G_{Ia} represent the strain energy release rates for the extension and the bending loading case, respectively. The expression for the strain energy release rate G_{II} for the sliding mode loading takes the form

$$G_{II} = 2\lim_{\delta\to 0}\frac{1}{\delta}\int_0^{\delta}\frac{1}{2}\tau_{\theta r}(\delta - r, 0)u_r(r,\pi)dr. \tag{2.106}$$

Introducing the expressions of $\tau_{\theta r}$ and u_r from equations (2.57) and (2.58), the strain energy release rate for Mode II loading, valid in the interior region, can be obtained as given below:

$$G_{II} = G_{IIs} + G_{IIa}, \tag{2.107}$$

where

$$G_{IIs} = \frac{1-\nu^2}{E}K^2{}_{IIs} \tag{2.108}$$

$$G_{IIa} = \frac{1-\nu^2}{E}K^2{}_{IIa}. \tag{2.109}$$

Like the (opening) Mode I, G_{IIs} is for extension loading case, whereas G_{IIa} represents bending loading case; the latter can not be obtained by two-dimensional method. The strain energy release rate on the surface region can be reduced by substitution of equations (2.83) and (2.84) into equation (2.106),

$$G_{II} = G_{IIs} + G_{IIa}, \tag{2.110}$$

where

$$G_{IIs} = \frac{K^2{}_{IIs}}{E} \tag{2.111}$$

$$G_{IIa} = \frac{K^2{}_{IIa}}{E}. \tag{2.112}$$

G_{IIs} the results are the same as two-dimensional generalized plane stress for extension loading case. G_{IIa} is for bending loading case that can not be obtained by the two-dimensional method. The calculation of the strain energy release rate G_{III} for antiplane shear loading or Mode III is computed as

$$G_{III} = 2\lim_{\delta\to 0}\frac{1}{\delta}\int_0^{\delta}\frac{1}{2}\tau_{\theta z}(\delta - r,0)u_z(r,\pi)dr, \tag{2.113}$$

which, together with equation (2.32) and (2.33), gives

$$G_{III} = G_{IIIs} + G_{IIIa}; \tag{2.114}$$

where

$$G_{IIIs} = \frac{1+\nu}{E}K^2_{IIIs} \tag{2.115}$$

$$G_{IIIa} = \frac{1+\nu}{E}K^2_{IIIa}. \tag{2.116}$$

G_{IIIs} is the same as its two-dimensional counterpart , whereas K_{IIIa} , the self-equilibrating stress intensity factor, can not be obtained by the two-dimensional method. The latter statement implies that the corresponding G_{IIIa}, the self-equilibrating strain energy release rate, can not be obtained by the two-dimensional method.

2.8 Approximate Determination of the Crack Front Yield Zone

Strictly speaking, the yield zone ahead of the crack front should be determined from an elastic-plastic analysis of the stress field around the crack front. However, some useful, albeit approximate, results regarding the shape of the yield zone can be obtained by

applying the Von Mises yield criterion to the present elastic analysis. The Von Mises expression is given in the form:

$$2\sigma_{ys}^2 = (\sigma_\theta - \sigma_r)^2 + (\sigma_\theta - \sigma_z)^2 + (\sigma_r - \sigma_z)^2 + 6(\tau_{\theta r}^2 + \tau_{z\theta}^2 + \tau_{zr}^2). \tag{2.117}$$

On substitution of equation (2.57) into equation (2.117), the following expression for the radius of the yield zone in the interior region for the opening mode (Mode I) can be obtained:

$$r_p = \frac{1}{4\pi}\left(\frac{K_I}{\sigma_{ys}}\right)^2 \left(\frac{3}{2}\sin^2\theta + (1-2\nu)^2(1+\cos\theta)\right). \tag{2.118}$$

Similarly, introducing equation (2.83) into equation (2.117), the radius of the yield zone ahead of the surface corner region at the crack front for Mode I can be derived as follows:

$$r_p = \frac{1}{4\pi(4+4\nu)^2}\left(\frac{K_I}{\sigma_{ys}}\right)^2 \left(6\cos^2\left(\frac{3\theta}{2}\right) + \left(4 + (5+4\nu)^2 + (3+4\nu)^2\right)\cos^2\left(\frac{\theta}{2}\right) -\right.$$

$$\left. 12\cos\left(\frac{\theta}{2}\right)\cos\left(\frac{3\theta}{2}\right) + 6\left(\sin\left(\frac{3\theta}{2}\right) + \sin\left(\frac{\theta}{2}\right)\right)^2\right). \tag{2.119}$$

The radius of the same yield zone for Mode I assuming the condition of (two-dimensional) plane stress in the surface layer is given by [78]:

$$r_{p2} = \frac{1}{4\pi}\left(\frac{K_I}{\sigma_{ys}}\right)^2 \left(\frac{3}{2}\sin^2\theta + 1 + \cos\theta\right). \tag{2.120}$$

Figures 2.16 and 2.17 show comparisons of the shapes of the yield zones for interior and surface regions ahead of the crack front for Mode I with their (two-

dimensional) plane stress approximate counterpart, for ν =0.25 and 0.5, respectively. It is interesting to observe that the yield zones on the surface region, computed using both the present three dimensional approach as well as (two-dimensional) plane stress analysis are much larger than that for the interior region. From equation (2.120), it is quite clear that the yield zone, computed using (two-dimensional) plane stress analysis, is independent of Poisson's ratio, ν. It is further interesting to observe from Figures 2.16 and 2.17 that the computed yield zones for both the interior and surface regions, decrease with the increase of Poisson's ratio, ν. $\theta = \pm\pi$, yield zone radius is zero for all cases (see Figures 2.16 and 2.17). Figure 2.18 presents the variations of the ratios of the yield zone radii, r_p/r_{p2}, with the wedge angle for ν = 0, 0.25, 0.5, wherein r_p and r_{p2} are computed using the present three-dimensional analysis for the surface region and the (two-dimensional) plane stress analysis, respectively. It is noteworthy that the yield zone radius for Mode I computed using the present three-dimensional approach shrinks with the increase of ν, until it reaches its minimum value r_p/r_{p2} = 0.584 at ν =0.5.

The yield zone radius, r_p , for the interior region corresponding to the sliding mode (Mode II) loading can be obtained in an analogous way as follows:

$$r_p = \frac{1}{4\pi}\left(\frac{K_{II}}{\sigma_{ys}}\right)^2\left[\left(8\nu^2 - 8\nu + \frac{19}{8}\right)\sin^2\frac{\theta}{2} - \frac{9}{4}\sin\frac{\theta}{2}\sin\frac{3\theta}{2} + \right.$$

$$\left.\frac{27}{8}\sin^2\frac{3\theta}{2} + \frac{3}{8}\left(\cos\frac{\theta}{2} + 3\cos\frac{3\theta}{2}\right)^2\right], \qquad (2.121)$$

whereas its counterpart for the surface region is given by

$$r_p = \frac{1}{4\pi(4+4\nu)^2}\left(\frac{K_{II}}{\sigma_{ys}}\right)^2\left(6(3+4\nu)^2\sin^2\left(\frac{3\theta}{2}\right) + \left(4 + (3+4\nu)^2 + (5+4\nu)^2\right)\sin^2\left(\frac{\theta}{2}\right) - \right.$$

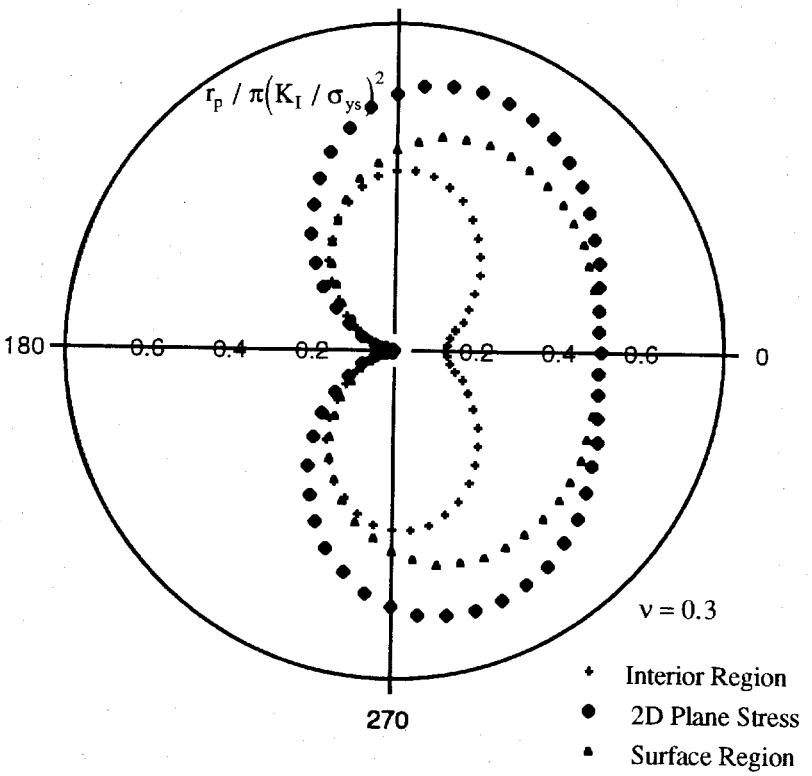

Figure 2.16. Development of the yield zone for Mode I in the vicinity of a semiinfinite crack front for ν=0.3.

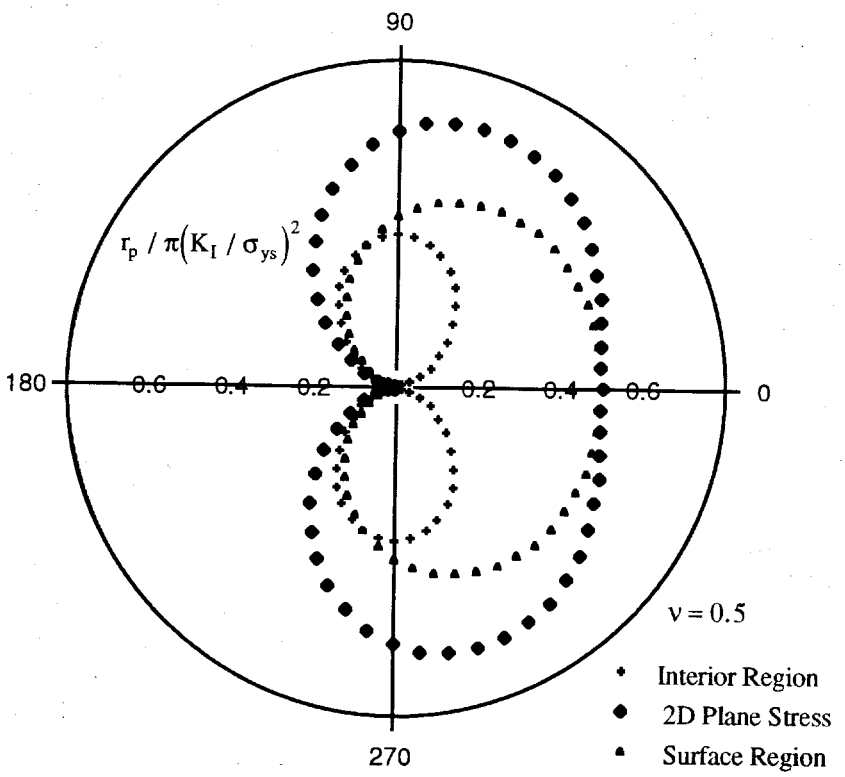

Figure 2.17. Development of the yield zone for Mode I in the vicinity of a semiinfinite crack front for ν=0.5.

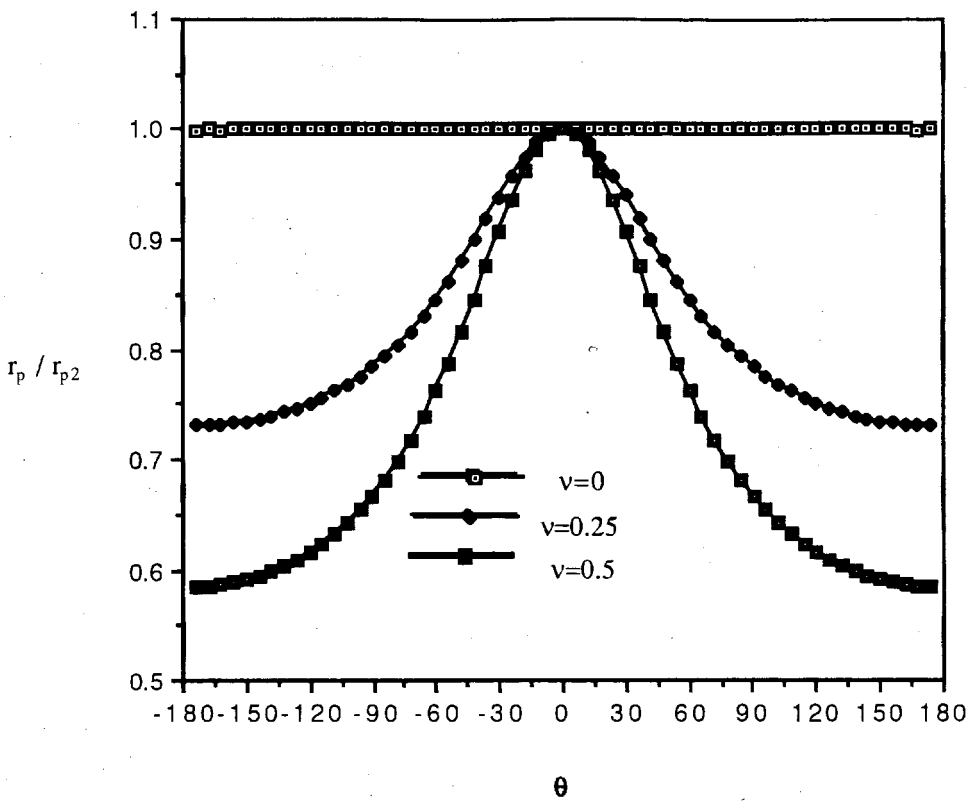

Figure 2.18 Variation of the ratio of the Mode I yield zone radii for surface region to two-dimensional plane stress solution vs angle, for different Poisson's ratios.

$$12(3+4\nu)\sin\left(\frac{3\theta}{2}\right)\sin\left(\frac{\theta}{2}\right)+6\left((3+4\nu)\cos\left(\frac{3\theta}{2}\right)+\cos\left(\frac{\theta}{2}\right)\right)^2). \tag{2.122}$$

The radius of the same yield zone for Mode II assuming the condition of (two-dimensional) plane stress in the surface layer is given by [78]

$$r_{p2}=\frac{1}{32\pi}\left(\frac{K_{II}}{\sigma_{ys}}\right)^2\left(19\sin^2\frac{\theta}{2}-18\sin\frac{\theta}{2}\sin\frac{3\theta}{2}+27\sin^2\frac{3\theta}{2}+\right.$$

$$\left.3\left(\cos\frac{\theta}{2}+3\cos\frac{3\theta}{2}\right)^2\right]. \tag{2.123}$$

Figures 2.19 and 2.20 show comparisons of the shapes of the yield zones for interior and surface regions ahead of the crack front for Mode II with their (two-dimensional) plane stress approximate counterpart, for ν =0.25 and 0.5, respectively. Similar to its Mode I counterpart, the yield zones on the surface region, computed using both the present three-dimensional approach as well as (two-dimensional) plane stress analysis are much larger than that for the interior region. However, in contrast to the Mode I case, the yield zone on the surface region, computed using the present three-dimensional approach is larger than (two-dimensional) plane stress analysis. From equation (2.123), it is quite clear that the yield zone, computed using (two-dimensional) plane stress analysis, is independent of Poisson's ratio, ν, whereas the same quantity when computed using the present three-dimensional approach for both interior and surface regions depends on Poisson's ratio. It is further interesting to observe from Figures 2.19 and 2.20 that the computed yield zones for the interior regions decrease with the increase of Poisson's ratio, ν, whereas the reverse is true for the surface region. Figure 2.21 presents the variations of the ratios of the yield zone radii, r_p/r_{p2}, with the wedge angle for ν = 0, 0.25, 0.5, wherein r_p and r_{p2} are computed using the present three-dimensional analysis for the surface region and the (two-dimensional) plane stress analysis, respectively. When ν = 0, the three-dimensional

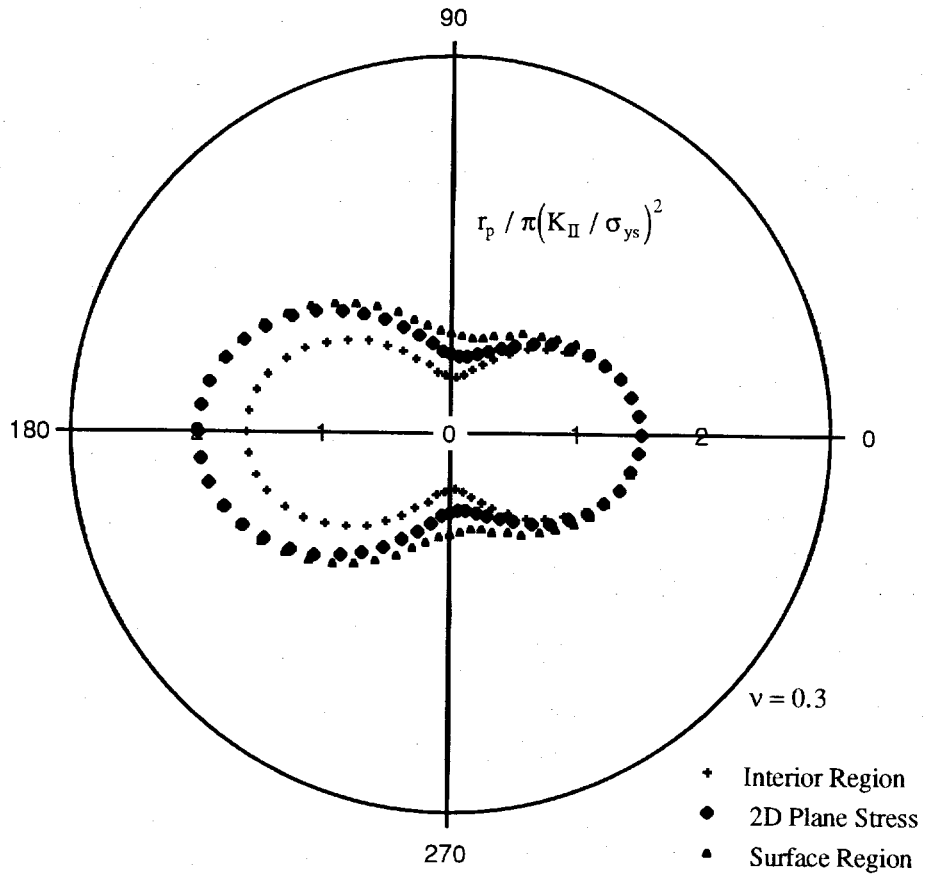

Figure 2.19 Development of the yield zone for Mode II in the vicinity of a semiinfinite crack front for ν=0.3.

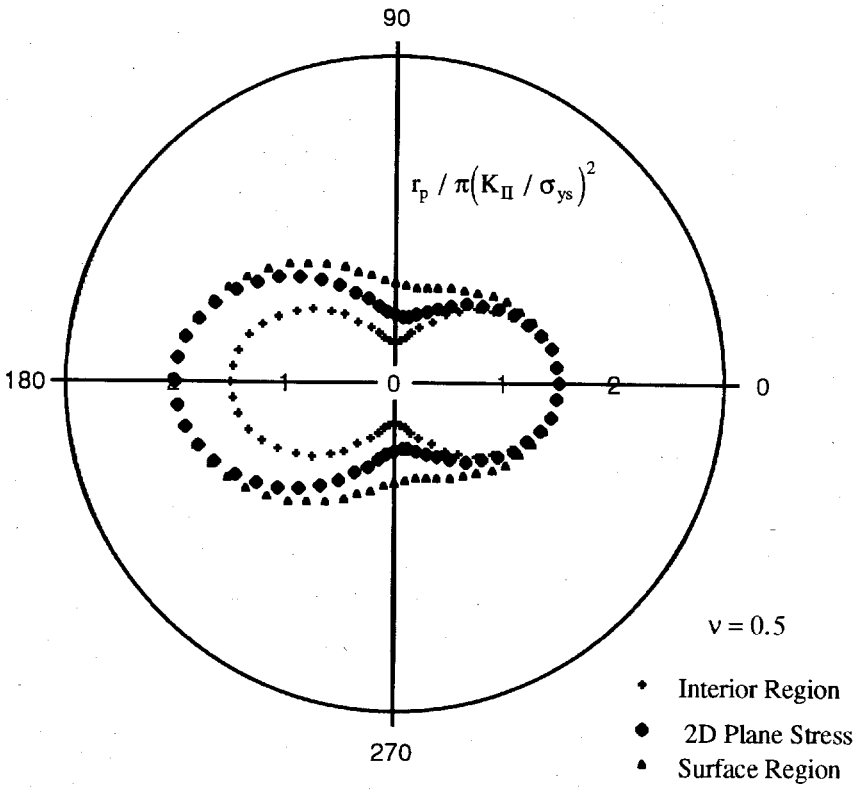

Figure 2.20 Development of the yield zone for Mode II in the vicinity of a semiinfinite crack front for ν=0.5.

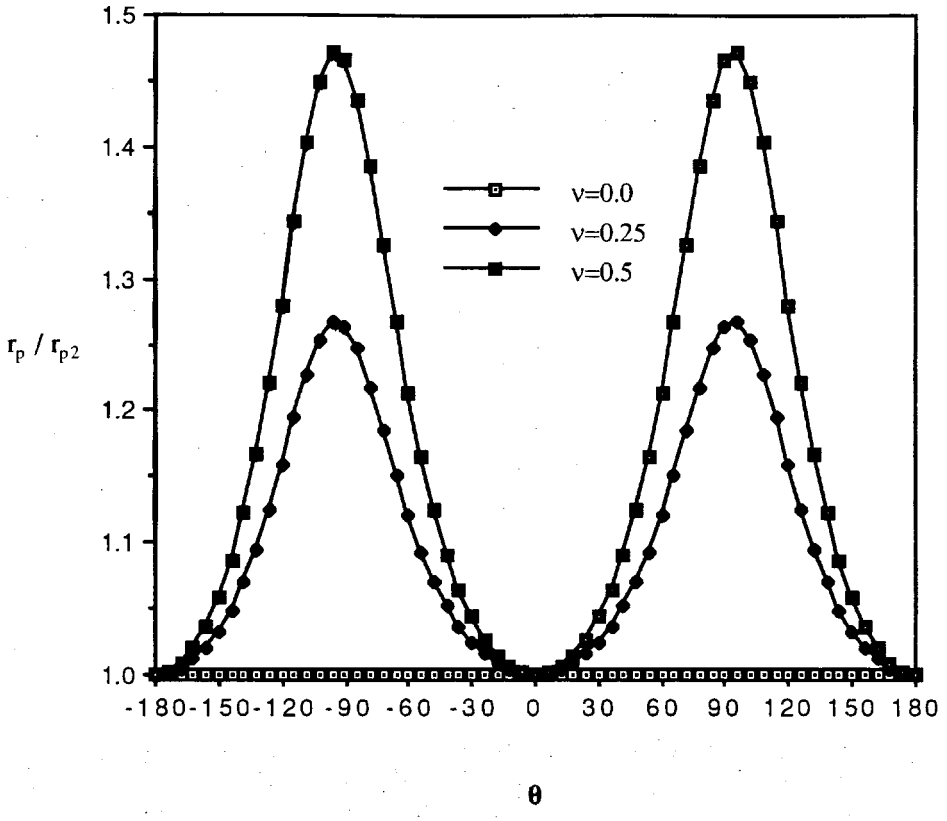

Figure 2.21 Variation of the ratio of the Mode II yield zone radii for surface region to two-dimensional plane stress solution vs wedge angle, for different Poisson's ratios.

surface solution reduces to its (two-dimensional) plane stress counterpart. It is noteworthy that the yield zone radius for Mode II computed using the present three-dimensional approach, in contrast to its Mode I counterpart, expands with the increase of ν, until it reaches its maximum value $r_p/r_{p2} = 1.47$ at $\nu = 0.5$ and $\theta = \pm\pi/2$.

Finally, for the antiplane shear mode (Mode III) loading, the yield zone assumes the shape of a circle centered at the crack tip with radius given by

$$r_p = \frac{3}{2\pi}\left(\frac{K_{III}}{\sigma_{ys}}\right)^2. \tag{2.124}$$

CHAPTER 3

THREE-DIMENSIONAL BIMATERIAL WEDGE PROBLEM

3.1 Statement of the Problem

As in the case of a homogeneous wedge, the cylindrical polar coordinate system (r,θ, z), is convenient to describe the deformation behavior of an infinite bimaterial wedge. Here, the z-axis is placed along the straight bimaterial wedge front, and the coordinates r, θ are used to define the position of an element in the plane of the plate (Figure 3.1). The components of the displacements in the radial and tangential directions are represented by U_{rj}, $U_{\theta j}$, while the component in the z-direction is denoted by U_{zj}.

In the absence of body forces, the coupled partial differential equations in terms of the displacement functions U_{rj}, $U_{\theta j}$, and U_{zj} are given as follows:

$$\left(\lambda_j + 2G_j\right)\frac{\partial^2 U_{rj}}{\partial r^2} + \frac{\left(\lambda_j + 2G_j\right)}{r}\frac{\partial U_{rj}}{\partial r} - \left(\lambda_j + 2G_j\right)\frac{U_{rj}}{r^2} + \frac{G_j}{r^2}\frac{\partial^2 U_{rj}}{\partial \theta^2} + \frac{\left(\lambda_j + G_j\right)}{r}\frac{\partial^2 U_{\theta j}}{\partial r \partial \theta} -$$

$$\frac{\left(\lambda_j + 3G_j\right)}{r^2}\frac{\partial U_{\theta j}}{\partial \theta} + G_j\frac{\partial^2 U_{rj}}{\partial z^2} + \left(\lambda_j + G_j\right)\frac{\partial^2 U_{zj}}{\partial r \partial z} = 0$$

$$\frac{\left(\lambda_j + G_j\right)}{r}\frac{\partial^2 U_{rj}}{\partial \theta \partial r} + \frac{\left(\lambda_j + 3G_j\right)}{r^2}\frac{\partial U_{rj}}{\partial \theta} + G_j\frac{\partial^2 U_{\theta j}}{\partial r^2} + G_j\frac{\partial U_{\theta j}}{r \partial r} - G_j\frac{U_{\theta j}}{r^2} + \left(\lambda_j + 2G_j\right)\frac{\partial^2 U_{\theta j}}{r^2 \partial \theta^2}$$

$$+ G_j\frac{\partial^2 U_{\theta j}}{\partial z^2} + \frac{\left(\lambda_j + G_j\right)}{r}\frac{\partial^2 U_{zj}}{\partial \theta \partial z} = 0$$

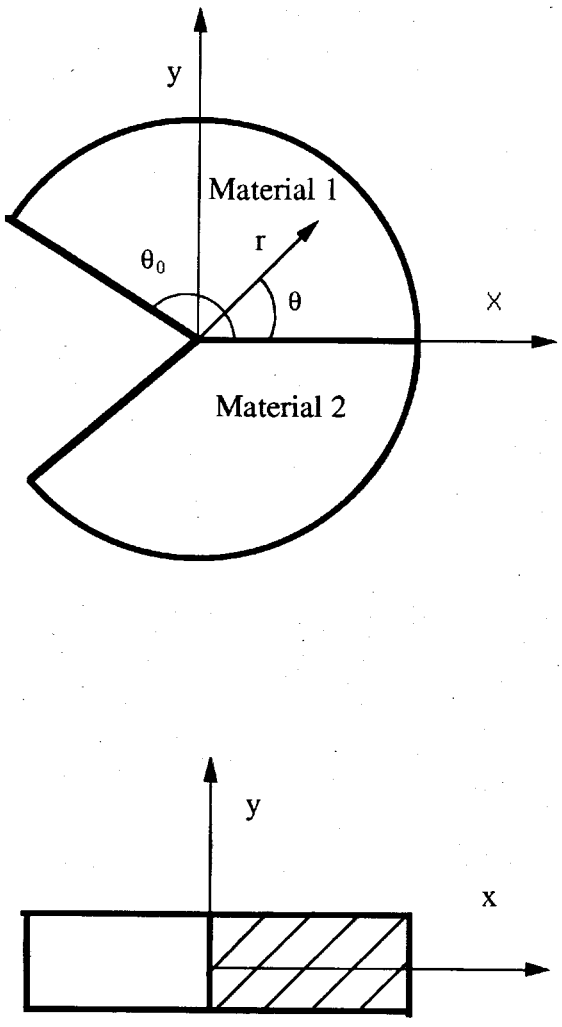

Figure 3.1 A Bimaterial Wedge

$$(\lambda_j + G_j)\frac{\partial^2 U_{rj}}{\partial r \partial z} + \frac{(\lambda_j + G_j)}{r}\frac{\partial U_{rj}}{\partial z} + \frac{(\lambda_j + G_j)}{r}\frac{\partial^2 U_{\theta j}}{\partial \theta \partial z} + (\lambda_j + 2G_j)\frac{\partial^2 U_{zj}}{\partial z^2} + G_j \frac{\partial^2 U_{zj}}{\partial r^2}$$

$$+ G_j \frac{\partial U_{zj}}{r \partial r} + \frac{G_j}{r^2}\frac{\partial^2 U_{zj}}{\partial \theta^2} = 0, \qquad j = 1,2$$

(3.1)

where λ_j and G_j. j=1,2 are Lame's coefficients for the material 1 and material 2. The boundary conditions at the bimaterial wedge-side surfaces are classified as follows:

$$\theta = \pm\theta_0,$$

1. Free-Free

$$\sigma_{\theta j} = \tau_{r\theta j} = \tau_{\theta z j} = 0; \qquad (3.2)$$

2. Clamped-Clamped

$$U_{rj} = U_{\theta j} = U_{zj} = 0; \qquad (3.3)$$

3. Clamped-Free

$$\theta = \theta_0$$

$$\sigma_{\theta 1} = \tau_{r\theta 1} = \tau_{\theta z 1} = 0 \qquad (3.4)$$

$$\theta = -\theta_0$$

$$U_{r2} = U_{\theta 2} = U_{z2} = 0. \qquad (3.5)$$

Assuming that the interface is perfectly bonded, it is easy to establish the continuity conditions of the stresses and displacements along the bimaterial interface, $\theta=0$, which are written as follows:

$$U_{\theta 1} = U_{\theta 2}, \quad U_{r1} = U_{r2}, \quad U_{z1} = U_{z2}$$

$$\sigma_{\theta 1} = \sigma_{\theta 2}, \quad \tau_{r\theta 1} = \tau_{r\theta 2}, \quad \tau_{\theta z1} = \tau_{\theta z2}. \tag{3.6}$$

The solution sought must satisfy the governing equations, boundary conditions and continuity conditions.

3.2 Singular Stress Fields at the Front of a Bimaterial Wedge Subjected to Antiplane Shear Loading

In what follows, the solution to the system of coupled differential equations (3.1) subjected to the boundary and interface conditions will be obtained for a bimaterial wedge subjected to antiplane shear loading. The general asymptotic displacement fields in the neighborhood of the wedge front can be obtained from equation (2.16) as follows:

$$U_{zj} = \frac{r^s}{G_j}\left(A_{1j}(z)\sin(s\theta) + A_{2j}(z)\cos(s\theta)\right) + 0\left(r^{s+2}\right)$$

$$U_{rj} = 0\left(r^{s+1}\right), \quad U_{\theta j} = 0\left(r^{s+1}\right); \qquad j = 1,2 \tag{3.7}$$

where

$$\overline{\overline{A}}_{1j,2j}\, B_{bj}(z) = \frac{A_{1j,2j} B_{bj}(z)}{G_j c_{sj}}$$

$$D_{1j} = -(ik)^s \overline{D}_{1j}, \qquad D_{2j} = i(ik)^s \overline{D}_{2j}$$

$$B_{bj}(z) = -D_{1j}\cos(kz) + D_{2j}\sin(kz). \tag{3.8}$$

The corresponding singular stress fields can be derived from equation (3.7) in the form:

$$\begin{aligned}
&\tau_{\theta zj} = r^{s-1}\, s\left(A_{1j}(z)\cos(s\theta) - A_{2j}(z)\sin(s\theta)\right) + 0\left(r^{s+1}\right) \\
&\tau_{rzj} = r^{s-1}\, s\left(A_{1j}(z)\sin(s\theta) + A_{2j}(z)\cos(s\theta)\right) + 0\left(r^{s+1}\right)
\end{aligned} \tag{3.9}$$

$$\tau_{r\theta j} = 0\left(r^{s+2}\right), \quad \sigma_{rj} = 0\left(r^{s}\right)$$

$$\sigma_{\theta j} = 0\left(r^{s}\right), \quad \sigma_{zj} = 0\left(r^{s}\right). \tag{3.10}$$

Satisfaction of stress free condition, given by equation (2.4), on the plate faces results in:

$$B_{bj}(\pm h) = B_{bjs}(\pm h) + B_{bja}(\pm h) = 0, \tag{3.11}$$

where

$$B_{bjs}(\pm h) = -D_{1j}\cos(\pm kh) \tag{3.12}$$

$$B_{bja}(\pm h) = D_{2j}\sin(\pm kh). \tag{3.13}$$

As in the case of a homogeneous wedge, the special case of symmetric deformation is obtained as follows:

$$k_i = \frac{(2i+1)}{2h}\pi \qquad i = 0, \pm 1, \pm 2, \cdots\cdots$$

$$B_{bjs}(z) = \sum_{i=0}^{\pm\infty} -D_{1ji}\cos\left(\frac{(2i+1)}{2h}\pi z\right). \tag{3.14}$$

The antisymmetric deformation case can also be obtained in a similar manner:

$$k_i = \frac{i\pi}{h} \qquad i = 0, \pm 1, \pm 2, \cdots\cdots$$

$$B_{bja}(z) = \sum_{i=0}^{\pm\infty} D_{2ji} \sin\left(\frac{i}{h}\pi z\right). \tag{3.15}$$

The expressions for stresses and displacements also need to satisfy continuity conditions at the bimaterial interface, given by equation (3.6), leading to the following two homogeneous linear algebraic equations:

$$A_{11}(z) - A_{12}(z) = 0$$

$$\frac{A_{21}(z)}{G_1} - \frac{A_{22}(z)}{G_2} = 0. \tag{3.16}$$

Additionally, the expressions for stresses and displacements also need to satisfy the boundary conditions on the wedge-side surfaces. The eigenvalues, which are related to the strength of the stress singularity, can be obtained from these relations. Three combinations of boundary conditions are considered: clamped-clamped, clamped-free and free-free.

3.2.1 Clamped-Clamped

Substitution of equation (3.7) into equation (3.3), the following characteristic equation is obtained:

$$\sin(2s\theta_0) = 0. \tag{3.17}$$

The minimum root (eigenvalue) contributing to the singular stresses is given by

$$s = \frac{\pi}{2\theta_0}. \tag{3.18}$$

It may be noted that when $\theta_0 \leq |\pm\pi/2|$, the stresses at the bimaterial wedge front are non-singular. The special case of $\theta_0 = \pm\pi/2$ represents the bimaterial half-space, which yields s=1. However, when $\theta_0 > |\pm\pi/2|$, the bimaterial wedge front has singular stresses. Another special case is given by $\theta_0 = \pm\pi$, which yields s=1/2.

3.2.2 Clamped-Free

Substitution of equations (3.7) and (3.9) into equations (3.4) and (3.5) supplies the following characteristic equation:

$$\tan^2(s\theta_0) = \frac{G_2}{G_1}.$$

$$s_2 = \frac{\pi}{\theta_0} - \frac{1}{\theta_0}\tan^{-1}\sqrt{\frac{G_2}{G_1}}. \tag{3.19}$$

The minimum roots (eigenvalues) contributing to the singular stresses are:

$$s_1 = \frac{1}{\theta_0}\tan^{-1}\sqrt{\frac{G_2}{G_1}} \tag{3.20}$$

$$s_2 = \frac{\pi}{\theta_0} - \frac{1}{\theta_0}\tan^{-1}\sqrt{\frac{G_2}{G_1}}. \tag{3.21}$$

If G_2 tends to infinity

$$s_1 = \frac{\pi}{2\theta_0}, \qquad s_2 = \frac{\pi}{2\theta_0}. \tag{3.22}$$

If G_1 tends to infinity

$$s_1 \to 0, \qquad s_2 = \frac{\pi}{\theta_0}. \tag{3.23}$$

In the special case, $G_1 = G_2$, equations (3.20) and (3.21) reduce to their homogeneous counterparts, i.e., equations (2.26) and (2.27).

3.2.3 Free-Free

Substitution of equation (3.9) into equation (3.2) supplies the following characteristic equation:

$$\sin(2s\theta_0) = 0. \tag{3.24}$$

The minimum root (eigenvalue) contributing to the singular stresses is given by

$$s = \frac{\pi}{2\theta_0}. \tag{3.25}$$

The eigenvalue given by equation (3.25) is identical to that for a homogeneous wedge. In the special case of a semiinfinite crack along the bimaterial interface, given by $\theta_0 = \pm\pi$, results in s=1/2.

It is noteworthy that as in the case of homogeneous case, the singularity of stresses remains unchanged all through the bimaterial plate thickness. The stress distribution in the vicinity of the front of a semiinfinite crack ($\theta_0 = \pm\pi$) along the bimaterial interface, i.e., $r \ll 1$, and for the case of free-free edge, can be expressed as follows:

$$\tau_{rzj} = \frac{K_{III}}{\sqrt{2\pi r}} \sin\left(\theta/2\right) \tag{3.26}$$

$$\tau_{r\theta j} = \frac{K_{III}}{\sqrt{2\pi r}} \cos\left(\theta/2\right), \tag{3.27}$$

where

$$K_{III} = K_{IIIs} + K_{IIIa} = \sqrt{\frac{\pi}{2}}\, A_{1j}\left(B_{bjs}(z) + B_{bja}(z)\right). \tag{3.28}$$

Thus, as in the case of a homogeneous material, the stress intensity factor for mode III can be separated into symmetric (K_{IIIs}) and antisymmetric (K_{IIIa}) parts. It is clear that

$$\int_{-h}^{h} K_{III\,a}\, dz = 0. \tag{3.29}$$

K_{IIIa} thus obtained represents the self-equilibrating stress intensity factor for a semiinfinite crack along the bimaterial interface, resulting in the residual stresses in the material. It must be noted that K_{IIIa} can not be determined by a two-dimensional approximation, which yields constant K_{IIIs}, whereas both K_{IIIa} and K_{IIIs}, obtained by the above three-dimensional approach, are functions of z.

3.3 Singular Stress Fields at the Front of the Interior Region of a Bimaterial Wedge Under Extension / Bending

In what follows, solution to the system of coupled differential equations (3.1) subjected to the boundary and interface conditions will be obtained for a bimaterial wedge subjected to extension and bending loading. The general asymptotic displacement fields in the neighborhood of the bimaterial wedge front can be obtained from equation (2.44) as follows:

$$U_{rj} = r_1^{s}\left[\frac{2^{-s}}{\Gamma(s+1)}\left(\overline{A}_{1j}(z)\sin(s+1)\theta + \overline{A}_{2j}(z)\cos(s+1)\theta\right) + \right.$$

$$a_{sj}\left(\overline{A}_{3j}(z)\sin(s-1)\theta + \overline{A}_{4j}(z)\cos(s-1)\theta\right)\ ] + 0\left(r^{s+2}\right)$$

$$U_{\theta j} = r_1^s\left[\frac{2^{-s}}{\Gamma(s+1)}\left(\overline{A}_{1j}(z)\cos(s+1)\theta - \overline{A}_{2j}(z)\sin(s+1)\theta\right) +\right.$$

$$\left. f_{1j}a_{sj}\left(\overline{A}_{3j}(z)\cos(s-1)\theta - \overline{A}_{4j}(z)\sin(s-1)\theta\right)\ \right] + 0\left(r^{s+2}\right)$$

$$U_{zj} = 0\left(r^{s+1}\right), \tag{3.30}$$

where

$$f_{1j} = \frac{\left(\lambda_j + G_j\right)s + \left(\lambda_j + 3G_j\right)}{\left(\lambda_j + G_j\right)s - \left(\lambda_j + 3G_j\right)}$$

$$B_{1j}(z) = D_{1j}\sin(kz) + D_{2j}\cos(kz) \tag{3.31}$$

$$\overline{A}_{ij}(z) = \overline{A}_{ij}B_{1j}(z), \qquad i = 1,2,3,4.$$

The fields of displacements and stresses can be written down in the form:

$$U_{rj} = \frac{r^s}{2G_j s}\left[\left(A_{1j}(z)\sin(s+1)\theta + A_{2j}(z)\cos(s+1)\theta\right) + \left(s - 3 + 4\nu_j\right)\right.$$

$$\left.\left(A_{3j}(z)\sin(s-1)\theta + A_{4j}(z)\cos(s-1)\theta\right)\ \right] + 0\left(r^{s+2}\right)$$

$$U_{\theta j} = \frac{r^s}{2G_j s}\left[\left(A_{1j}(z)\cos(s+1)\theta - A_{2j}(z)\sin(s+1)\theta\right) + \left(s + 3 - 4\nu_j\right)\right.$$

$$\left.\left(A_{3j}\cos(s-1)\theta - A_{4j}\sin(s-1)\theta\right)\ \right] + 0\left(r^{s+2}\right)$$

$$\sigma_{rj} = r^{s-1}\Big[\Big(A_{1j}(z)\sin(s+1)\theta + A_{2j}(z)\cos(s+1)\theta\Big) + (s-3)$$

$$\Big(A_{3j}(z)\sin(s-1)\theta + A_{4j}(z)\cos(s-1)\theta\Big)\ \Big] + 0\Big(r^{s+1}\Big)$$

$$\sigma_{\theta j} = -r^{s-1}\Big[\Big(A_{1j}(z)\sin(s+1)\theta + A_{2j}(z)\cos(s+1)\theta\Big) + (s+1)$$

$$\Big(A_{3j}(z)\sin(s-1)\theta + A_{4j}(z)\cos(s-1)\theta\Big)\ \Big] + 0\Big(r^{s+1}\Big)$$

$$\tau_{r\theta j} = r^{s-1}\ \Big[\Big(A_{1j}(z)\cos(s+1)\theta - A_{2j}(z)\sin(s+1)\theta\Big) + (s-1)$$

$$\Big(A_{3j}(z)\cos(s-1)\theta - A_{4j}(z)\sin(s-1)\theta\Big)\ \Big] + 0\Big(r^{s+1}\Big)$$

$$\sigma_{zj} = -4\nu_j r^{s-1}\Big(A_{3j}(z)\sin(s-1)\theta + A_{4j}(z)\cos(s-1)\theta\Big) + 0\Big(r^{s+1}\Big)$$

$$U_{zj} = 0\Big(r^{s+1}\Big)\ ,\quad \tau_{rzj} = 0\Big(r^{s}\Big)\ ,\quad \tau_{\theta zj} = 0\Big(r^{s}\Big), \tag{3.32}$$

where

$$\overline{A}_{1j,2j}(z) = \frac{1}{2G_j s} A_{1j,2j}(z)\frac{\Gamma(s+1)2^s}{(ik)^s}$$

$$\overline{A}_{3j,4j}(z) = \frac{\big(\lambda_j + G_j\big)s - \big(\lambda_j + 3G_j\big)}{2sG_j\big(\lambda_j + G_j\big)a_{sj}(ik)^s}\ A_{3j,4j}(z)$$

$$A_{ij}(z) = A_{ij}B_{1j}(z), \qquad i = 1,2,3,4. \tag{3.33}$$

The expressions for stresses and displacements also need to satisfy continuity conditions at the bimaterial interface, given by equation (3.6), leading to the following four homogeneous linear algebraic equations:

$$A_{21}(z)+(s+c_{21})A_{41}(z)-k\left(A_{22}(z)+(s+c_{22})A_{42}(z)\right)=0$$

$$A_{11}(z)+(s-c_{21})A_{31}(z)-k\left(A_{12}(z)+(s-c_{22})A_{32}(z)\right)=0$$

$$A_{21}(z)+(s+1)A_{41}(z)-\left(A_{22}(z)+(s+1)A_{42}(z)\right)=0$$

$$A_{11}(z)+(s-1)A_{31}(z)-\left(A_{12}(z)+(s-1)A_{32}(z)\right)=0, \qquad (3.34)$$

where

$$c_{2j}=-3+4\nu_j \qquad j=1,2$$

$$k=\frac{G_1}{G_2}.$$

Additionally, the expressions for stresses and displacements also need to satisfy the boundary conditions on the bimaterial wedge-side surfaces. The eigenvalues, which are related to the strength of the stress singularity, can be obtained from these relations. Three combinations of boundary conditions are considered: clamped-clamped, clamped-free and free-free.

3.3.1 Clamped-Clamped

Substitution of equation (3.32) into equation (3.3) yields the following characteristic equations:

$$A_{11}(z)\sin(s+1)\theta_0 + A_{21}(z)\cos(s+1)\theta_0 +$$

$$(s+c_{21})\left(A_{31}(z)\sin(s-1)\theta_0 + A_{41}(z)\cos(s-1)\theta_0\right) = 0$$

$$A_{11}(z)\cos(s+1)\theta_0 - A_{21}(z)\sin(s+1)\theta_0 +$$

$$(s-c_{21})\left(A_{31}(z)\cos(s-1)\theta_0 - A_{41}(z)\sin(s-1)\theta_0\right) = 0$$

$$-A_{12}(z)\sin(s+1)\theta_0 + A_{22}(z)\cos(s+1)\theta_0 +$$

$$(s+c_{22})\left(-A_{32}(z)\sin(s-1)\theta_0 + A_{42}(z)\cos(s-1)\theta_0\right) = 0$$

$$A_{12}(z)\cos(s+1)\theta_0 + A_{22}(z)\sin(s+1)\theta_0 +$$

$$(s-c_{22})\left(A_{32}(z)\cos(s-1)\theta_0 + A_{42}(z)\sin(s-1)\theta_0\right) = 0. \tag{3.35}$$

In the special case of $\theta_0=\pm\pi$, the above system of eight homogeneous algebraic equations, given by equations (3.34) and (3.35), reduce to one characteristic equation, given as follows:

$$\cot^2 s\pi + \left(\frac{c_{21}(1+c_{22}) - kc_{22}(1+c_{21})}{kc_{22}(1-c_{21}) + c_{21}(1-c_{22})}\right)^2 = 0. \tag{3.36}$$

The eigenvalues can be explicitly obtained from equation (3.36), which is given below:

$$s = \frac{1}{2} \pm i\varepsilon \tag{3.37}$$

$$\varepsilon = \frac{1}{2\pi}\ln\left(\frac{1-c}{1+c}\right) \tag{3.38}$$

$$c = \frac{c_{21}(1+c_{22}) - kc_{22}(1+c_{21})}{kc_{22}(1-c_{21}) + c_{21}(1-c_{22})},$$

where ε is the imaginary part of a complex root, implying the oscillatory character at the front of the bi-material slit along the interface. In the special case of a homogeneous wedge, given by $E_1=E_2$, and $\nu_1=\nu_2$, the imaginary part, ε, representing the oscillatory character vanishes.

3.3.2 Clamped-Free

Substitution of equation (3.32) into equations (3.4) and (3.5) yields the following characteristic equations:

$$A_{11}(z)\sin(s+1)\theta_0 + A_{21}(z)\cos(s+1)\theta_0 +$$

$$(s+1)\left(A_{31}(z)\sin(s-1)\theta_0 + A_{41}(z)\cos(s-1)\theta_0\right) = 0$$

$$A_{11}(z)\cos(s+1)\theta_0 - A_{21}(z)\sin(s+1)\theta_0 +$$

$$(s-1)\left(A_{31}(z)\cos(s-1)\theta_0 - A_{41}(z)\sin(s-1)\theta_0\right) = 0$$

$$-A_{12}(z)\sin(s+1)\theta_0 + A_{22}(z)\cos(s+1)\theta_0 +$$

$$(s+c_{22})\left(-A_{32}(z)\sin(s-1)\theta_0 + A_{42}(z)\cos(s-1)\theta_0\right) = 0$$

$$A_{12}(z)\cos(s+1)\theta_0 + A_{22}(z)\sin(s+1)\theta_0 +$$

$$(s-c_{22})\left(A_{32}(z)\cos(s-1)\theta_0 + A_{42}(z)\sin(s-1)\theta_0\right) = 0. \tag{3.39}$$

3.3.3 Free-Free

Substitution of equation (3.32) into equations (3.2) yields the following characteristic equations:

$$A_{11}(z)\sin(s+1)\theta_0 + A_{21}(z)\cos(s+1)\theta_0 +$$

$$(s+1)\left(A_{31}(z)\sin(s-1)\theta_0 + A_{41}(z)\cos(s-1)\theta_0\right) = 0$$

$$A_{11}(z)\cos(s+1)\theta_0 - A_{21}(z)\sin(s+1)\theta_0 +$$

$$(s-1)\left(A_{31}(z)\cos(s-1)\theta_0 - A_{41}(z)\sin(s-1)\theta_0\right) = 0$$

$$-A_{12}(z)\sin(s+1)\theta_0 + A_{22}(z)\cos(s+1)\theta_0 +$$

$$(s+1)\left(-A_{32}(z)\sin(s-1)\theta_0 + A_{42}(z)\cos(s-1)\theta_0\right) = 0$$

$$A_{12}(z)\cos(s+1)\theta_0 + A_{22}(z)\sin(s+1)\theta_0 +$$

$$(s-1)\left(A_{32}(z)\cos(s-1)\theta_0 + A_{42}(z)\sin(s-1)\theta_0\right) = 0. \tag{3.40}$$

In the special case of a semiinfinite crack along the bimaterial interface, $\theta_0=\pm\pi$, the above system of eight homogeneous algebraic equations, given by equations (3.34) and (3.40) reduces to one characteristic equation, given as follows:

$$\cot^2 s\pi + \left(\frac{k(1-2\nu_2)-(1-2\nu_1)}{2k(1-\nu_2)+2(1-\nu_1)} \right)^2 = 0. \tag{3.41}$$

The eigenvalues can be explicitly obtained from equation (3.36). The eigenvalues are given below:

$$s = \frac{1}{2} \pm i\varepsilon$$

$$\varepsilon = \frac{1}{2\pi} \ln\left(\frac{k_1 / G_1 + 1/G_2}{k_2 / G_2 + 1/G_1} \right)$$

$$k_j = 3 - 4\nu_j, \tag{3.42}$$

where ε is the imaginary part of a eigenvalue, implying the oscillatory character at the front of the bimaterial slit along the interface. In the special case of a homogeneous wedge, given by $E_1=E_2$, and $\nu_1=\nu_2$, the imaginary part, ε, representing the oscillatory character vanishes.

The asymptotic stress fields in the vicinity of the front of a semiinfinite crack along the bimaterial interface, confined to the interior region, are given as follows:

$$\sigma_{r2} = \frac{1}{\sqrt{2\pi r}\cosh \varepsilon\pi} \left(K_I \left(\left(\frac{1}{4}\right) \cos\left(\frac{3}{2}\theta - \varepsilon \ln(r)\right) e^{\varepsilon(\theta+\pi)} - \frac{1}{2}\cos\left(\frac{3}{2}\theta + \varepsilon \ln(r)\right) e^{-\varepsilon(\theta+\pi)} + \right.\right.$$

$$\frac{\varepsilon}{2}\sin\left(\frac{3}{2}\theta - \varepsilon \ln(r)\right) e^{\varepsilon(\theta+\pi)} + \frac{5}{4}\cos\left(\frac{\theta}{2} + \varepsilon \ln(r)\right) e^{\varepsilon(\theta+\pi)} + \frac{\varepsilon}{2}\sin\left(\frac{\theta}{2} + \varepsilon \ln(r)\right) e^{\varepsilon(\theta+\pi)} \Big) +$$

$$K_{II}\left(\frac{1}{4}\sin\left(\frac{3}{2}\theta - \varepsilon \ln(r)\right) e^{\varepsilon(\theta+\pi)} + \frac{1}{2}\sin\left(\frac{3}{2}\theta + \varepsilon \ln(r)\right) e^{-\varepsilon(\theta+\pi)} - \right.$$

$$\frac{\varepsilon}{2}\cos\left(\frac{3}{2}\theta-\varepsilon\ln(r)\right)e^{\varepsilon(\theta+\pi)}-\frac{5}{4}\sin\left(\frac{\theta}{2}+\varepsilon\ln(r)\right)e^{\varepsilon(\theta+\pi)}+\frac{\varepsilon}{2}\cos\left(\frac{\theta}{2}+\varepsilon\ln(r)\right)e^{\varepsilon(\theta+\pi)}\Big)\Big)$$

$$\sigma_{\theta 2}=\frac{1}{\sqrt{2\pi r}\cosh\varepsilon\pi}\Bigg(K_I\Bigg(-\left(\frac{1}{4}\right)\cos\left(\frac{3}{2}\theta-\varepsilon\ln(r)\right)e^{\varepsilon(\theta+\pi)}+\frac{1}{2}\cos\left(\frac{3}{2}\theta+\varepsilon\ln(r)\right)e^{-\varepsilon(\theta+\pi)}-$$

$$\frac{\varepsilon}{2}\sin\left(\frac{3}{2}\theta-\varepsilon\ln(r)\right)e^{\varepsilon(\theta+\pi)}-\frac{\varepsilon}{2}\sin\left(\frac{\theta}{2}+\varepsilon\ln(r)\right)e^{\varepsilon(\theta+\pi)}+\frac{3}{4}\cos\left(\frac{\theta}{2}+\varepsilon\ln(r)\right)e^{\varepsilon(\theta+\pi)}\Big)-$$

$$K_{II}\Bigg(\frac{1}{4}\sin\left(\frac{3}{2}\theta-\varepsilon\ln(r)\right)e^{\varepsilon(\theta+\pi)}+\frac{1}{2}\sin\left(\frac{3}{2}\theta+\varepsilon\ln(r)\right)e^{-\varepsilon(\theta+\pi)}-$$

$$\frac{\varepsilon}{2}\cos\left(\frac{3}{2}\theta-\varepsilon\ln(r)\right)e^{\varepsilon(\theta+\pi)}+\frac{3}{4}\sin\left(\frac{\theta}{2}+\varepsilon\ln(r)\right)e^{\varepsilon(\theta+\pi)}+\frac{\varepsilon}{2}\cos\left(\frac{\theta}{2}+\varepsilon\ln(r)\right)e^{\varepsilon(\theta+\pi)}\Big)\Big)$$

$$\tau_{\theta r2}=-\frac{1}{\sqrt{2\pi r}\cosh\varepsilon\pi}\Bigg(K_I\Bigg(\left(\frac{1}{4}\right)\sin\left(\frac{3}{2}\theta-\varepsilon\ln(r)\right)e^{\varepsilon(\theta+\pi)}-\frac{1}{2}\sin\left(\frac{3}{2}\theta+\varepsilon\ln(r)\right)e^{-\varepsilon(\theta+\pi)}-$$

$$\frac{\varepsilon}{2}\cos\left(\frac{3}{2}\theta-\varepsilon\ln(r)\right)e^{\varepsilon(\theta+\pi)}+\frac{\varepsilon}{2}\cos\left(\frac{\theta}{2}+\varepsilon\ln(r)\right)e^{\varepsilon(\theta+\pi)}-\frac{1}{4}\sin\left(\frac{\theta}{2}+\varepsilon\ln(r)\right)e^{\varepsilon(\theta+\pi)}\Big)-$$

$$K_{II}\Bigg(\frac{1}{4}\cos\left(\frac{3}{2}\theta-\varepsilon\ln(r)\right)e^{\varepsilon(\theta+\pi)}+\frac{1}{2}\cos\left(\frac{3}{2}\theta+\varepsilon\ln(r)\right)e^{-\varepsilon(\theta+\pi)}+$$

$$\frac{\varepsilon}{2}\sin\left(\frac{3}{2}\theta-\varepsilon\ln(r)\right)e^{\varepsilon(\theta+\pi)}+\frac{1}{4}\cos\left(\frac{\theta}{2}+\varepsilon\ln(r)\right)e^{\varepsilon(\theta+\pi)}+\frac{\varepsilon}{2}\sin\left(\frac{\theta}{2}+\varepsilon\ln(r)\right)e^{\varepsilon(\theta+\pi)}\Big)\Big) \tag{3.43}$$

where

$$A_{42}(z)=a_{42}B_{12}(z)+i\bar{a}_{42}B_{12}(z) \tag{3.44}$$

$$K_I=K_{Is}+K_{Ia}=-\sqrt{2\pi}\left(1+e^{-2\pi\varepsilon}\right)a_{42}\left(B_{12s}(z)+B_{12a}(z)\right) \tag{3.45}$$

$$K_{II} = K_{IIs} + K_{IIa} = -\sqrt{2\pi}\left(1 + e^{-2\pi\varepsilon}\right)\bar{a}_{42}\left(B_{12s}(z) + B_{12a}(z)\right). \tag{3.46}$$

The stress field in the vicinity of the front of a semiinfinite crack under in plane extension can be recovered if

$$B_{12}(z) = B_{12s}(z) = D_{22}\cos(kz).$$

By using the boundary condition of free plate surface, the general form of B_{1sj} can be obtained as

$$B_{12s}(z) = \sum_{i=0}^{\pm\infty} D_{2i2}\cos\left(\frac{(2i+1)}{2h}\pi z\right). \tag{3.47}$$

Here $K_I = K_{Is}$ and $K_{II} = K_{IIs}$ are symmetric stress intensity factors. If the odd functions are selected from $B_{12}(z)$, it can yield the out-of-plane bending case given by

$$B_{12}(z) = B_{12a}(z) = D_{12}\sin(kz). \tag{3.48}$$

B_{12a} that satisfies free boundary condition is

$$B_{12a}(z) = \sum_{i=0}^{\pm\infty} D_{1i2}\sin\left(\frac{i\pi}{h}z\right). \tag{3.49}$$

Here $K_I = K_{Ia}$ and $K_{II} = K_{IIa}$ are antisymmetric stress intensity factors. If the boundary conditions on the free plate faces are satisfied, all the stresses and displacements on the plate faces in the vicinity of the front of a semiinfinite bimaterial crack vanish in a manner similar to their homogeneous wedge counterparts. It is contrary to the experimental results except for $\nu_1=\nu_2=0$, which leads to the prediction of another solution on the surface.

3.4 Singular Stress Fields at the Front of the Surface Region of a Bimaterial Wedge Under Extension / Bending

In what follows, the solution to the system of coupled differential equations (3.1) subjected to the boundary and interface conditions will be obtained for a bimaterial wedge subjected to extensional and bending loading. The asymptotic expressions for displacements and stresses in the vicinity of the surface corner point located at the bimaterial interface wedge front can be obtained from equations (2.75) to (2.79) as follows:

$$U_{rj} = \frac{r^s}{2G_j s}\Big[\Big(A_{1j}(\pm h)\sin(s+1)\theta + A_{2j}(\pm h)\cos(s+1)\theta\Big) + \Big(s - 3 + 2\nu_j\Big)$$

$$\Big(A_{3j}(\pm h)\sin(s-1)\theta + A_{4j}(\pm h)\cos(s-1)\theta\Big)\Big] + 0\Big(r^{s+2}\Big)$$

$$U_{\theta j} = \frac{r^s}{2G_j s}\Big[\Big(A_{1j}(\pm h)\cos(s+1)\theta - A_{2j}(\pm h)\sin(s+1)\theta\Big) + \Big(s + 3 - 2\nu_j\Big)$$

$$\Big(A_{3j}(\pm h)\cos(s-1)\theta - A_{4j}(\pm h)\sin(s-1)\theta\Big)\Big] + 0\Big(r^{s+2}\Big)$$

$$\sigma_{rj} = r^{s-1}\Big[\Big(A_{1j}(\pm h)\sin(s+1)\theta + A_{2j}(\pm h)\cos(s+1)\theta\Big) + \Big(s - 3 - 2\nu_j\Big)$$

$$\Big(A_{3j}(\pm h)\sin(s-1)\theta + A_{4j}(\pm h)\cos(s-1)\theta\Big)\Big] + 0\Big(r^{s+1}\Big)$$

$$\sigma_{\theta j} = -r^{s-1}\Big[\Big(A_{1j}(\pm h)\sin(s+1)\theta + A_{2j}(\pm h)\cos(s+1)\theta\Big) + \Big(s + 1 + 2\nu_j\Big)$$

$$\Big(A_{3j}(\pm h)\sin(s-1)\theta + A_{4j}(\pm h)\cos(s-1)\theta\Big)\Big] + 0\Big(r^{s+1}\Big)$$

$$\tau_{\theta rj} = r^{s-1}\Big[\Big(A_{1j}(\pm h)\cos(s+1)\theta - A_{2j}(\pm h)\sin(s+1)\theta\Big) + (s-1)$$

$$\left(A_{3j}(\pm h)\cos(s-1)\theta - A_{4j}(\pm h)\sin(s-1)\theta\right)] + 0\left(r^{s+1}\right)$$

$$U_{zj} = 0\left(r^{s+1}\right), \qquad \sigma_{zj} = 0\left(r^{s+1}\right), \qquad \tau_{rzj} = 0\left(r^{s}\right), \quad \tau_{\theta zj} = 0\left(r^{s}\right), \tag{3.50}$$

where

$$A_{ij}(\pm h) = A_{ij}B_{2j}(\pm h), \qquad i = 1,2,3,4.$$

The solutions for stresses and displacements satisfy the boundary condition on the free plate surface. Substitution of equations (3.50) into equations (3.6) leads to the following equations:

$$A_{21}(\pm h) + (s + c_{21})A_{41}(\pm h) - k\left(A_{22}(\pm h) + (s + c_{22})A_{42}(\pm h)\right) = 0$$

$$A_{11}(\pm h) + (s - c_{21})A_{31}(\pm h) - k\left(A_{12}(\pm h) + (s - c_{22})A_{32}(\pm h)\right) = 0$$

$$A_{21}(\pm h) + (s + c_{11})A_{41}(\pm h) - \left(A_{22}(\pm h) + (s + c_{12})A_{42}(\pm h)\right) = 0$$

$$A_{11}(\pm h) + (s - 1)A_{31}(\pm h) - \left(A_{12}(\pm h) + (s - 1)A_{32}(\pm h)\right) = 0, \tag{3.51}$$

where

$$c_{1j} = 1 + 2\nu_j, \qquad c_{2j} = -3 + 2\nu_j \qquad j = 1,2$$

$$k = \frac{G_1}{G_2}. \tag{3.52}$$

Additionally, the expressions for stresses and displacements also need to satisfy the boundary conditions on the bimaterial wedge-side surfaces. The eigenvalues, which are

related to the strength of the stress singularity, can be obtained from these relations. Three combinations of boundary conditions are considered: clamped-clamped, clamped-free and free-free.

3.4.1 Clamped-Clamped

On substitution of equations (3.50) into equation (3.3), the following characteristic equations are obtained:

$$A_{11}(\pm h)\sin(s+1)\theta_0 + A_{21}(\pm h)\cos(s+1)\theta_0 +$$

$$(s+c_{21})\left(A_{31}(\pm h)\sin(s-1)\theta_0 + A_{41}(\pm h)\cos(s-1)\theta_0\right) = 0$$

$$A_{11}(\pm h)\cos(s+1)\theta_0 - A_{21}(\pm h)\sin(s+1)\theta_0 +$$

$$(s-c_{21})\left(A_{31}(\pm h)\cos(s-1)\theta_0 - A_{41}(\pm h)\sin(s-1)\theta_0\right) = 0$$

$$-A_{12}(\pm h)\sin(s+1)\theta_0 + A_{22}(\pm h)\cos(s+1)\theta_0 +$$

$$(s+c_{22})\left(-A_{32}(\pm h)\sin(s-1)\theta_0 + A_{42}(\pm h)\cos(s-1)\theta_0\right) = 0$$

$$A_{12}(\pm h)\cos(s+1)\theta_0 + A_{22}(\pm h)\sin(s+1)\theta_0 +$$

$$(s-c_{22})\left(A_{32}(\pm h)\cos(s-1)\theta_0 + A_{42}(\pm h)\sin(s-1)\theta_0\right) = 0. \qquad (3.53)$$

In the special case of $\theta_0=\pm\pi$, the above system of eight homogeneous algebraic equations, given by equations (3.51) and (3.53), reduce to one characteristic equation, given as follows:

$$\cot^2 s\pi = c, \tag{3.54}$$

where

$$c = \frac{\left(c_{21}(1+c_{22}) - kc_{22}(1+c_{21})\right)\left(c_{21}(c_{12}+c_{22}) - kc_{22}(c_{11}+c_{21})\right)}{\left(kc_{22}(1-c_{21}) + c_{21}(1-c_{22})\right)\left(kc_{22}(c_{21}-c_{11}) + c_{21}(c_{22}-c_{12})\right)}. \tag{3.55}$$

Equation (3.54) leads to two different eigenvalues. If $c \geq 0$, the oscillatory character of the stresses disappears, and the eigenvalue is given by

$$s = \frac{\cot^{-1}\left(\sqrt{c}\right)}{\pi}. \tag{3.56}$$

If $c<0$, the oscillatory character of the stresses is recovered

$$s = \frac{1}{2} \pm i\varepsilon \tag{3.57}$$

$$\varepsilon = \frac{1}{2\pi} \ln\left(\frac{1-\sqrt{c}}{1+\sqrt{c}}\right), \tag{3.58}$$

where ε is the imaginary part of a complex root, implying the oscillatory character at the front of the bimaterial slit along the interface. In the special case of a homogeneous wedge, given by $E_1=E_2$, and $v_1=v_2$, the imaginary part, ε, representing the oscillatory character vanishes.

3.4.2 Clamped-Free

Substitution of equations (3.50) into equations (3.4) and (3.5) leads to the following characteristic equations:

$$A_{11}(\pm h)\sin(s+1)\theta_0 + A_{21}(\pm h)\cos(s+1)\theta_0 +$$

$$(s+c_{11})\left(A_{31}(\pm h)\sin(s-1)\theta_0 + A_{41}(\pm h)\cos(s-1)\theta_0\right) = 0$$

$$A_{11}(\pm h)\cos(s+1)\theta_0 - A_{21}(\pm h)\sin(s+1)\theta_0 +$$

$$(s-1)\left(A_{31}(\pm h)\cos(s-1)\theta_0 - A_{41}(\pm h)\sin(s-1)\theta_0\right) = 0$$

$$-A_{12}(\pm h)\sin(s+1)\theta_0 + A_{22}(\pm h)\cos(s+1)\theta_0 +$$

$$(s+c_{22})\left(-A_{32}(\pm h)\sin(s-1)\theta_0 + A_{42}(\pm h)\cos(s-1)\theta_0\right) = 0$$

$$A_{12}(\pm h)\cos(s+1)\theta_0 + A_{22}(\pm h)\sin(s+1)\theta_0 +$$

$$(s-c_{22})\left(A_{32}(\pm h)\cos(s-1)\theta_0 + A_{42}(\pm h)\sin(s-1)\theta_0\right) = 0. \qquad (3.59)$$

3.4.3 Free-Free

Substitution of equations (3.50) into equations (3.2) yields the following characteristic equations:

$$A_{11}(\pm h)\sin(s+1)\theta_0 + A_{21}(\pm h)\cos(s+1)\theta_0 +$$

$$(s+c_{11})\left(A_{31}(\pm h)\sin(s-1)\theta_0 + A_{41}(\pm h)\cos(s-1)\theta_0\right) = 0$$

$$A_{11}(\pm h)\cos(s+1)\theta_0 - A_{21}(\pm h)\sin(s+1)\theta_0 +$$

$$(s-1)\left(A_{31}(\pm h)\cos(s-1)\theta_0 - A_{41}(\pm h)\sin(s-1)\theta_0\right) = 0$$

$$-A_{12}(\pm h)\sin(s+1)\theta_0 + A_{22}(\pm h)\cos(s+1)\theta_0 +$$

$$(s+c_{12})\left(-A_{32}(\pm h)\sin(s-1)\theta_0 + A_{42}(\pm h)\cos(s-1)\theta_0\right) = 0$$

$$A_{12}(\pm h)\cos(s+1)\theta_0 + A_{22}(\pm h)\sin(s+1)\theta_0 +$$

$$(s-1)\left(A_{32}(\pm h)\cos(s-1)\theta_0 + A_{42}(\pm h)\sin(s-1)\theta_0\right) = 0. \tag{3.60}$$

In the special case of a semiinfinite crack along the bimaterial interface, $\theta_0=\pm\pi$, the above system of eight homogeneous algebraic equations, given by equations (3.51) and (3.60), reduce to one characteristic equation, given as follows:

$$\cot^2 s\pi + L = 0, \tag{3.61}$$

where

$$L = \frac{(D_3+D_4)(c_{12}D_1 - D_2)}{(D_1+D_2+c_{12}+1)(c_{12}D_3 - D_4 + c_{12}+1)} = \frac{L_1 \cdot L_2}{L_3 \cdot L_4} \tag{3.62}$$

$$L_1 = D_3 + D_4 \qquad L_2 = c_{12}D_1 - D_2$$

$$L_3 = D_1 + D_2 + c_{12} + 1 \qquad L_4 = c_{12}D_3 - D_4 + c_{12} + 1$$

$$D_1 = \frac{k - c_{21} + c_{11}(k-1)}{1 - c_{21}}, \qquad D_2 = \frac{c_{21} + c_{11} - kc_{22}(c_{11}+1)}{1 - c_{21}}$$

$$D_3 = \frac{c_{21} + 1 - k(c_{11}+1)}{c_{21} - c_{11}}, \qquad D_4 = \frac{c_{12}(1+c_{21}) - kc_{22}(c_{11}+1)}{c_{21} - c_{11}}.$$

Equation (3.61) can result in two different eigenvalues. If equation (3.64) is satisfied, the oscillatory character of stresses disappears, and the eigenvalues are

$$s = \frac{\cot^{-1}\left(\sqrt{-L}\right)}{\pi} \tag{3.63}$$

$$\frac{1}{2} \le \left(\frac{\nu_1 - \nu_2 g}{1-g}\right) \le 1, \tag{3.64}$$

where

$$g = \frac{E_1}{E_2}.$$

The eigenvalues for $\nu_2 = 0.5$ and various g values are shown in Figure 3.2 with respect to ν_1. At g=1, the oscillatory character appears for all ν_1 values shown in the plot whereas for g=1.5, the oscillatory character appears in some ν_1 area. At g=5 and beyond (e. g., g=50), the oscillatory character disappears for all ν_1 values shown in the plot keeping the eigenvalues independent of the ratio, g. It is further noteworthy that disappearance of the oscillatory character renders the eigenvalue to become smaller than 0.5. The oscillatory character of the stresses is recovered when equation (3.64) is not satisfied

$$s = \frac{1}{2} \pm i\varepsilon \tag{3.65}$$

$$\varepsilon = \frac{1}{2\pi} \ln\left(\frac{1-\sqrt{L}}{1+\sqrt{L}}\right), \tag{3.66}$$

where ε is the imaginary part of eigenvalue, implying an oscillatory nature of the stresses near the front of the bimaterial slit along the interface. In the special case of a

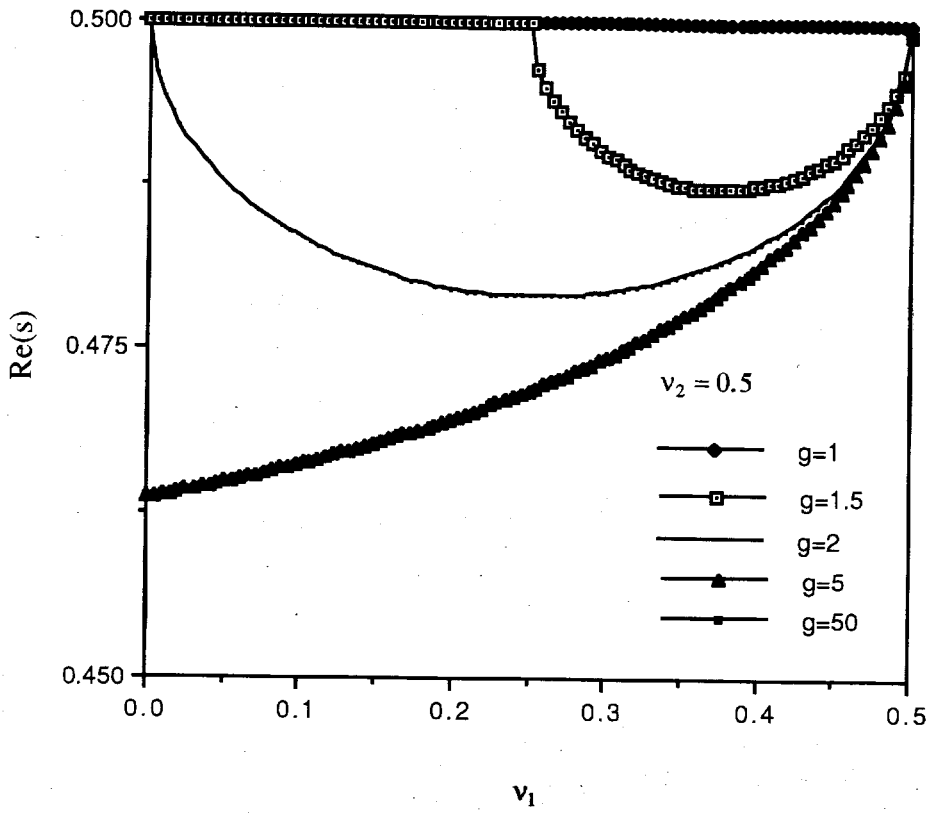

Figure 3.2 Variation of the lowest real eigenvalue with respect to the Poisson's ratio of material 1(ν_1), for various g=E_1/E_2.

homogeneous wedge, given by $E_1=E_2$, and $\nu_1=\nu_2$, the imaginary part, ε, representing the oscillatory character vanishes. The relationship of coefficients is expressed as follows:

$$\begin{Bmatrix} A_{12} \\ A_{22} \\ A_{32} \end{Bmatrix} = \begin{Bmatrix} \dfrac{L_4\left(L_2-(s+c_{22})(1+D_1)\right)\cot s\pi}{(1+D_3)L_2} \\ -\left(s+\dfrac{D_4-1}{D_3+1}\right) \\ \dfrac{(1+D_1)L_4\cot s\pi}{(1+D_3)L_2} \end{Bmatrix} A_{42} = \begin{Bmatrix} f_{r12}+if_{c12} \\ f_{r22}+if_{c22} \\ f_{r32}+if_{c32} \end{Bmatrix} A_{42}. \tag{3.67}$$

The nonoscillatory asymptotic stress fields in the vicinity of the front of a semiinfinite crack along the bimaterial interface, confined to the interior region, are given as follows:

$$\sigma_{r2} = -\frac{r^{s-1}K_I}{\sqrt{2\pi}\left(f_{r22}+(s+1+2\nu_2)\right)}\left(f_{r12}\sin(s+1)\theta + f_{r22}\cos(s+1)\theta + \right.$$

$$\left.(s-3-2\nu_2)\left(f_{r32}\sin(s-1)\theta+\cos(s-1)\theta\right)\right.$$

$$\sigma_{\theta 2} = \frac{r^{s-1}K_I}{\sqrt{2\pi}\left(f_{r22}+(s+1+2\nu_2)\right)}\left(f_{r12}\sin(s+1)\theta + f_{r22}\cos(s+1)\theta + \right.$$

$$\left.(s+1+2\nu_2)\left(f_{r32}\sin(s-1)\theta+\cos(s-1)\theta\right)\right.$$

$$\tau_{r\theta 2} = \frac{r^{s-1}K_{II}}{\sqrt{2\pi}\left(f_{r12}+(s-1)f_{32}\right)}\left(f_{r12}\cos(s+1)\theta - f_{r22}\sin(s+1)\theta + \right.$$

$$\left.(s-1)\left(f_{r32}\cos(s-1)\theta-\sin(s-1)\theta\right),\right. \tag{3.68}$$

where

$$K_I = K_{Is}+K_{Ia} = -\sqrt{2\pi}\left(f_{r22}+(s+1+2\nu_2)\right)A_{42}\left(B_{22s}(\pm h)+B_{22a}(\pm h)\right) \tag{3.69}$$

$$K_{II} = K_{IIs} + K_{IIa} = \sqrt{2\pi}\left(f_{r12} + (s-1)f_{r32}\right)A_{42}\left(B_{22s}(\pm h) + B_{22a}(\pm h)\right). \tag{3.70}$$

The asymptotic oscillatory stress fields in the vicinity of the front of a semiinfinite crack along the bimaterial interface, confined to the interior region, are given as follows:

$$\sigma_{r2} = R_e \frac{r^{i\varepsilon}(1+D_3)}{\sqrt{2\pi r}}\left(\left(f_{r12} + if_{c12}\right)\sin\left(\frac{3}{2} + i\varepsilon\right)\theta + \left(f_{r22} + if_{c22}\right)\cos\left(\frac{3}{2} + i\varepsilon\right)\theta -\right.$$

$$\left.\left(\frac{5}{2} + 2\nu_2 - i\varepsilon\right)\left(\left(f_{r32} + if_{c32}\right)\sin\left(-\frac{1}{2} + i\varepsilon\right)\theta + \cos\left(-\frac{1}{2} + i\varepsilon\right)\theta\right)\right)\left(-\frac{K_I}{L_4} + i\frac{\sqrt{L}K_{II}}{(D_3 + D_4)}\right)$$

$$\sigma_{\theta 2} = -R_e \frac{r^{i\varepsilon}(1+D_3)}{\sqrt{2\pi r}}\left(\left(f_{r12} + if_{c12}\right)\sin\left(\frac{3}{2} + i\varepsilon\right)\theta + \left(f_{r22} + if_{c22}\right)\cos\left(\frac{3}{2} + i\varepsilon\right)\theta +\right.$$

$$\left.\left(\frac{3}{2} + 2\nu_2 + i\varepsilon\right)\left(\left(f_{r32} + if_{c32}\right)\sin\left(-\frac{1}{2} + i\varepsilon\right)\theta + \cos\left(-\frac{1}{2} + i\varepsilon\right)\theta\right)\right)\left(-\frac{K_I}{L_4} + i\frac{\sqrt{L}K_{II}}{(D_3 + D_4)}\right)$$

$$\tau_{r\theta 2} = R_e \frac{r^{i\varepsilon}(1+D_3)}{\sqrt{2\pi r}}\left(\left(f_{r12} + if_{c12}\right)\cos\left(\frac{3}{2} + i\varepsilon\right)\theta - \left(f_{r22} + if_{c22}\right)\sin\left(\frac{3}{2} + i\varepsilon\right)\theta -\right.$$

$$\left.\left(\frac{1}{2} - i\varepsilon\right)\left(\left(f_{r32} + if_{c32}\right)\cos\left(-\frac{1}{2} + i\varepsilon\right)\theta - \sin\left(-\frac{1}{2} + i\varepsilon\right)\theta\right)\right)\left(-\frac{K_I}{L_4} + i\frac{\sqrt{L}K_{II}}{(D_3 + D_4)}\right), \tag{3.71}$$

where

$$K_I = K_{Is} + K_{Ia} = -\sqrt{2\pi}\left(\frac{L_4}{1+D_3}\right)a_{42}\left(B_{22s}(\pm h) + B_{22a}(\pm h)\right) \tag{3.72}$$

$$K_{II} = K_{IIs} + K_{IIa} = \sqrt{\frac{2\pi}{L}}\left(\frac{(D_4 + D_3)}{(1+D_3)}\right)\bar{a}_{42}\left(B_{22s}(\pm h) + B_{22a}(\pm h)\right). \tag{3.73}$$

K_{Is} and K_{IIs} are symmetric stress intensity factors. K_{Ia} and K_{IIa} are antisymmetric stress intensity factors.

3.5 Results and Discussions

The eigenequations for the interior or surface region for the different boundary conditions can be written down into the form:

$$[\Delta(s)]\{A_{ij}\} = 0. \tag{3.73}$$

The existence of a nontrivial solution for A_{ij} requires vanishing of the coefficient determinant

$$|\Delta(s)| = 0. \tag{3.74}$$

$\Delta(s)$ is a 8*8 matrix involving s in a transcendental form. Thus, equation (3.74) is a transcendental characteristic equation for a standard eigenvalue problem. A physically meaningful solution is

$$0 < R_e(s) < 1. \tag{3.75}$$

3.5.1 Clamped-Clamped

3.5.1.1 Interior Region

The variation of the lowest real part of the eigenvalue for the interior region with respect to the included angle, θ_0, is plotted in Figure 3.3 with $\nu_1=\nu_2=0.3$, and various k. It is interesting to note that the lowest real part of the eigenvalue, computed for, for k=10, and k=100, does not decrease monotonically with respect to the included angle, θ_0. It is due to the effect of the imaginary part. The relationship of the real and imaginary parts is displayed in Figure 3.4. Like a homogeneous wedge with free-clamped boundary

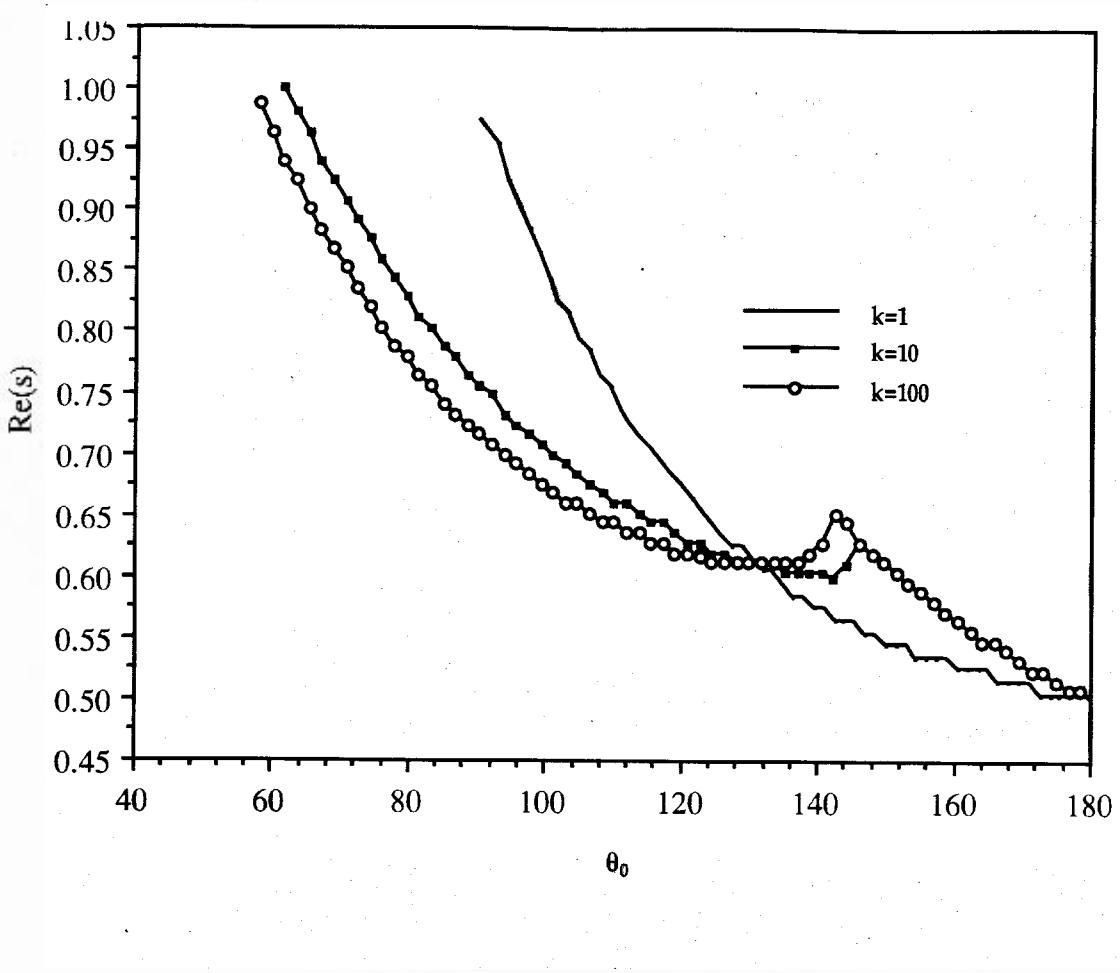

Figure 3.3 Variation of the lowest real eigenvalue in interior region with respect to wedge angle, for a clamped-clamped with $\nu_1=\nu_2=0.3$ and $k=G_1/G_2$.

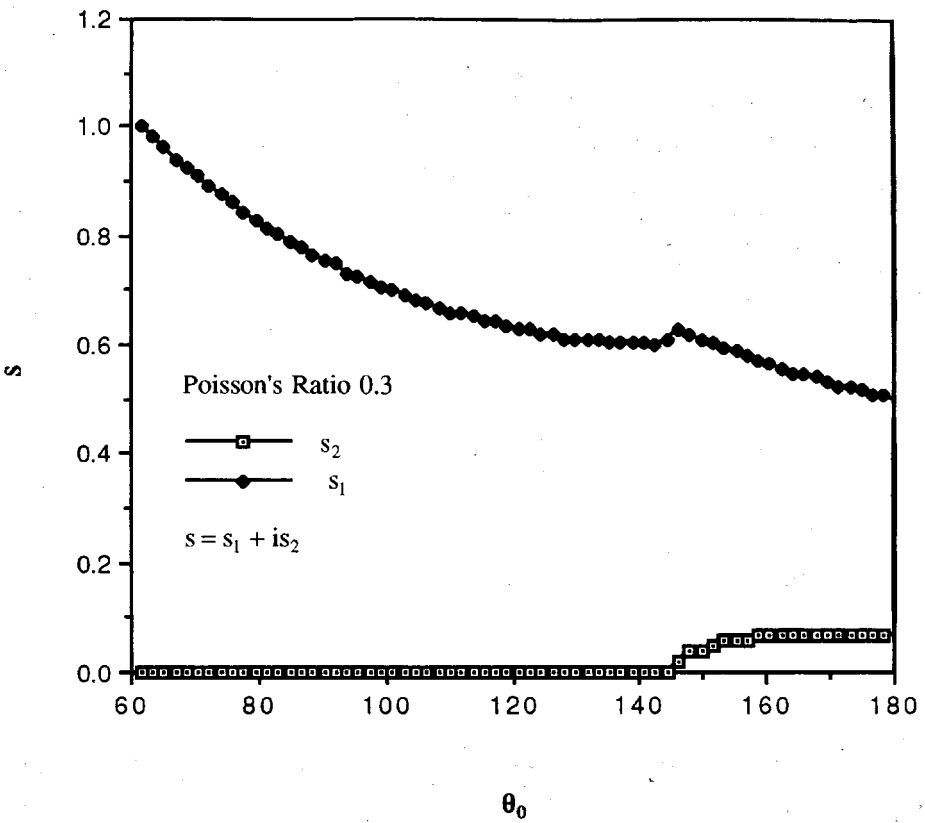

Figure 3.4 Variation of the imaginary and lowest real parts of eigenvalue in the interior region of a bimaterial clamped-clamped wedge with respect to the wedge angle.

condition, the occurrence of the nonvanishing imaginary part starting at $\theta_0 = 146^0$ is accompanied by the appearance of a clearly visible cusp in the real part at the same, θ_0 . In contrast, the lowest real part of the eigenvalue, computed for k=1, decreases monotonically with the increase of the included angle, θ_0, because the computed eigenvalue in this case is always real. The phenomenon that monotonicity of the lowest real part of the eigenvalue is disturbed by the appearance of the imaginary part happens not only for a clamped-clamped edge, but is also found for free-free and free-clamped edges. The variation of the lowest real part of the eigenvalue with $\nu_1=\nu_2=0.5$ and for various k values, with respect to the included angle, θ_0, is shown in Figure 3.5. Because the computed eigenvalues for $\nu_1=\nu_2=0.5$ are always real, they decrease monotonically as k and θ_0 increase. The lowest real part of the eigenvalue with $\nu_1=0.3$, $\nu_2=0.5$ and for various k values is depicted in Figure 3.6.

3.5.1.2 Surface Region

The variation of the lowest real part of the eigenvalue for the surface region with respect to the included angle, θ_0, is shown in Figure 3.7 with $\nu_1=\nu_2=0.3$, and for various k values. Trends are similar to those for the interior region shown in Figure 3.3 with $\nu_1=\nu_2=0.3$, and for various k values. Figure 3.8 shows the lowest real part of the eigenvalue with $\nu_1=\nu_2=0.5$, and various k. Also it is similar to the results of Figure 3.5 computed for $\nu_1=\nu_2=0.5$, and various k values. The lowest real part of the eigenvalue, for $\nu_1=0.3$, $\nu_2=0.5$ and various k values, is shown in Figure 3.9.

Comparisons of the lowest real part of the eigenvalue for the interior region, surface region, and antiplane shear loading are illustrated in Figure 3.10 with k=10. In the range of angle, $\theta_0 = 0^0 - \pm 140^0$, the largest eigenvalue arises from the antiplane shear loading. The smallest eigenvalue occurs for the interior region. As Poisson's ratio increases, the lowest real part of the eigenvalue decreases except for some local range of the included angle, θ_0, affected by the imaginary part.

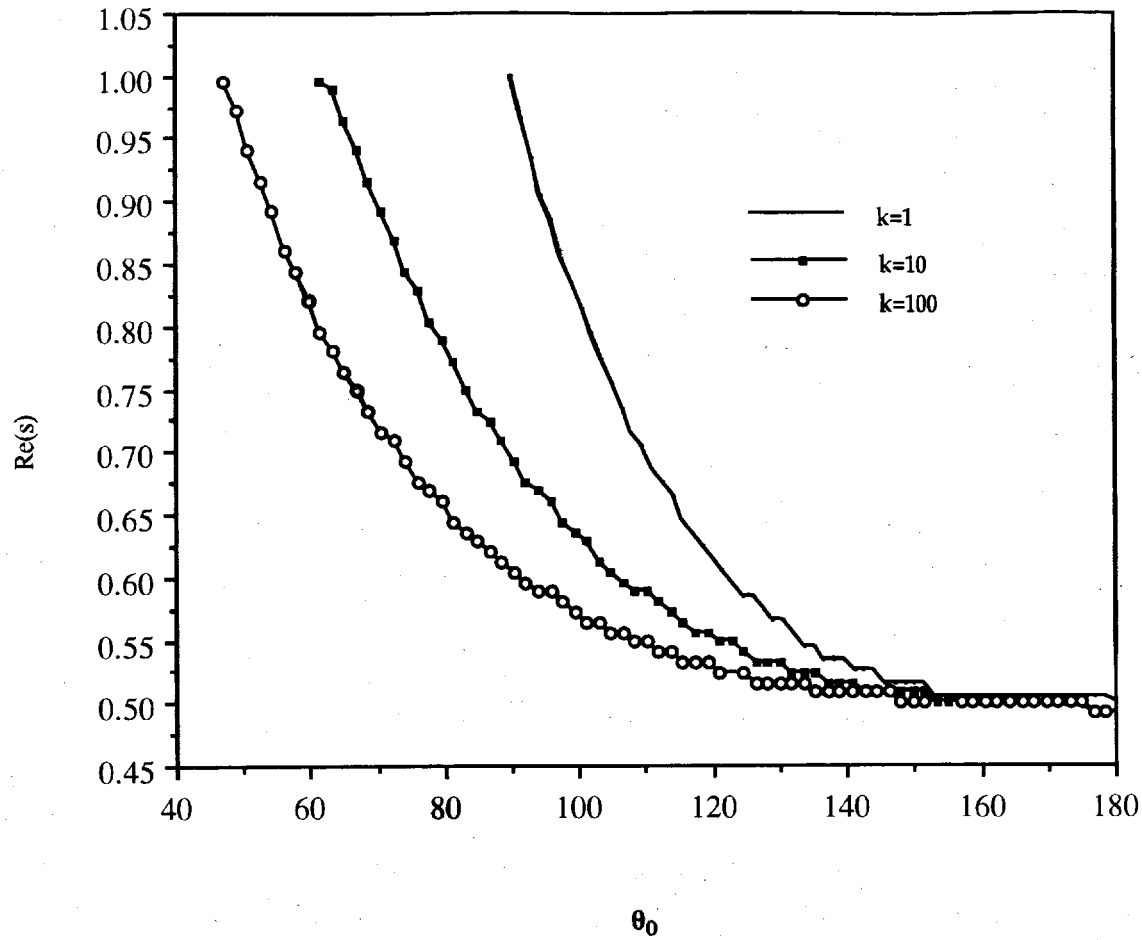

Figure 3.5 Variation of the lowest real eigenvalue in interior region with respect to wedge angle, for a clamped-clamped bimaterial wedge where $\nu_1=\nu_2=0.5$ and $k=G_1/G_2$.

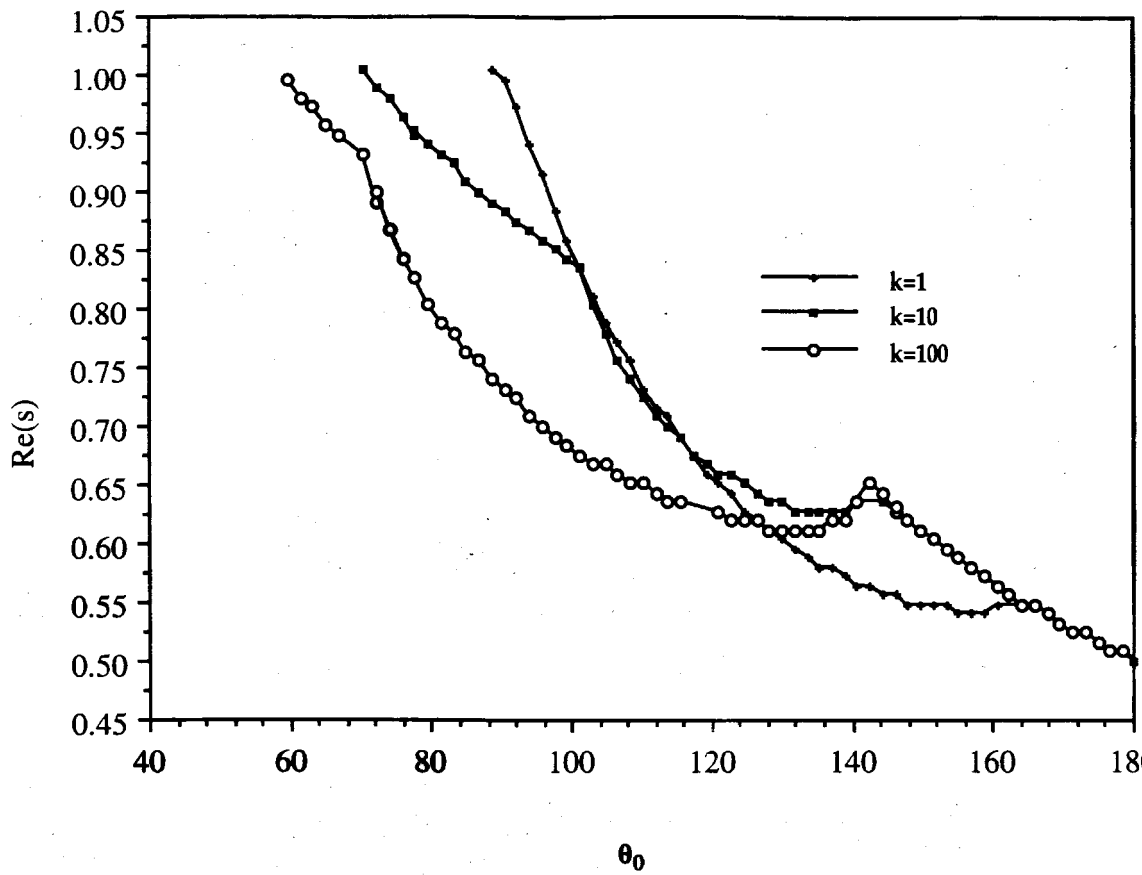

Figure 3.6 Variation of the lowest real eigenvalue in interior region with respect to wedge angle, for a clamped-clamped bimaterial wedge where ν_1=0.3, ν_2=0.5 and k=G_1/G_2.

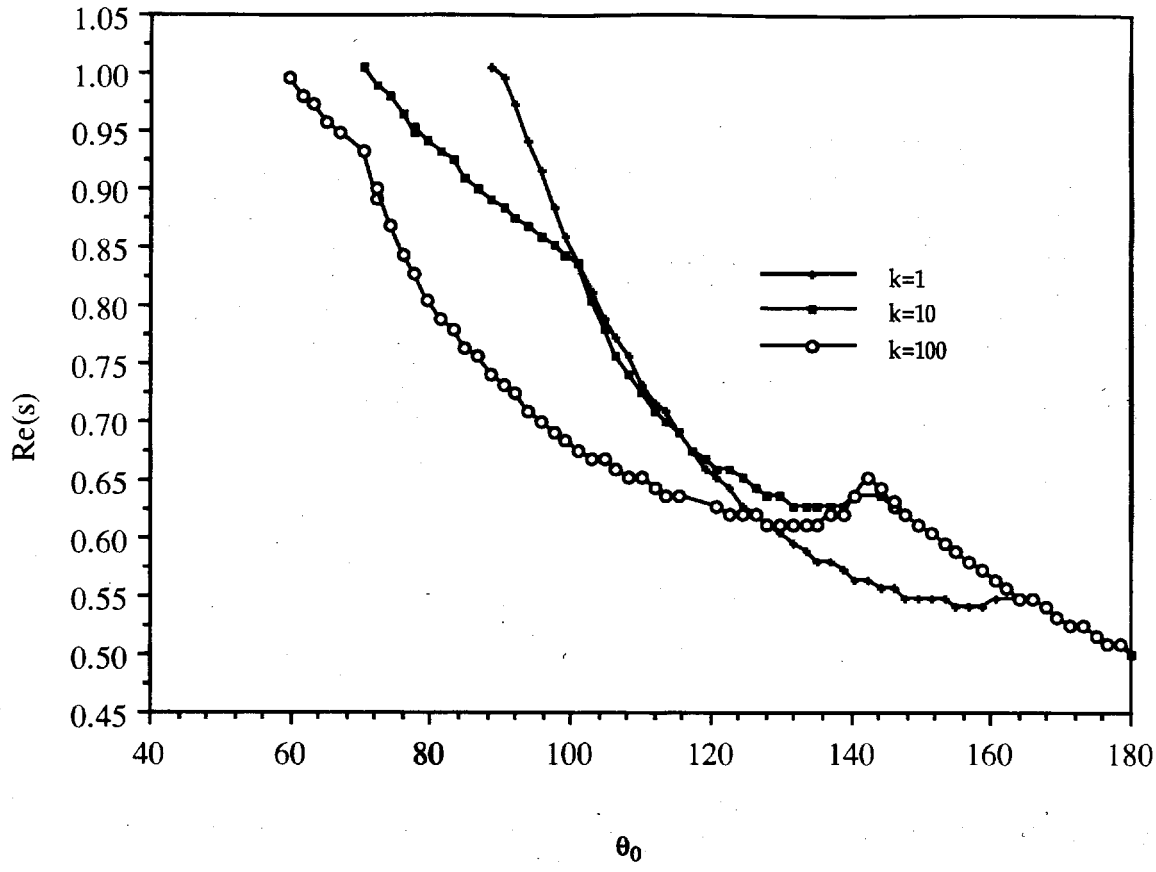

Figure 3.7 Variation of the lowest real eigenvalue on surface region with respect to wedge angle, for a clamped-clamped bimaterial wedge where $\nu_1=\nu_2=0.3$ and $k=G_1/G_2$.

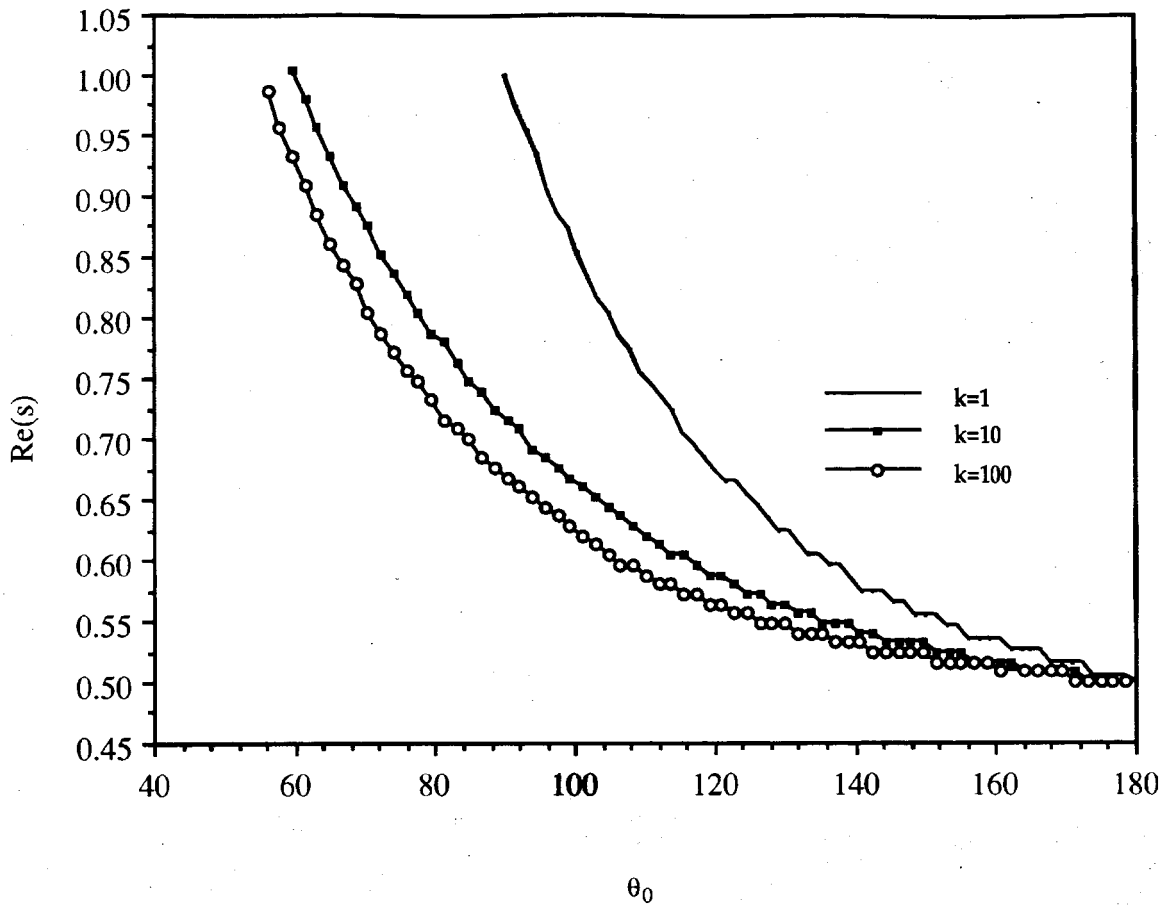

Figure 3.8 Variation of the lowest real eigenvalue on surface region with respect to wedge angle, for a clamped-clamped bimaterial wedge where $\nu_1=\nu_2=0.5$ and $k=G_1/G_2$.

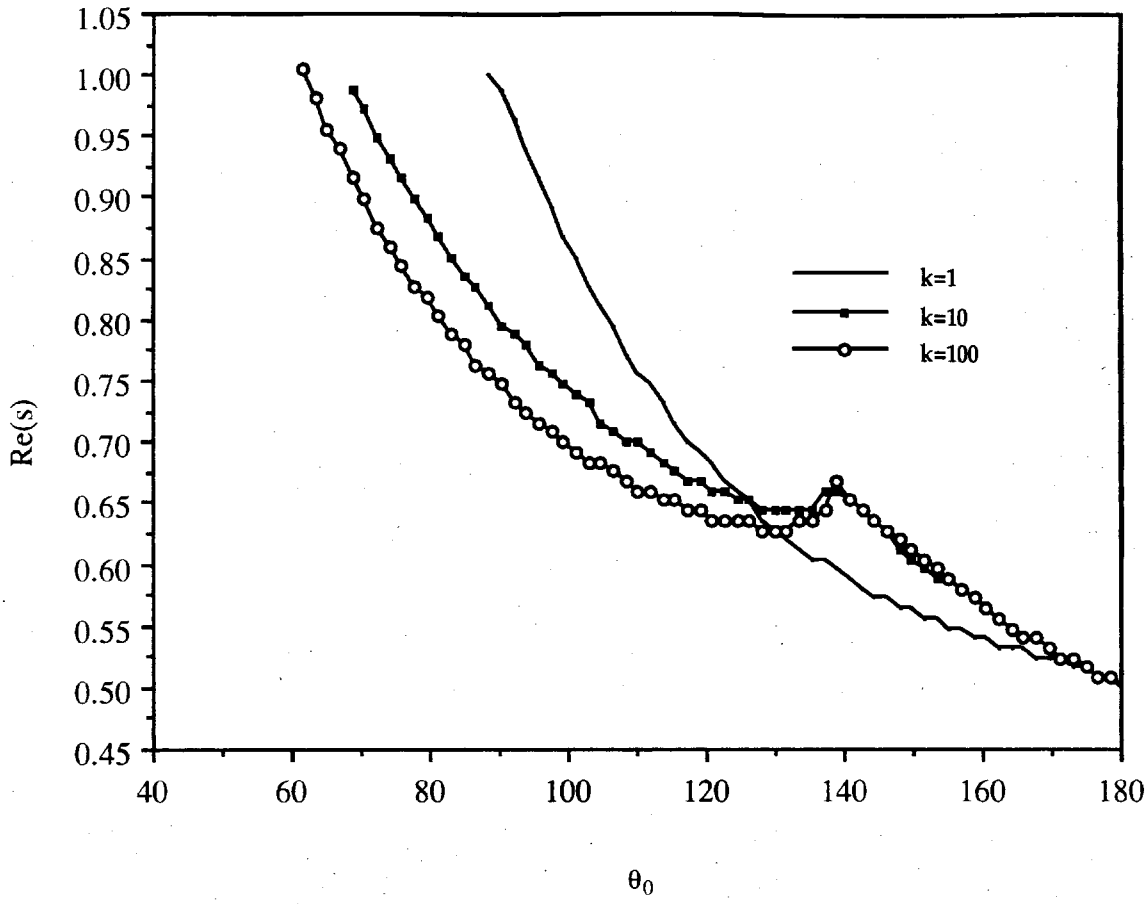

Figure 3.9 Variation of the lowest real eigenvalue on surface region with respect to wedge angle, for a clamped-clamped bimaterial wedge where ν_1=0.3, ν_2=0.5 and k=G_1/G_2.

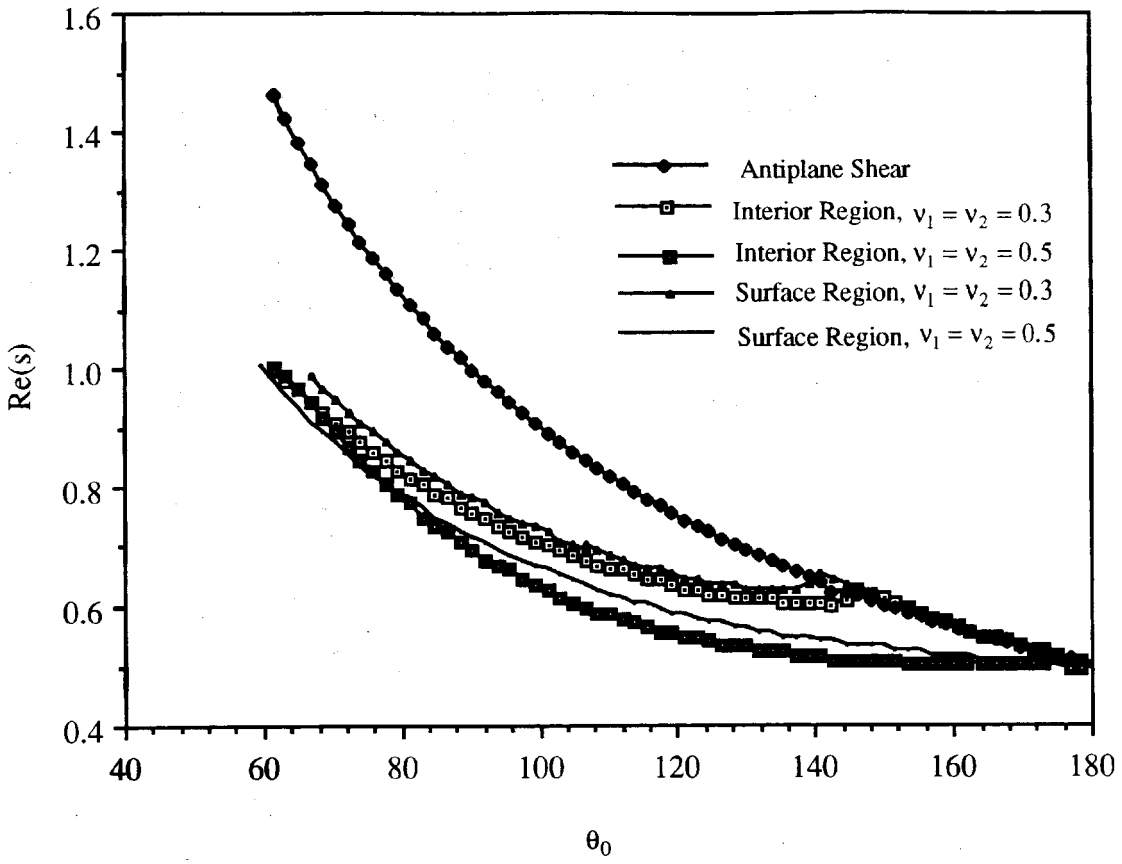

Figure 3.10 Variation of the lowest real eigenvalue for a clamped-clamped bimaterial wedge with respect to wedge angle, $k=G_1/G_2=10$.

3.5.2 Free-Clamped

3.5.2.1 Interior Region

The lowest real part of the eigenvalue with $\nu_1=\nu_2=0.3$ and various k values is shown in Figure 3.11. The lowest real part of the eigenvalue decreases as both angle, θ_0, and k increase except for in some local region affected by the imaginary part. The lowest real part of the eigenvalue depends heavily on the shear modulus ratio, k, of the two materials. The same trend continues for $\nu_1=\nu_2=0.5$ (Figure 3.12), and $\nu_1=0.3$, $\nu_2=0.5$ (Figure 3.13). The lowest real part of the eigenvalue decreases as θ_0 and k increase except for some local range of the included angle, affected by the imaginary part. The relationship of the lowest real part of the eigenvalue with respect to Poisson's ratio and shear modulus ratio, k, is also shown in Table 3.1. As k increases, the most severe stress singularity occurs in the vicinity of the bimaterial wedge front.

3.5.2.2 Surface Region

The lowest real part of the eigenvalue for the surface region is similar to its interior region counterpart (Figures 3.14, 3.15, and 3.16). The dependence of this eigenvalue on

3.1 Comparison of the lowest real part of the eigenvalue
for the interior region from different property, $\theta_0=\pi$

	$\nu_1=\nu_2=0.3$	$\nu_1=\nu_2=0.5$	$\nu_1=0.3,\nu_2=0.5$
k=0.1	0.400	0.4504	0.4258
k=1	0.25	0.25	0.2724
k=10	0.09415	0.08425	0.10900

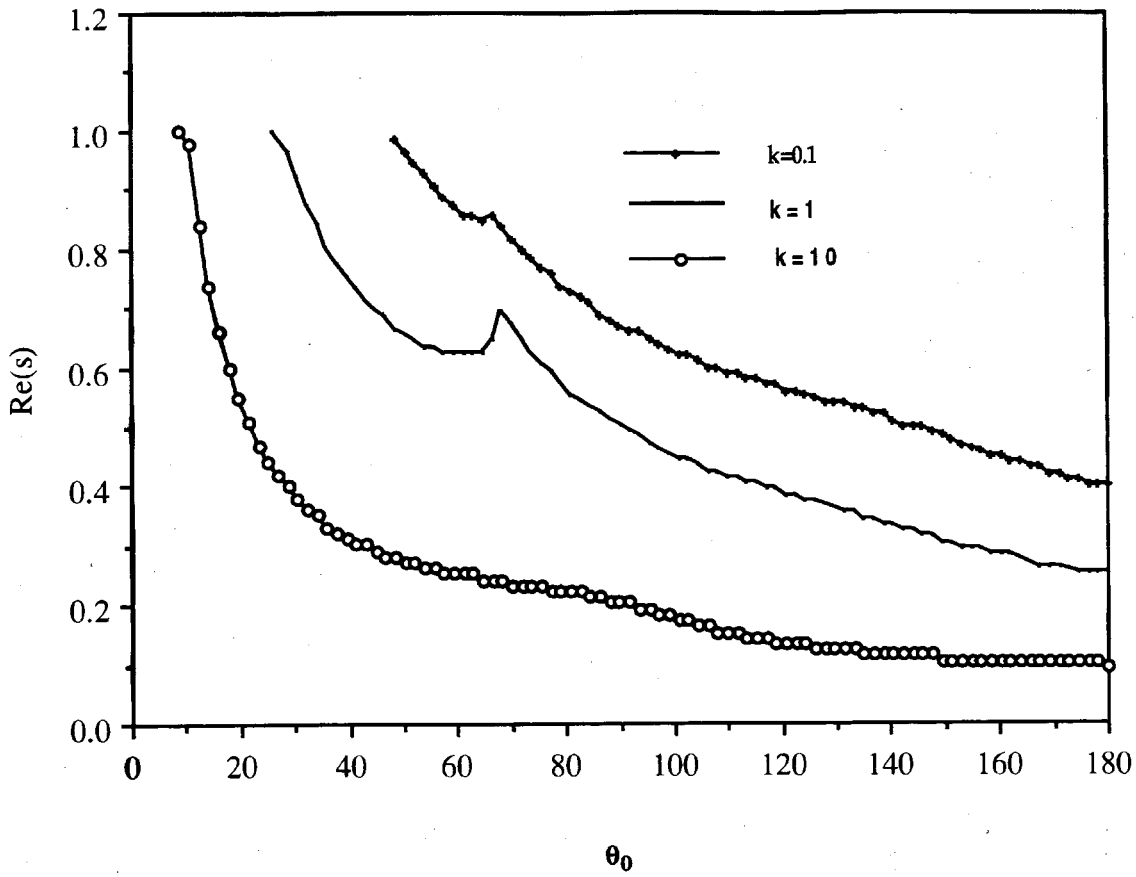

Figure 3.11 Variation of the lowest real eigenvalue in interior region with respect to wedge angle, for a free-clamped bimaterial wedge with $\nu_1=\nu_2=0.3$ and $k=G_1/G_2$.

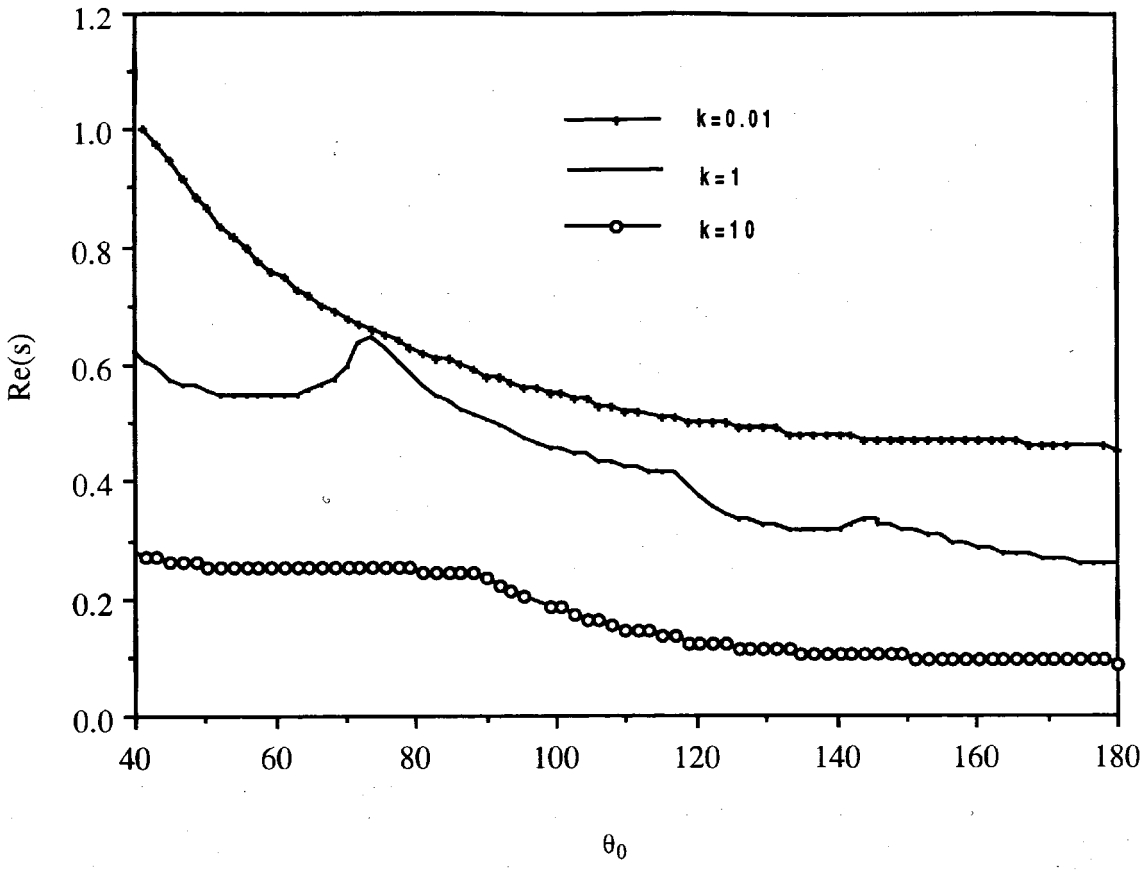

Figure 3.12 Variation of the lowest real eigenvalue in interior region with respect to wedge angle, for a free-clamped bimaterial wedge where $\nu_1=\nu_2=0.5$ and $k=G_1/G_2$.

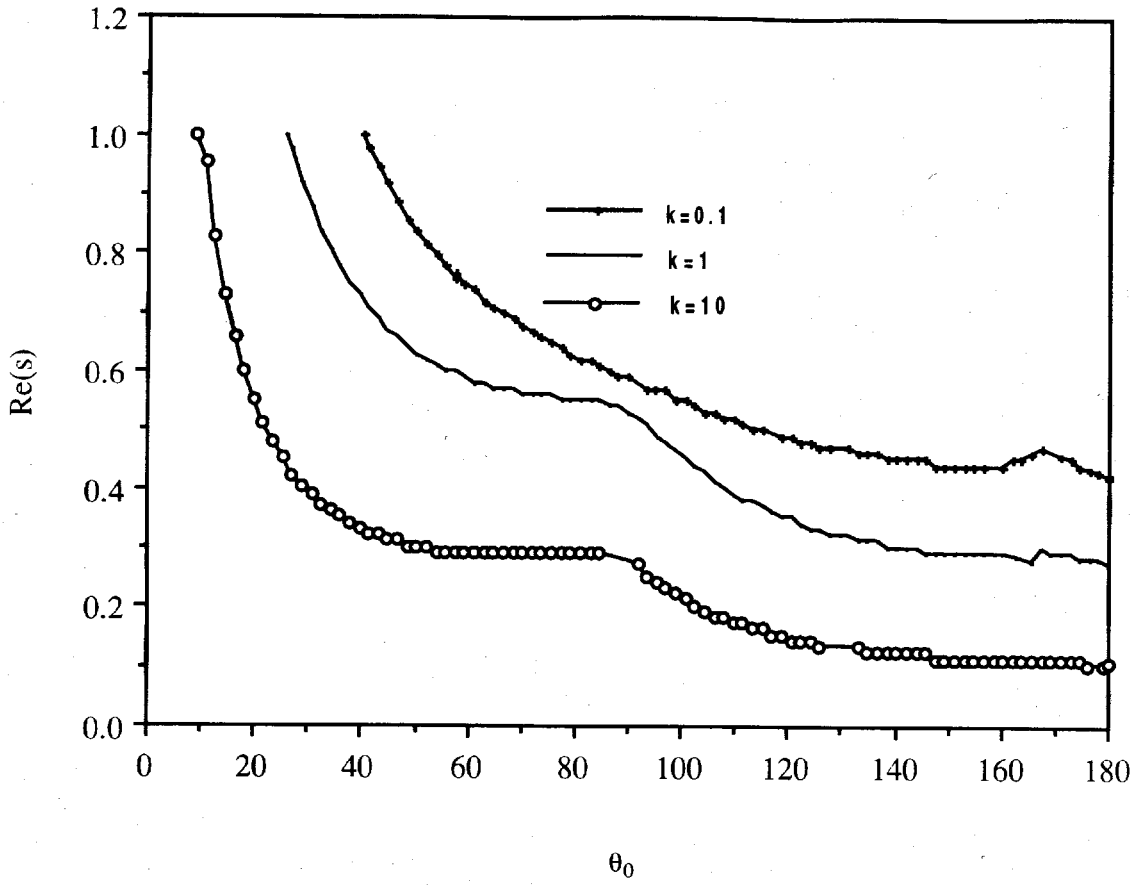

Figure 3.13 Variation of the lowest real eigenvalue in interior region with respect to wedge angle, for a free-clamped bimaterial wedge where ν_1=0.3, ν_2=0.5 and k=G_1/G_2.

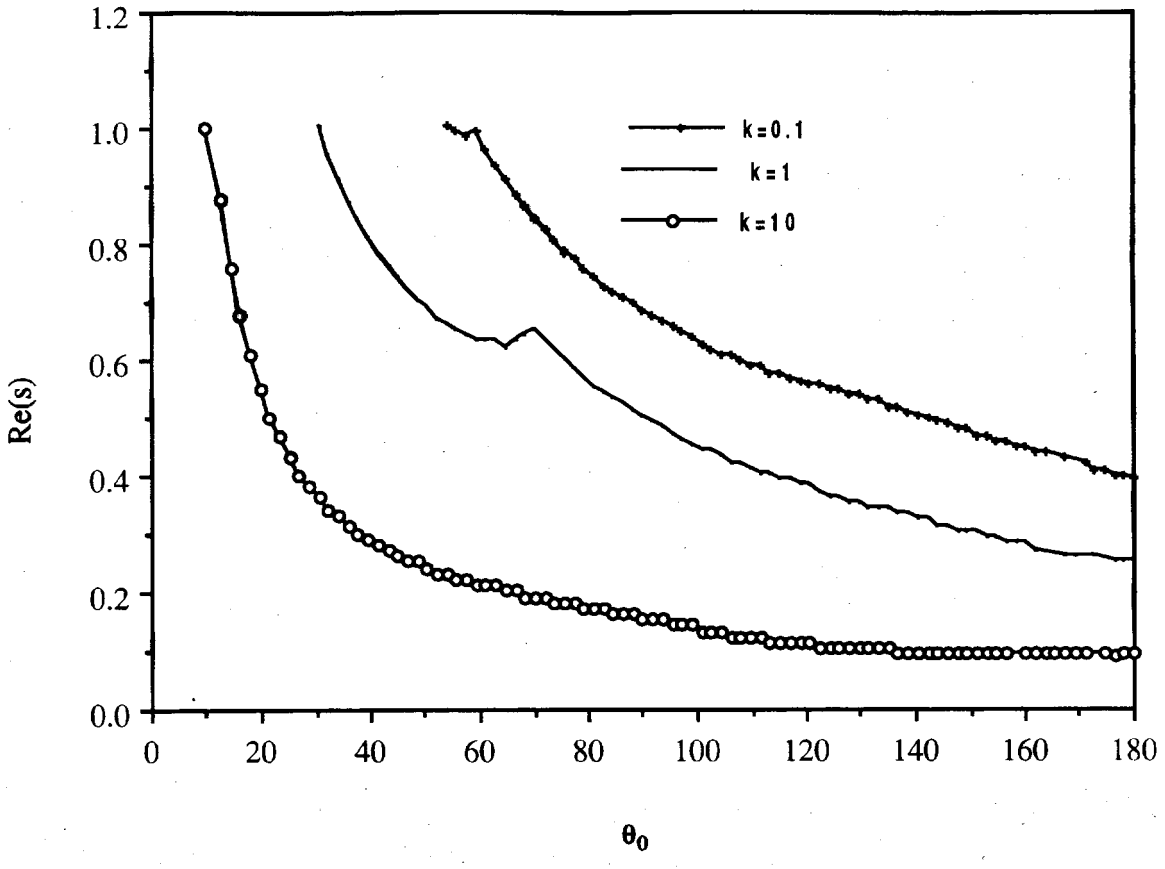

Figure 3.14 Variation of the lowest real eigenvalue on surface region with respect to wedge angle, for a free-clamped bimaterial wedge with $\nu_1=\nu_2=0.3$ and $k=G_1/G_2$.

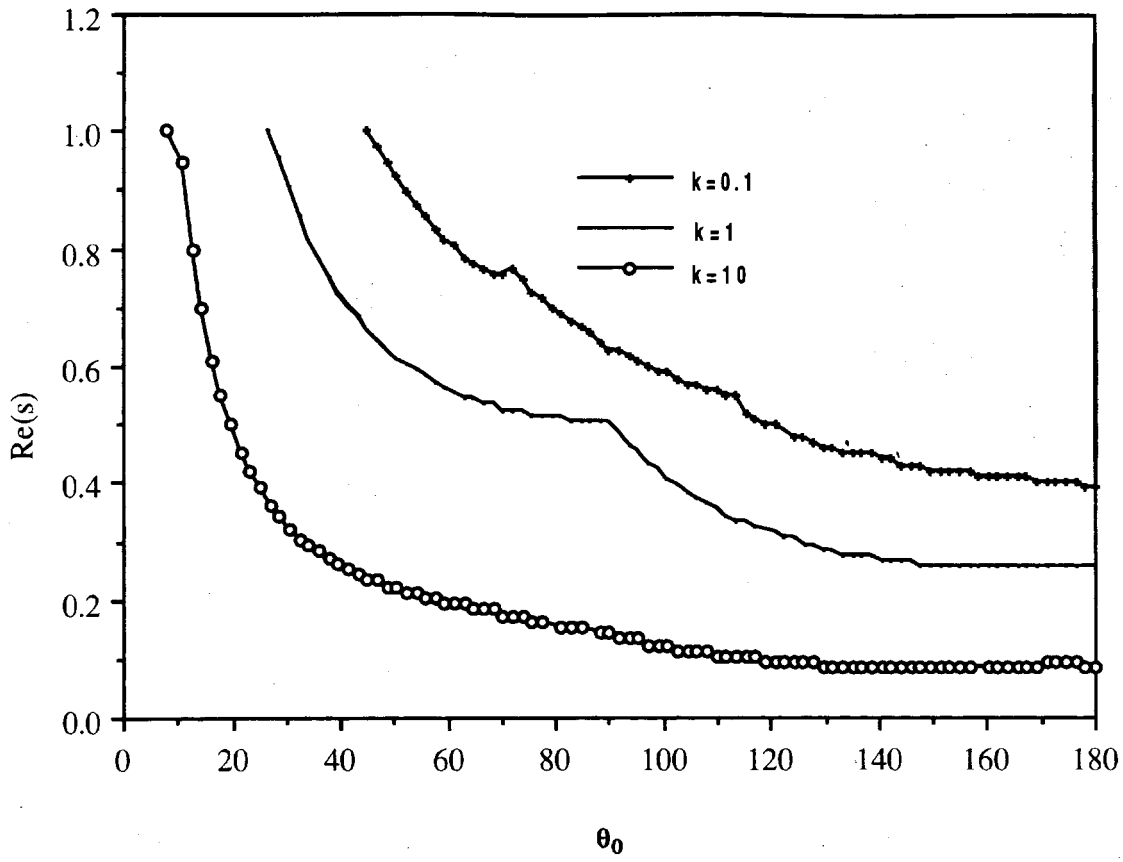

Figure 3.15 Variation of the lowest real eigenvalue on surface region with respect to wedge angle, for a free-clamped bimaterial wedge with $\nu_1=\nu_2=0.5$ and $k=G_1/G_2$.

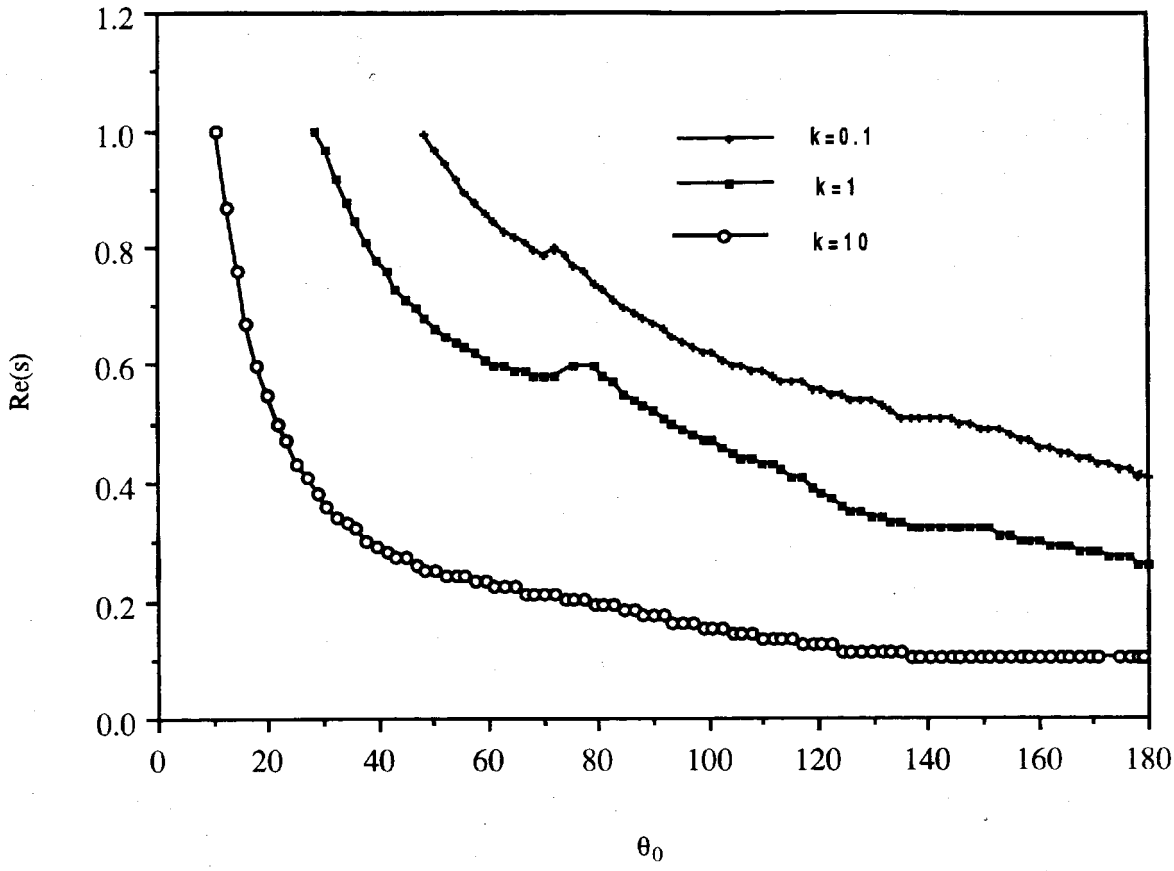

Figure 3.16 Variation of the lowest real eigenvalue on surface region with respect to wedge angle, for a free-clamped bimaterial wedge with ν_1=0.3, ν_2=0.5 and k=G_1/G_2.

material properties, such as the Poisson's ratio and shear modulus ratio, k, is shown in Table 3.2.

Comparison of Table 3.1 with the Table 3.2 shows that the lowest real part of the eigenvalue on the surface region is smaller than that in the interior region for k=0.1. However, the lowest real parts of the eigenvalue, computed using k=10, for both the regions are almost identical. Comparisons of the lowest real part of the eigenvalue for the interior region, surface region, and antiplane shear loading are shown in Figure 3.17 with k=10. The lowest real part of the eigenvalue, computed for all the cases, is nearly identical. The only exception is the eigenvalue for the antiplane shear loading, which is significantly different from the rest in the range of $\theta_0 = 10^0$ to 60^0.

3.5.3 Free-Free

3.5.3.1 Interior Region

Variation of the lowest real part of the eigenvalue for the interior region with respect to the included angle, θ_0, is plotted in Figure 3.18 with $\nu_1=\nu_2=0.3$, and various k values. As in the case of the clamped-clamped boundary condition discussed above, the lowest real part of the eigenvalue k=10, and k=100 does not decrease monotonically due to the effect of imaginary part. The lowest real part of the eigenvalue with $\nu_1=\nu_2=0.5$ and various

Table 3.2 Comparison of the lowest real part of the eigenvalue of surface region from different property, $\theta_0=\pi$

	$\nu_1=\nu_2=0.3$	$\nu_1=\nu_2=0.5$	$\nu_1=0.3,\nu_2=0.5$
k=0.1	0.3961	0.3912	0.4109
k=1	0.25	0.25	0.2625
k=10	0.09415	0.08425	0.10405

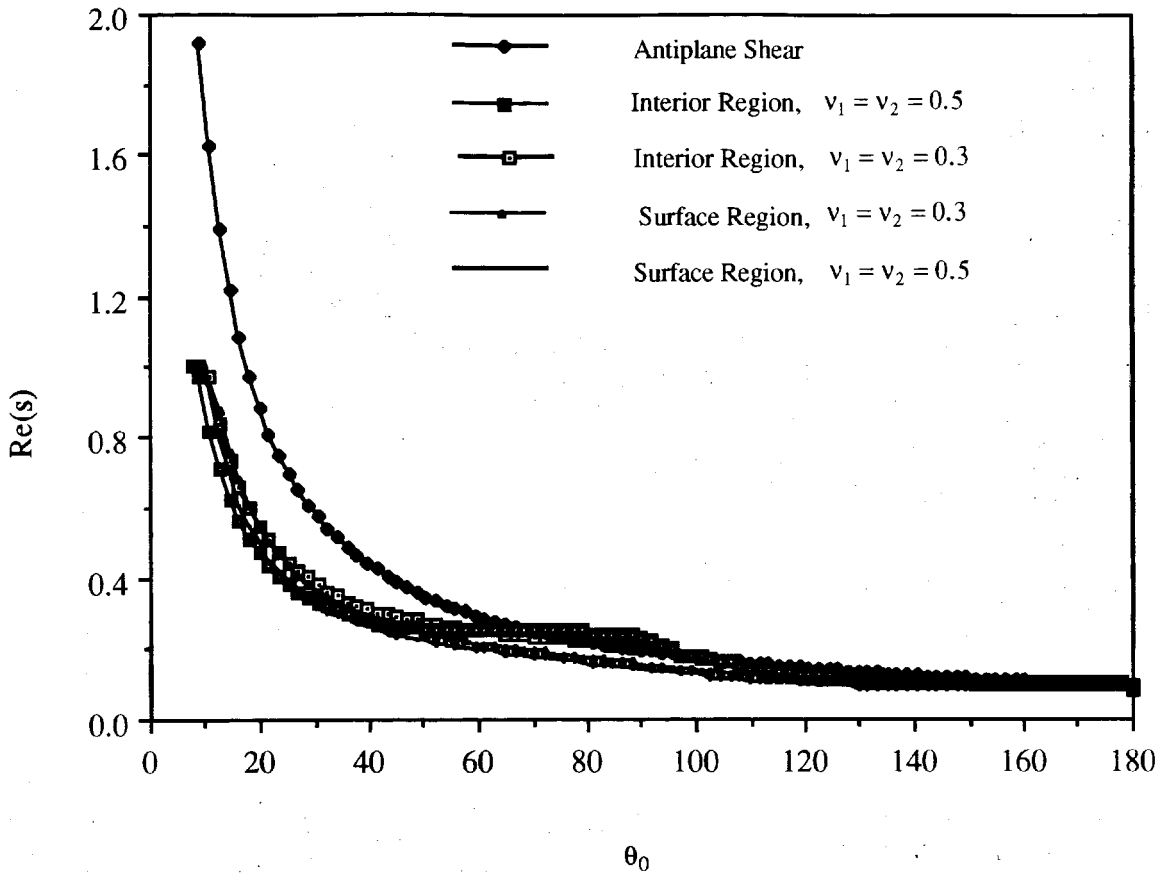

Figure 3.17 Variation of the lowest real eigenvalue for a free-clamped bimaterial wedge with respect to wedge angle, $k=G_1/G_2=10$.

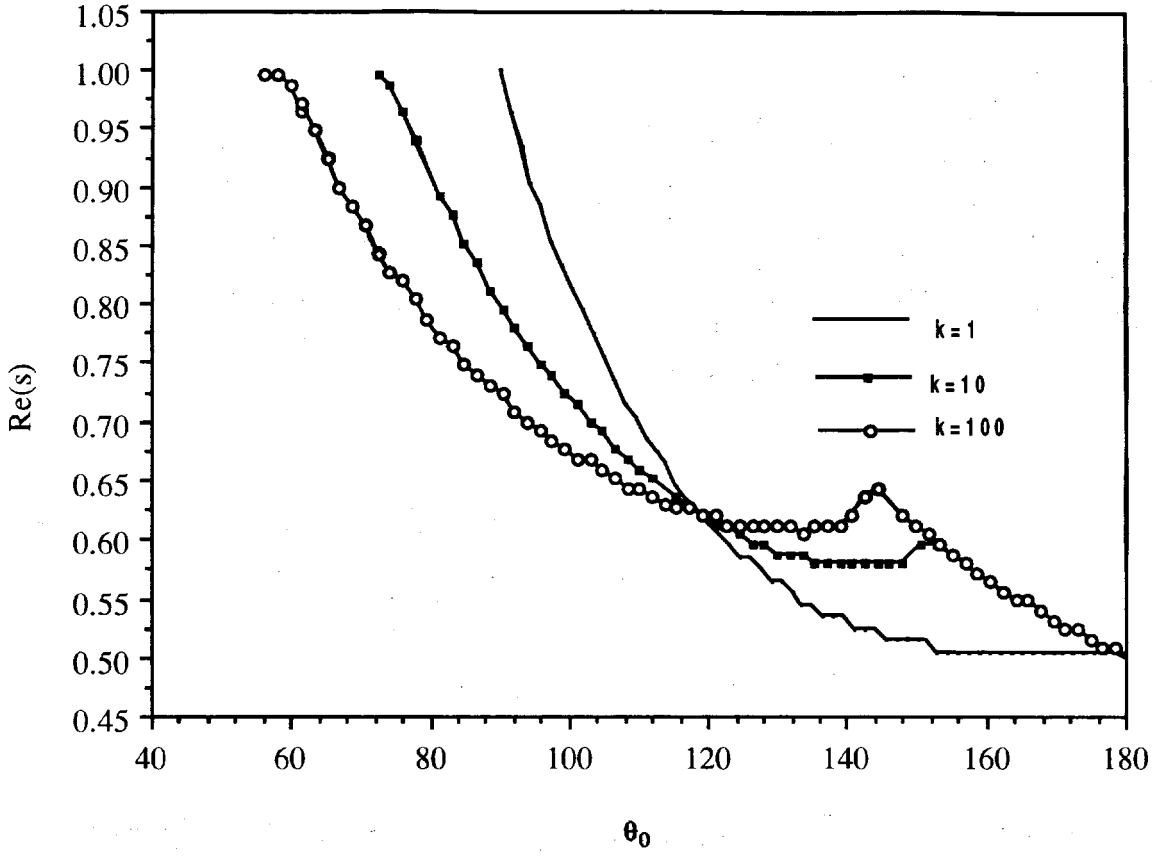

Figure 3.18 Variation of the lowest real eigenvalue in interior region with respect to wedge angle, for a free-free bimaterial wedge with $\nu_1=\nu_2=0.3$ and $k=G_1/G_2$.

k is shown in Figure 3.19. Like the clamped-clamped case, the lowest real part of the eigenvalue decreases monotonically as k and θ_0 increase. The lowest real part of the eigenvalue with ν_1=0.3,ν_2=0.5 and various k is shown in Figure 3.20.

3.5.3.2 Surface Region

As in the case of its homogeneous counterpart, the rigid body mode also exists in the bimaterial wedge with free-free edge condition (see Figure 3.21). The remaining eigenvalues that have physical meaning in regards to the stress singularity are plotted in Figures 3.22, 3.23, and 3.24.

Comparisons of the lowest real part of the eigenvalue for interior region, surface region, and antiplane shear loading are shown in Figure 3.25 with k=10. These results are similar to their clamped-clamped counterparts, shown in Figure 3.10.

3.6 The Study of Boundary-Layer Effects in Bonded Dissimilar Materials with Right Angle

The study of boundary-layer effects in bonded dissimilar materials with right angle (see Figure 3.26) has been a subject of intensive investigation for the past several decades. The stress singularity at the free edge of an interface is one of the factors responsible for the delamination. Rongved [76] has analyzed the problem of a concentrated force applied interior to one of two bonded elastic half-spaces. The corresponding two-dimensional solution was given by Frasier and Rongved [77]. Williams [6] has considered an elastic wedge bonded to a rigid base, and obtained the singularity of stress field. Two elastic edge bonded results have been obtained by Bogy [22], [23] using the Mellin transform method. Unfortunately, however, all the above-cited results are based on two-dimensional approaches.

Wang and Choi [35], [36] have investigated the free orthogonal edge of an interface in a laminated composite by Lekhnitskii's stress potentials. Ting and Chou [8] have

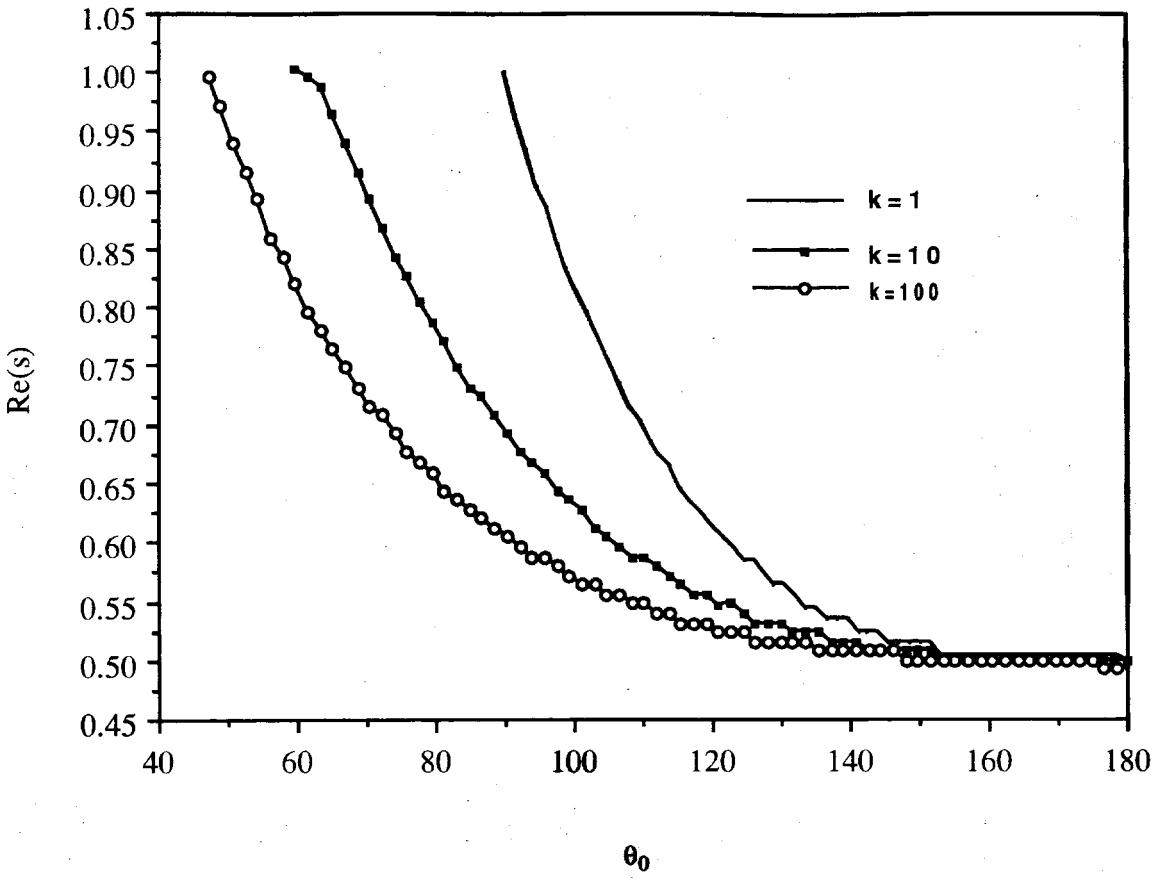

Figure 3.19 Variation of the lowest real eigenvalue in interior region with respect to wedge angle, for a free-free bimaterial wedge with $\nu_1=\nu_2=0.5$ and $k=G_1/G_2$.

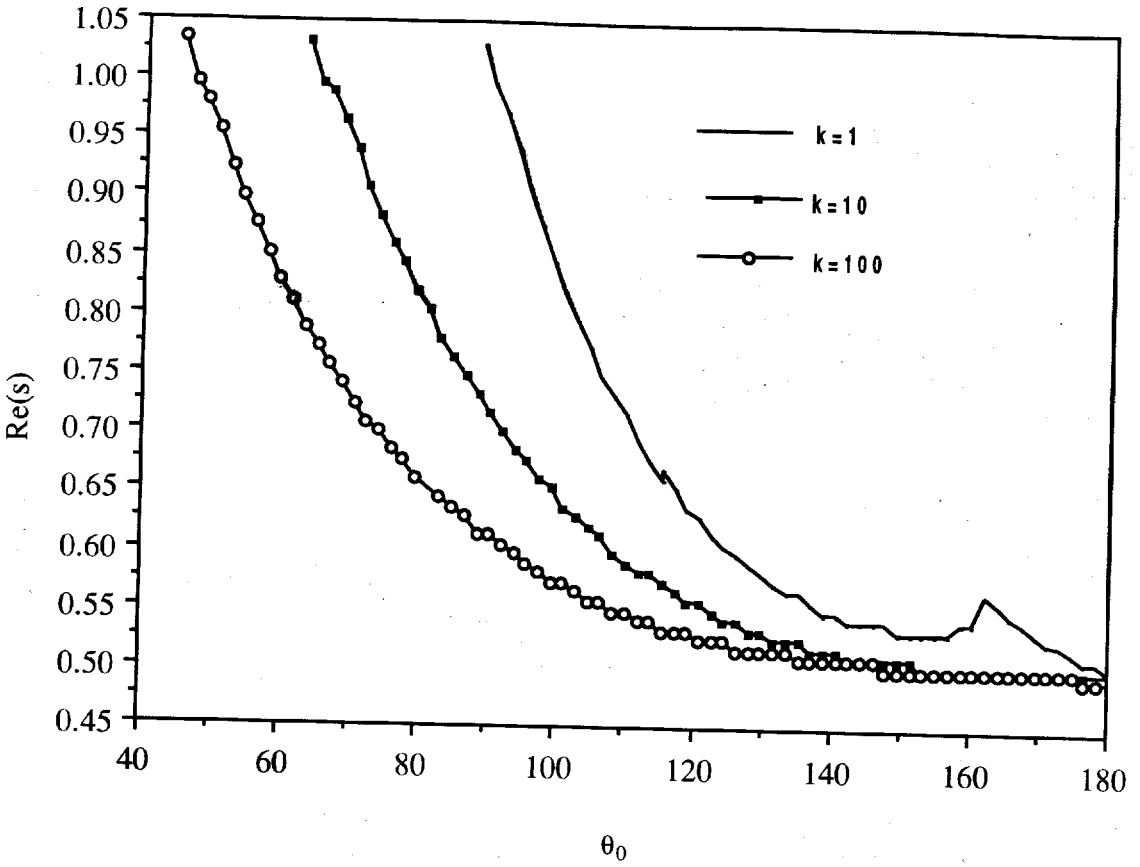

Figure 3.20 Variation of the lowest real eigenvalue in interior region with respect to wedge angle, for a free-free bimaterial wedge with ν_1=0.3, ν_2=0.5 and k=G_1/G_2.

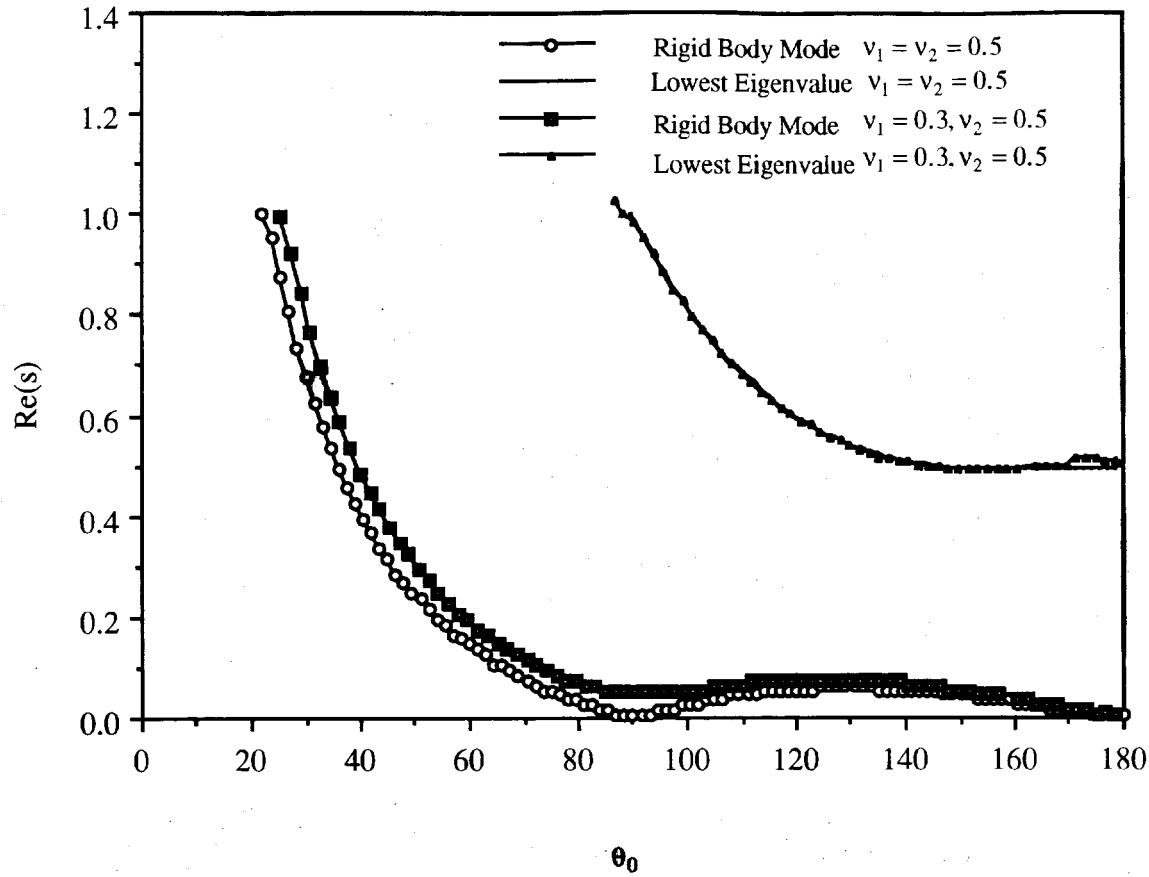

Figure 3.21 Variation of the rigid body eigenvalue and lowest eigenvalue, for a free-free bimaterial wedge with respect to wedge angle.

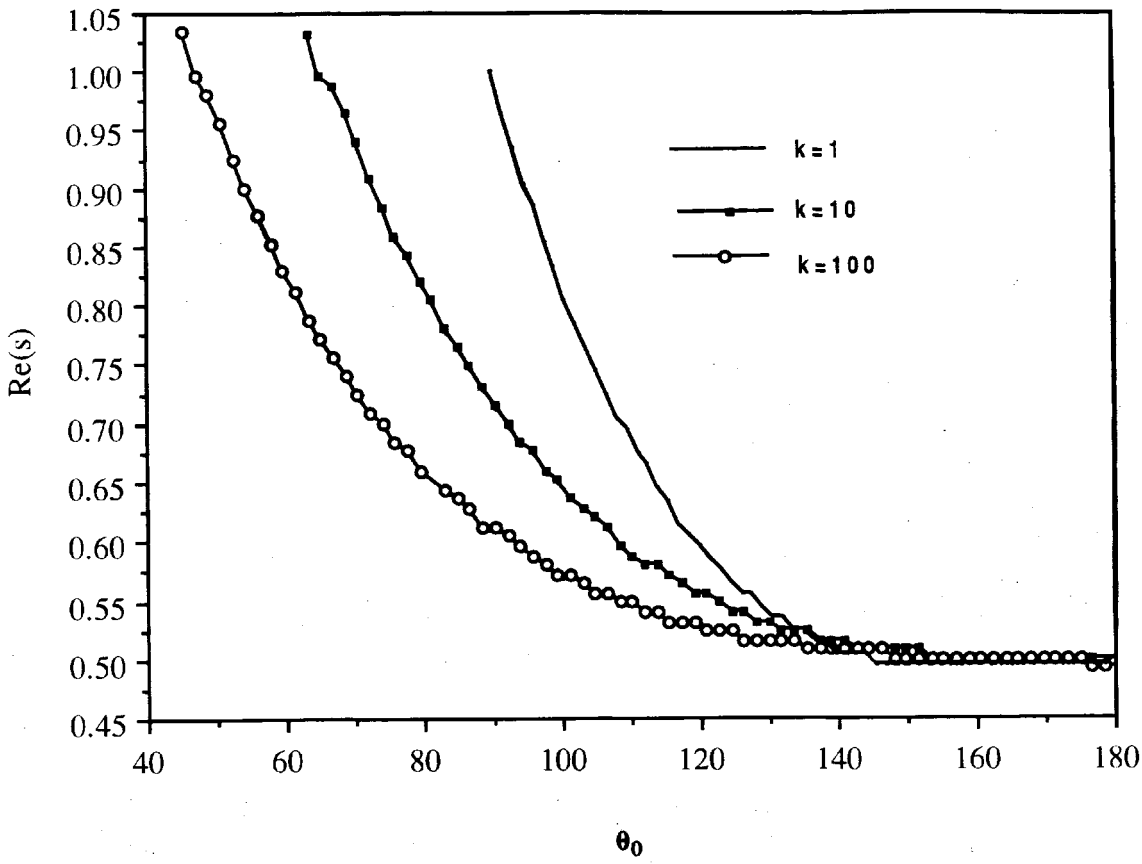

Figure 3.22 Variation of the lowest real eigenvalue on surface region with respect to wedge angle, for a free-free bimaterial wedge with $\nu_1=\nu_2=0.3$ and $k=G_1/G_2$.

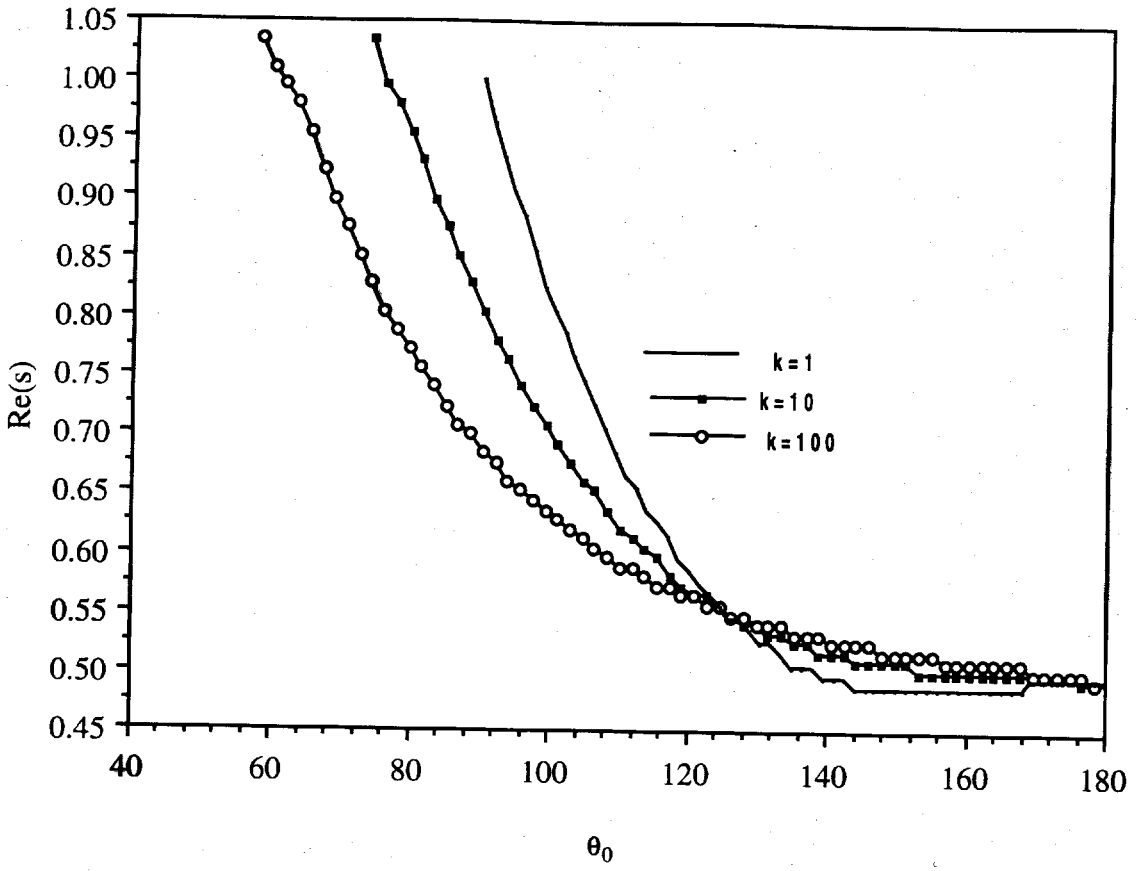

Figure 3.23 Variation of the lowest real eigenvalue on surface region with respect to wedge angle, for a free-free bimaterial wedge with $\nu_1=\nu_2=0.5$ and $k=G_1/G_2$.

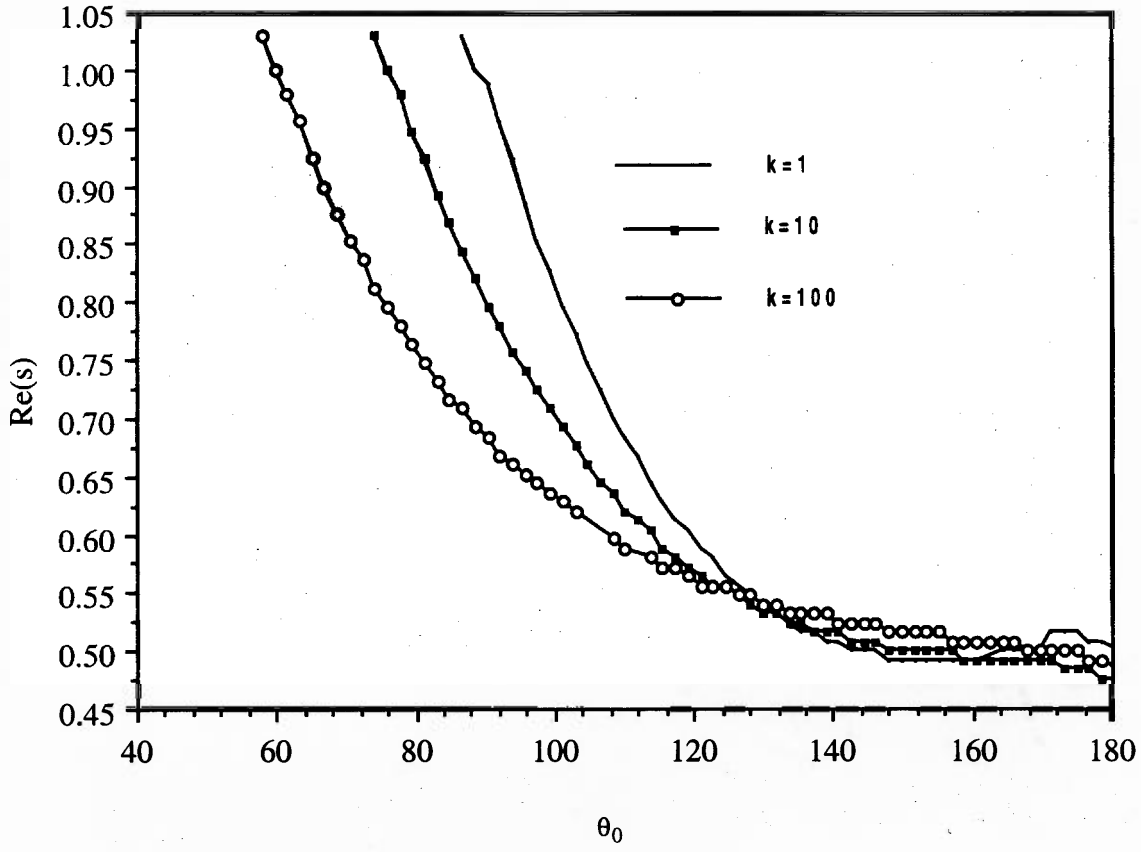

Figure 3.24 Variation of the lowest real eigenvalue on surface region with respect to wedge angle, for a free-free bimaterial wedge with ν_1=0.3, ν_2=0.5 and k=G_1/G_2.

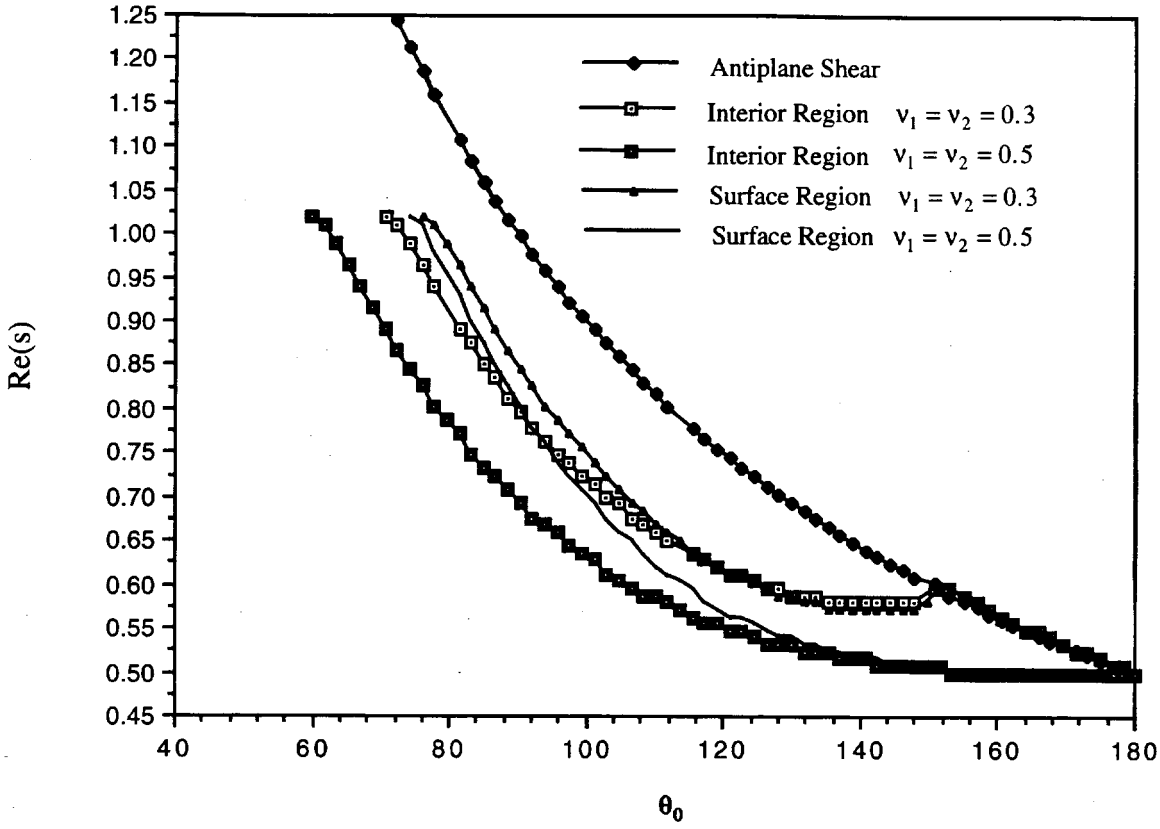

Figure 3.25 Variation of the lowest real eigenvalue for a free-free bimaterial wedge with respect to wedge angle, $k=G_1/G_2=10$.

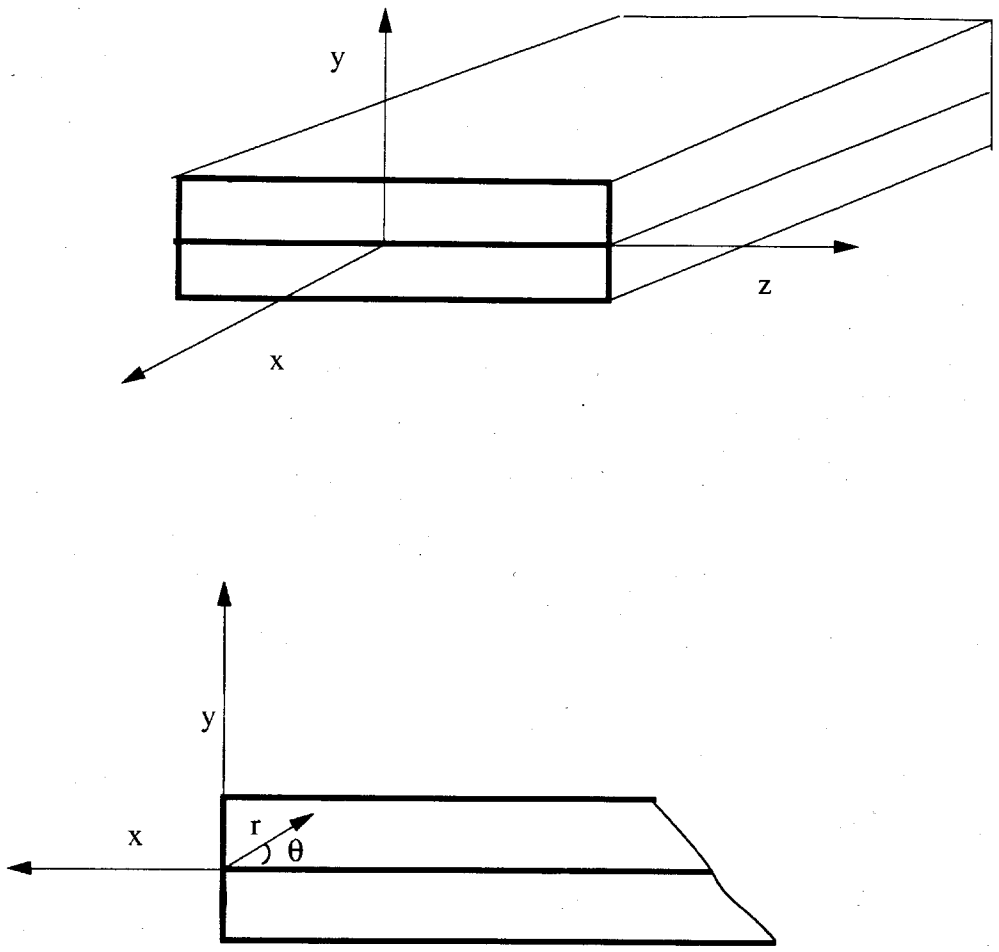

Figure 3.26 Edge-bonded orthogonal wedge

analyzed the same problem by the Stroh method, wherein the coupling between in-plane and transverse deformations and stresses near the edge of a composite laminate is investigated. The results obtained are based on the assumption that the stresses in the laminated composite are independent of the z-coordinate. As a result, the results are not truly three-dimensional So far, the problem of an edge-bonded orthogonal wedge has not been analyzed using a three-dimensional method. A three-dimensional theoretical investigation pertaining to singular stresses in a dissimilar edge, with right angle and made of an isotropic materials, is presented here for the first time.

3.6.1 Singular Stress Fields at the Inside Region on the Bimaterial Interface

The boundary conditions at the surface of edge-bonded orthogonal wedge (see Figure 3.25) are:

$$\theta_o = \pm\frac{\pi}{2}$$

$$\sigma_{\theta j} = \tau_{r\theta j} = \tau_{\theta z j} = 0. \tag{3.76}$$

The expressions for stresses and displacements need to satisfy the boundary conditions on the surfaces given by equation (3.76). The eigen equation, which can be obtained by substitution of equation (3.32) into equation (3.76), is as given below:

$$A_{11}(z)\sin(s+1)\frac{\pi}{2} + A_{21}(z)\cos(s+1)\frac{\pi}{2} +$$

$$(s+1)\left(A_{31}(z)\sin(s-1)\frac{\pi}{2} + A_{41}(z)\cos(s-1)\frac{\pi}{2}\right) = 0$$

$$A_{11}(z)\cos(s+1)\frac{\pi}{2} - A_{21}(z)\sin(s+1)\frac{\pi}{2} +$$

$$(s-1)\left(A_{31}(z)\cos(s-1)\frac{\pi}{2}-A_{41}(z)\sin(s-1)\frac{\pi}{2}\right)=0$$

$$-A_{12}(z)\sin(s+1)\frac{\pi}{2}+A_{22}(z)\cos(s+1)\frac{\pi}{2}+$$

$$(s+1)\left(-A_{32}(z)\sin(s-1)\frac{\pi}{2}+A_{42}(z)\cos(s-1)\frac{\pi}{2}\right)=0$$

$$A_{12}(z)\cos(s+1)\frac{\pi}{2}+A_{22}(z)\sin(s+1)\frac{\pi}{2}+$$

$$(s-1)\left(A_{32}(z)\cos(s-1)\frac{\pi}{2}+A_{42}(z)\sin(s-1)\frac{\pi}{2}\right)=0, \tag{3.77}$$

where

$$c_{1j}=-3+4\nu_j$$

$$k=\frac{G_1}{G_2}.$$

The eigenvalues can be computed by combining equation (3.77) with equation (3.34). If the boundary conditions on the free plate faces are satisfied, all the stresses and displacements on the plate near the corner junction point are zero. This is contrary to the experimental results except for $\nu_1=\nu_2=0$. It means that there is another solution for stresses in the vicinity of the corner junction point.

3.6.2 Singular Stress Fields in the Vicinity of the Corner Junction Point

With substitution of equation (3.50) into equation (3.76), the eigen equations can be derived in the form:

$$A_{11}(\pm h)\sin(s+1)\frac{\pi}{2}+A_{21}(\pm h)\cos(s+1)\frac{\pi}{2}+$$

$$(s+c_{21})\left(A_{31}(\pm h)\sin(s-1)\frac{\pi}{2}+A_{41}(\pm h)\cos(s-1)\frac{\pi}{2}\right)=0$$

$$A_{11}(\pm h)\cos(s+1)\frac{\pi}{2}-A_{21}(\pm h)\sin(s+1)\frac{\pi}{2}+$$

$$(s-1)\left(A_{31}(\pm h)\cos(s-1)\frac{\pi}{2}-A_{41}(\pm h)\sin(s-1)\frac{\pi}{2}\right)=0$$

$$-A_{12}(\pm h)\sin(s+1)\frac{\pi}{2}+A_{22}(\pm h)\cos(s+1)\frac{\pi}{2}+$$

$$(s+c_{22})\left(-A_{32}(\pm h)\sin(s-1)\frac{\pi}{2}+A_{42}(\pm h)\cos(s-1)\frac{\pi}{2}\right)=0$$

$$A_{12}(\pm h)\cos(s+1)\frac{\pi}{2}+A_{22}(\pm h)\sin(s+1)\frac{\pi}{2}+$$

$$(s-1)\left(A_{32}(\pm h)\cos(s-1)\frac{\pi}{2}+A_{42}(\pm h)\sin(s-1)\frac{\pi}{2}\right)=0, \tag{3.78}$$

where

$$c_{2j}=-3+2\nu_j.$$

The eigenvalues can be computed by combining equation (3.78) with equation (3.51).

3.6.3 Numerical Results and Discussion

The comparison of the variation of the lowest eigenvalue under bending/extension computed for three different cases — (i) an inside point on the bimaterial interface, (ii) near the corner junction point under bending/extension, and (iii) two-dimensional (plane stress)

condition — with respect to $k=G_1/G_2$, is shown in Figure 3.27, with $\nu_1=0$, $\nu_2=0.5$. It is interesting to observe that the lowest eigenvalue for the inside region is the smallest in the entire range of k, whereas its two-dimensional (plane stress) counterpart is the largest. The smallest eigenvalue on the corner junction point is 0.667, whereas its two-dimensional (plane stress) and inside region counterparts are 0.689, and 0.595, respectively.

The comparison of the variation of the lowest eigenvalues with k, computed for the aforementioned three cases of an edge-bonded orthogonal wedge with Poisson's ratio, $\nu_1=\nu_2=0.25$, is plotted in Figure 3.28. As before, the eigenvalue for the inside region is also the smallest in the entire range of k. The eigenvalue for two-dimensional (plane stress) condition, in $0<k<25$ range, is smaller than that its corner junction point counterpart. In the remaining range of k, the eigenvalue for the two-dimensional (plane stress) condition is larger than that for the corner junction point.

The comparison of the variation of the lowest eigenvalues, computed for the aforementioned three cases of edge-bonded orthogonal wedge with respect to $\nu_1=\nu_2$, is displayed in Figure 3.29 with k=5. However the lowest eigenvalues for two-dimensional plane stress are smaller than those corresponding to the corner junction point. The comparison of the variation of the lowest eigenvalues with respect to $\nu_1=\nu_2$ is shown in the Figure 3.30 with k=100. Also the smallest eigenvalue is in the interior region. Unlike the case shown in Figure 3.29, the lowest eigenvalues for the the corner junction point are smaller than their two-dimensional (plane stress) counterparts.

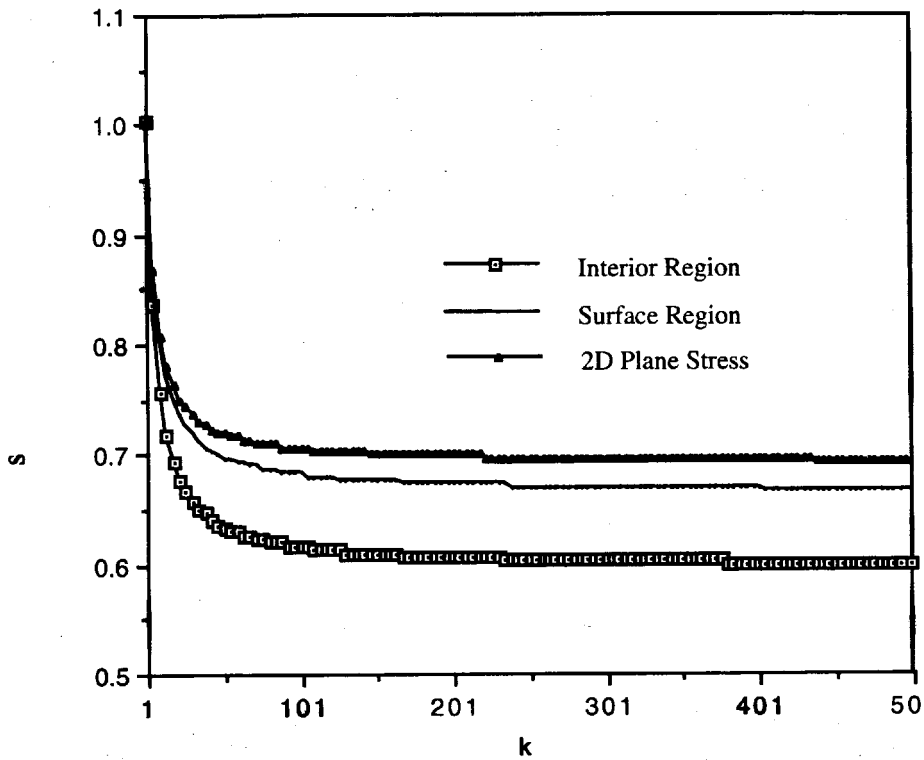

Figure 3.27 Dependence of the lowest eigenvalue on $k=G_1/G_2$ for a edge-bonded orthogonal wedge with $\nu_1=0$, $\nu_2=0.5$.

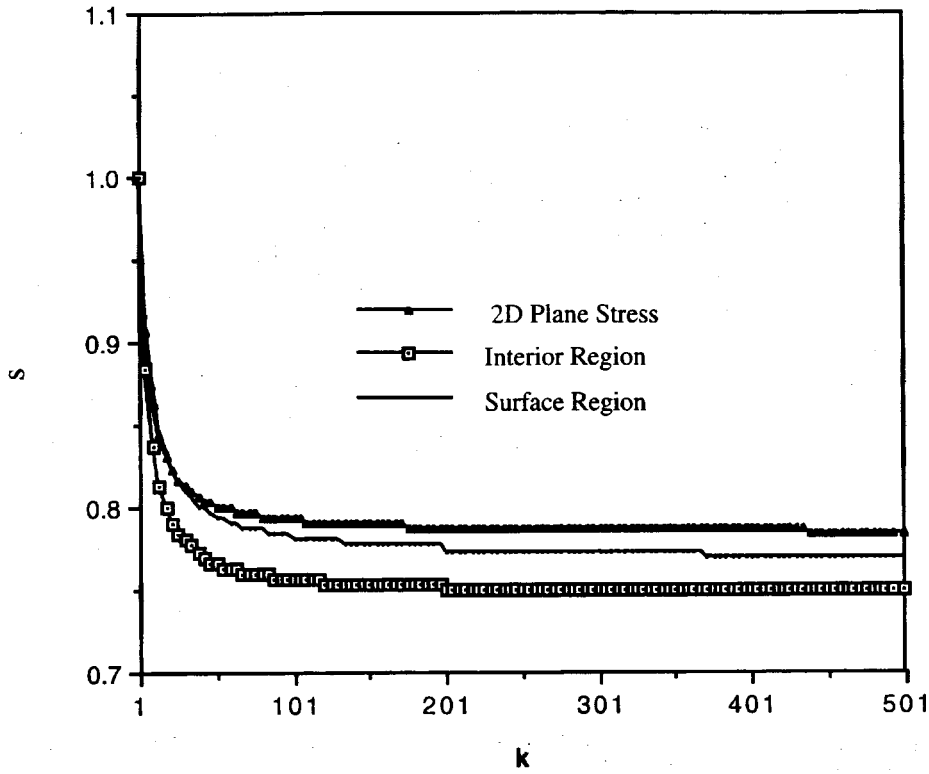

Figure 3.28 Dependence of the lowest eigenvalue on $k=G_1/G_2$ for a edge-bonded orthogonal wedge with $\nu_1=\nu_2=0.25$.

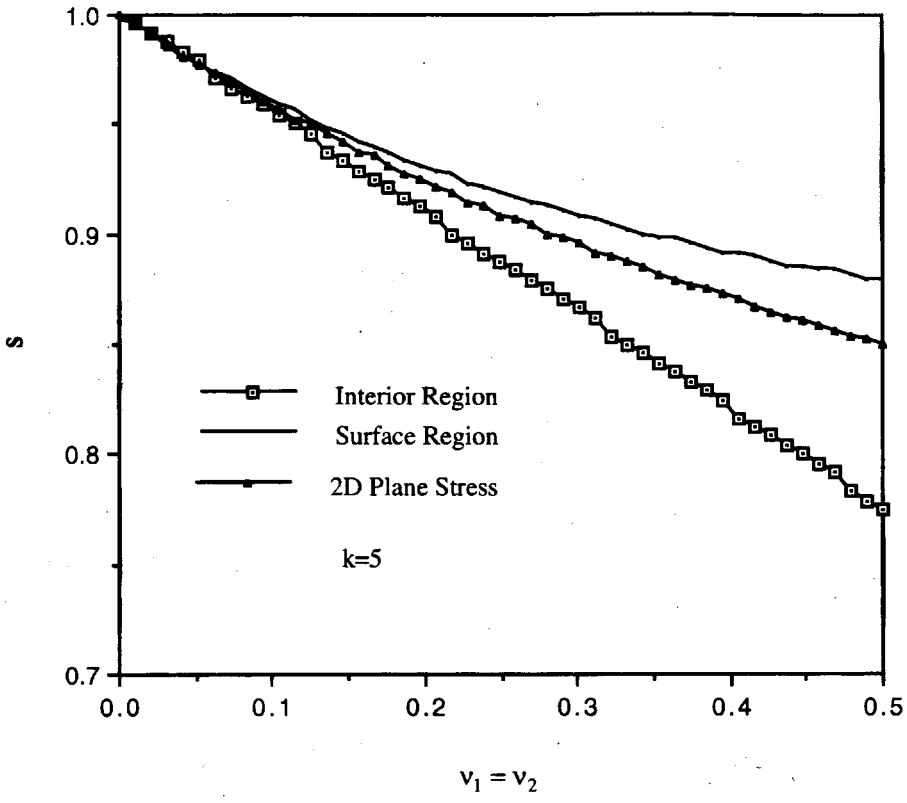

Figure 3.29 Dependence of the lowest eigenvalue on $\nu_1=\nu_2$ for a edge-bonded orthogonal wedge with $k=G_1/G_2=5$.

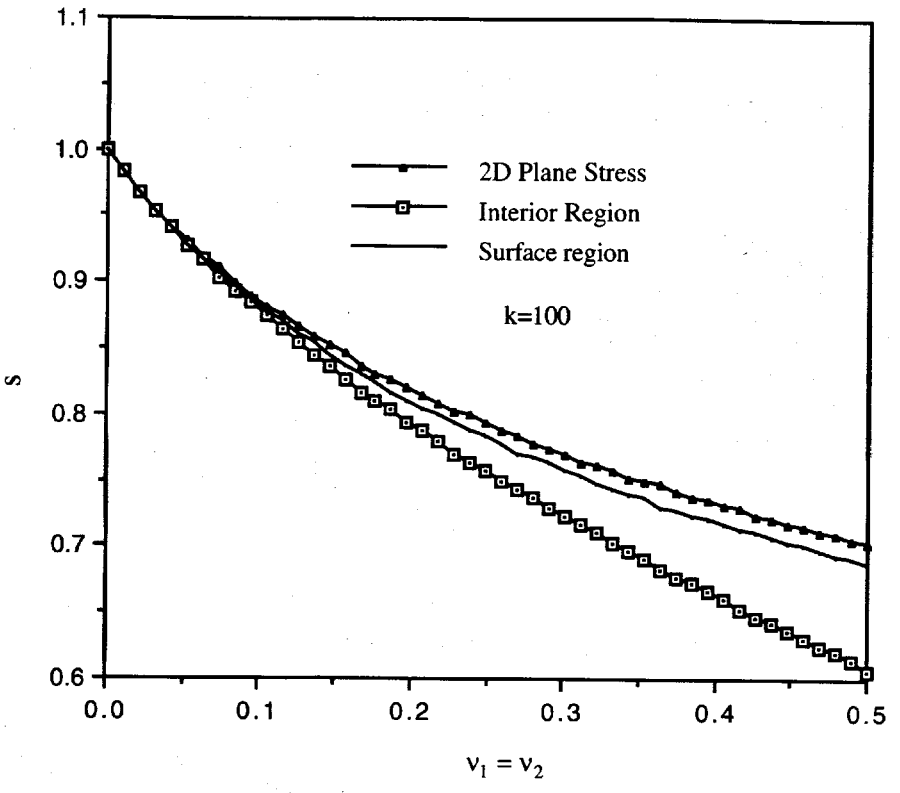

Figure 3.30 Dependence of the lowest eigenvalue on $\nu_1=\nu_2$ for a edge-bonded orthogonal wedge with $k=G_1/G_2=100$.

CHAPTER 4

CONCLUSIONS AND RECOMMENDATIONS

4.1 Summary and Conclusions

The mathematical difficulties posed by the three-dimensional homogeneous and bi-material wedge problems are substantially greater than their two-dimensional counterparts, available in the literature. A new eigenfunction expansion method is developed to obtain three-dimensional asymptotic stress fields in the vicinity of (a) an interior point and (b) the surface corner point located at the front of a (i) homogeneous and (ii) bimaterial wedge, subjected to three combinations of wedge-side boundary conditions — clamped-clamped, clamped-free and free-free. In comparison with the method due to Hartranft and Sih [47], the present method is much easier to implement and also computationally more efficient in the sense that it does not need to resort to iterative schemes to solve the three partial differential equations, which limit the former's applicability to more complex geometric shape, such as a wedge. The expressions for singular stress fields in the neighborhood of these points located at the front of a semiinfinite crack — a special case of a homogeneous wedge — are also presented. Likewise, the expressions for singular stress fields in the neighborhood of these points located at the front of a semiinfinite crack along the interface— a special case of a bimaterial wedge — are also presented.

Additionally, heretofore unavailable numerical results, especially for three-dimensional stress fields in the vicinity of the surface corner point at the front of a (i) homogeneous and (ii) bimaterial wedge subjected to the aforementioned wedge-side boundary conditions, and their comparisons with their two-dimensional (i.e., plane stress)

counterparts, are also presented. Furthermore, the general stress intensity factor (for $\theta_0 \neq \pm\pi$) and the corresponding expression of singular stresses for homogeneous wedges are also obtained. Important conclusions drawn from this study are grouped, under the headings of homogeneous and bimaterial wedge.

4.1.1 Homogeneous Wedge

(i) Although the two-dimensional approximation can still yield acceptable (in the engineering sense) results for a generalized plane stress problem, which does not involve stress singularity, the presence of such a singularity renders the two-dimensional approximation to be in significant error. This type of discrepancy can be resolved only through the use of a three-dimensional approach.

(ii) Such important quantities as the self-equilibrating stress intensity factor, K_{IIIa}, and the self-equilibrating strain energy release rate, G_{IIIa}, which can not be obtained by any two-dimensional analysis, are obtained by this new three-dimensional method.

(iii) The eigenvalue for a homogeneous wedge subjected to the antiplane shear loading is independent of the material property for any kind of boundary condition.

(iv) For a homogeneous wedge with free-free boundary condition, the eigenvalues corresponding to the Modes I, II and III have the following relationship :

$$s_2 \geq s_3 \geq s_1,$$

which suggests that the opening mode (Mode I) yields the most severe stress singularity, and the onset of fracture is triggered by an applied load corresponding to this mode. The sliding mode (Mode II) has the largest eigenvalue, which yields the least dangerous stress singularity. However, in the special case of a semiinfinite crack (i.e., $\theta_0 = \pm\pi$), the three eigenvalues become identical and are equal to 1/2.

(v) In the special case of a homogeneous wedge becoming cracklike, i. e., $\theta_0=\pm\pi$, the computed eigenvalues for the surface region, interior region, and antiplane shear loading become identical. Additionally, they are independent of the material properties, and depend only on the boundary condition. For example:

1. Free-Free

$$\sigma_{ij} \sim 0\left(r^{-\frac{1}{2}}\right),$$

2. Clamped-Clamped

$$\sigma_{ij} \sim 0\left(r^{-\frac{1}{2}}\right);$$

3. Free-Clamped

$$\mathrm{Re}\,\sigma_{ij} \sim 0\left(r^{-\frac{3}{4}}\right) + 0\left(r^{-\frac{1}{4}}\right).$$

(vi) For the free-free boundary condition, the lowest eigenvalue in the interior region is larger than the one on the surface region. Additionally, the smallest eigenvalue for the interior region occurs at $\theta_0=\pm\pi$. The same is not true for the surface region. The smallest eigenvalue occurs in the range of approximately $0.85\pi<\theta_0<\pi$. These two facts imply that in the case of the free-free boundary condition, a semiinfinite crack may open up, resulting in a failure that initiates at the surface corner point and then propagates inward. Furthermore, the two-dimensional (plane stress) approximation is on the nonconsevative side in estimating the structural integrity on the surface region.

(vii) For the free-free boundary condition, the second eigenvalue in the interior region, in contrast to the lowest one, is smaller than the one on the surface region. However, the reverse order is true for the clamped-clamped boundary condition.

(viii) For the free-free boundary condition, the lowest eigenvalue for the surface region monotonically decreases with the increase of Poisson's ratio, implying thereby an increase in severity of the stress singularity at the surface corner point at the wedge front. The reverse is, however, true for the second eigenvalue. The eigenvalues for the interior region are insensitive to the change in Poisson's ratio.

(ix) For the opening mode (Mode I), the strain energy release rate on the surface region is different from the one computed two-dimensional plane stress approximation; however, for the sliding mode (Mode II), it is the same as its two-dimensional plane stress counterpart.

(x) For the free-clamped boundary condition, the eigenvalue consists of both real and imaginary parts for a certain range of the included wedge angle. The occurrence of the nonvanishing imaginary part is always accompanied by the appearance of a clearly visible cusp in the real part, thus disturbing monotonicity of variation of the lowest real part with the included wedge angle.

(xi) The yield zone on the surface region for the sliding mode (Mode II) computed using the present analysis is larger than its approximate two-dimensional plane stress counterpart. Furthermore, the size of the yield zone computed using the present analysis for Mode II increases with the increase of Poisson's ratio. The reverse is true, however, for the opening mode (Mode I).

4.1.2 Bimaterial Wedge

(i) The eigenvalue for a bimaterial wedge subjected to the antiplane shear loading is independent of the material property except for the free-clamped boundary condition.

(ii) The asymptotic expressions of stresses and displacements in the vicinity of a

semiinfinite crack along the bimaterial interface are the same as their homogeneous crack counterparts, when the plate is subjected to the antiplane shear loading

(iii) When $\theta_0=\pm\pi$, the stress singularity in the interior region of clamped-clamped and free-free bimaterial wedges is always given by the oscillatory phenomenon

$$s=\frac{1}{2}\pm i\varepsilon.$$

On the surface region, however, the oscillatory phenomenon vanishes for the case of free-free boundary condition (i. e., a semiinfinite crack along the bimaterial interface) if the material parameters satisfies the following condition:

$$\frac{1}{2}\le\left(\frac{\nu_1-\nu_2(E_1/E_2)}{1-(E_1/E_2)}\right)\le 1.$$

In this particular case, the lowest eigenvalue is smaller than 1/2, implying a more severe stress singularity.

(iv) The lowest real part of the eigenvalue for a free-clamped bimaterial wedge depends heavily on the $k=G_1/G_2$ (the wedge-side surface for material 1 is free). As k increases, the eigenvalue decreases significantly, the most severe stress singularity occurring in the vicinity of bimaterial wedge front.

(v) In general, the lowest real part of the eigenvalue for any boundary condition in a bimaterial wedge decreases as k and θ_0 increase except for some local angle, θ_0, region affected by imaginary part.

(vi) The fields of stress and displacement of extension and bending from the two-dimensional method is different for a bimaterial crack [9]. For the three-dimensional point of view, the expressions of stress and displacement are the same.

(vii) The smallest eigenvalue for edge-bonded orthogonal wedge is 0.595, 0.667, and 0.689 for (i) a inside point on the bimaterial interface computed using the present three-dimensional analysis, (ii) a point on corner junction point computed using the present three-dimensional analysis, (iii) the two-dimensional (plane stress) approximation, respectively.

4.2 Recommendations and Future Work

It is recommended that the following issues be addressed in future:

(i) The three-dimensional asymptotic stress fields in the vicinity of the front of homogeneous wedge and bimaterial wedge are obtained. However, the effect of the higher order terms (in terms of r) on stress fields in the vicinity of the homogeneous and bi-material wedge fronts needs careful consideration.

(ii) The present study needs to be extended to include (a) orthotropic material property and (b) anisotropic material property.

(iii) Numerical techniquess, such as the Sinc method, can be formulated to handle more complex geometries.

(iv) Since the oscillatory phenomenon exists for a semiinfinite interface bimaterial crack, the strain energy release rate cannot be obtained by the conventional approach. Hence, a new approach needs to be developed in the future.

APPENDIX

The objective of this appendix is to show that the solution technique used by Iyengar et al. [55] can not keep the displacement components at the crack front finite, unless $M_{3/2}$ and $f(d_{k-.5})$ vanish.The transverse displacement is given by Ref. [5] as follows:

$$W = \Psi_2\, \Psi + X_2\, X, \tag{A-1}$$

where

$$\Psi_2(\xi) = 2(1-\mu)X\overline{X} + \delta\xi\Sigma\overline{X} - \eta\delta\overline{\Sigma}X \tag{A-2}$$

$$X_2(\xi) = 2(1-\mu) - \delta^2\eta^2\left(2(1-\mu) + \mu\left(1 - \xi^2/\eta^2\right)\right) \tag{A-3}$$

$$\Psi(r,\theta) = R_e \sum_n \sum_{k=1}^{\infty} d_{kn}\, I_n\left(\omega_k r/\eta\right)\cos(n\theta) \tag{A-4}$$

$$X(r,\theta) = \sum_n \sum_{m=o}^{\infty} r^t\left[M_t \cos(t-2)\theta + N_t \cos(t\theta)\right] \tag{A-5}$$

$$C = \cos\delta\xi \qquad S = \sin\delta z \qquad \xi = z/a \tag{A-6}$$

$$\overline{C} = \cos\delta\overline{\xi} \qquad \overline{S} = \sin\delta\overline{z} \qquad \eta = h/a \tag{A-7}$$

$$\delta^2 = \frac{\partial^2}{\partial r^2} + \frac{1}{r}\frac{\partial}{\partial r} + \frac{1}{r^2}\frac{\partial^2}{\partial \theta^2} \tag{A-8}$$

$$\sin(2\omega_k) - 2\omega_k = 0 \qquad k = 1,2,\cdots\cdots \tag{A-9}$$

a is the half length of a crack, while h is the thickness of the plate. M_t and N_t are unknown constants, and μ is shear modulus. I_n represents the Bessel function. The Ψ_2 can be expanded into the form:

$$\Psi_2(\xi) = \sum_{k=o}^{\infty} C_k(z)\delta^{2k} \tag{A-10}$$

The $C_k(z)$ is known as z function and is given as follows for k=0, 2, ……:

$$C_0 = 2(1-\mu) \qquad C_2 = -2(1-\mu)\left(\frac{\xi^2}{2} + \frac{\bar{\xi}^2}{2}\right) + \xi z - \eta\bar{z} \quad \cdots\cdots \tag{A-11}$$

Using equation (10) of Ref. [55], given by

$$\left[\delta^2 - (\omega_i/\eta)^2\right]\Psi(r,\theta) = 0 \qquad i = 1,2\cdots\cdots \tag{A-12}$$

the result can be derived in a straightforward manner

$$\delta^{2n}\Psi(r,\theta) = (\omega_i/\eta)^{2n}\Psi(r,\theta) \qquad i = 1,2\cdots\cdots \tag{A-13}$$

where n is given as n=±1/2+j, j=1,2 ....., as n=-1/2,

$$\Psi(r,\theta) = R_e\left(d_{1-1/2}I_{-1/2}\left(\frac{\omega_1 r}{\eta}\right) + d_{2-1/2}I_{-1/2}\left(\frac{\omega_2 r}{\eta}\right) + d_{3-1/2}I_{-1/2}\left(\frac{\omega_3 r}{\eta}\right)\cdots\cdots\right)\cos(\theta/2) \tag{A-14}$$

The above equation can be simplified into the form:

$$\Psi(r,\theta) = R_e\left(d_{1-1/2}\left(\frac{\omega_1}{\eta}\right)^{-1/2} + d_{2-1/2}\left(\frac{\omega_2}{\eta}\right)^{-1/2} + d_{3-1/2}\left(\frac{\omega_3}{\eta}\right)^{-1/2} \cdots\cdots \right)\sqrt{2}\sqrt{\pi}^{-1}\cos(\theta/2)r^{-1/2} \tag{A-15}$$

which yields

$$\Psi(r,\theta) = \sqrt{2}\sqrt{\pi}^{-1}\cos(\theta/2)r^{-1/2}R_e\sum_{i=1}^{\infty} d_{i-1/2}\left(\frac{\omega_i}{\eta}\right)^{-1/2} \tag{A-16}$$

which, when combined with equation (A-10), will yields the following equation

$$\Psi_2\Psi(r,\theta) = \sqrt{2}\sqrt{\pi}^{-1}\cos(\theta/2)r^{-1/2}R_e\sum_{i=1}^{\infty} d_{i-1/2}\left(\frac{\omega_i}{\eta}\right)^{-1/2}\sum_{i=0}^{\infty} C_i(z)\left(\frac{\omega_k}{\eta}\right)^{2i} \qquad k = 1,2\cdots\cdots \tag{A-17}$$

For t=3/2, χ becomes Williams' symmetric solution

$$\chi = r^{3/2}(M_{3/2}\cos(\theta/2) + N_{3/2}\cos(3\theta/2)) \tag{A-18}$$

$$\chi_2\chi = -2\eta^2\left(2(1-\mu) + \mu\left(1-\frac{\xi^2}{\eta^2}\right)\right)r^{-1/2}M_{3/2}\cos(\theta/2) + 0(r) \tag{A-19}$$

The normal transverse displacement term, which can lead to singular stresses, is given by

$$W = \Psi_2\,\Psi + X_2\,X \tag{A-20}$$

$$W = r^{-1/2}\cos(\theta/2)\left(A(z)M_{3/2} + B(z)f\left(d_{k-1/2}\right)\right) + 0(r) \tag{A-21}$$

where

$$A(z) = -2\eta^2\left(2(1-\mu)+\left(1-\xi^2/\eta^2\right)\right) \tag{A-22}$$

$$B(z) = \sum_{i=0}^{\infty} C_i(z)\left(\omega_i/\eta\right)^{2i} \tag{A-23}$$

$$f\left(d_{k-1/2}\right) = \sum_{k=0}^{\infty} \frac{\left(\sqrt{2\eta}\, d_{k-1/2}\right)}{\sqrt{\omega_k \pi}} \tag{A-24}$$

In order for the condition of finite displcement to be satisfied for all z, $M_{3/2}$ and $f(d_{k-1/2})$ must be equal to zero, and vice versa. The same applies to the displacement functions U, and V.

REFERENCES

1. H. J. Garala, Structural evaluation of externally pressurized, 4-inch diameter, graphite-composite cylinder. *DTRC report 86/071*, (1986).

2. H. J. Garala, Structural evaluation of 8-inch diameter graphite-epoxy composite cylinders subjected to external hydrostatic compressive loading. *DTRC report 89/016*, (1989).

3. R. A. Chaudhuri, Prediction of the compressive strength of thick-section advanced composite laminates. *J. Composite Materials*. **25**, 1244 -1276, (1991).

4. R. A. Chaudhuri and H. J. Garala, On deformation and failure behavior of thick advanced composites under compression. presented at ICTAM, Haifa, *ISRAEL Paper # 984*, (1992).

5. H. J. Garala and R. A. Chaudhuri, Structural evaluation of advanced composite thick-section cylinders under biaxial compression. invited by Dr. Rajapakse, ONR; presented at the First Joint ASCE-EMD, ASME-AMD, *SES meeting*, Charlottesville, VA, (1993).

6. M. L. Williams, Stress singularities resulting from various boundary conditions in angular corners of plates in extensiom. *J. Appl. Mech.* **19**, 526-528 (1952).

7. M. L. Williams, On the stress distribution at the base of a stationary crack. *J. Appl. Mech.* **24**, 109-114 (1957).

8. M. L. Williams, The stresses around a fault or crack in dissimilar media. *Bull. Seis Soc. Am.* **49**, 199-204 (1959).

9. G. C. Sih and J. R. Rice, The bending of plates of dissimilar materials with cracks. *J. Appl. Mech.* **31**, 477-482 (1964).

10. J. R. Rice and G. C. Sih, Plane problems of cracks in dissimilar media. *J. Appl. Mech.* **32**, 418-423 (1965).

11. F. Erdogan, Stress distribution in a nonhomogeneous elastic plane with cracks. *J. Appl. Mech.* **30**, 232-236 (1963).

12. F. Erdogan, Stress distribution in bonded dissimlar materials with crack. *J. Appl. Mech.* **32**, 403-410 (1965).

13. A. H. England, A crack between dissimilar media. *J. Appl. Mech.* **32**, 400-402 (1965).

14. M. Comninou, The interface crack with friction in the contact zone. *J. Appl. Mech.* **44**, 631-636 (1977).

15. M. Comninou and D.Schmuese, The interface crack in a combined tension-compression and shear field. *J. Appl. Mech.* **46**, 345-358 (1979).

16. J. D. Achenbach, L. M. Keer, R. P. Khetan and H. S. Chen. Loss of adhesion at the tip of an interface crack. *J. Elasticity* **9**, 397-424 (1979).

17. J. K. Knowles and E. Sternberg, Largc deformations near a tip of an interface crack between two neohookean sheets. *J. Elasticity* **13**, 257-793 (1983).

18. A. K. Gautesen and J. Dundurs, The interface crack under combined loading. *J. Appl. Mech.* **55**, 580-586 (1988).

19. A. K. Zak and M. L. Williams, Crack point stress singularities at a bimaterials interface. *J. Appl. Mech.* **30**, 142-143 (1963).

20. J. P. Dempsey and G. B. Sinclair, On the stress singularities in the plane elasticity of the composite wedge. *J. Elasticity* **9**, 373-391 (1979).

21. J. P. Dempsey and G. B. Sinclair, On the singular hehavior at the vertex of a bi-material wedge. *J. Elasticity* **11**, 317-327 (1981).

22. D. B. Bogy, Two edge-bonded dissimilar orthogonal elaslic wedges under normal and shear loadin. *J. Appl. Mech.* **35**, 460-466 (1968).

23. D. B. Bogy, Two edge-bonded elaslic wedges of different materials and wedge angles under surface tractions. *J. Appl. Mech.* **38**, 377-386 (1971).

24. V.L.Hein and F. Erdogan, stress singularity in a two-material wedge. *Int. J. Fracture. Mech.* **7**, 317-330 (1971).

25. G. C. Sih, Stress distiution near internal crack tips for longitudinal shear cracks. *J. Appl. Mech.* **32**, 51-58 (1965).

26. C. C. Ma and B. L. Hour, Antiplane problems in composite anisotropic materials with an inclined crack terminatig at a bimaterial interface. *Int. J. Solids Struct.* **26**, 1387-1400 (1990).

27. G. C. Sih, P. C. Paris and G. R. Irwin, On cracks in rectilineary anisotropic bodies. *Int. J. Fracture. Mech.* **1**,189-302 (1965).

28. D. B. Bogy, The plane solution for anisotropic elastic wedges under normal and shear loading. *J. Appl. Mech.* **39**, 1103-1109 (1972).

29. M. C. Kuo and D. B. Bogy, Plane solutions for the displacement and traction-displacement problems for anisotropic elastic wedges. *J. Appl. Mech.* **41**, 197-203 (1974).

30. M. Gotoh, Some problems of bonded anisotropic plates with cracks along the bond. *Int. J. Fracture. Mech.* **3**, 253-260 (1967).

31. J. R. Willis, Fracture mechanics of interfacial cracks. *J. Mech. Phys. Solids.* **19**, 353 -368 (1971).

32. D. L. Clements, A crack between dissimilar anisotropic media. *Int. J. Eng. Sci.* **9**, 257-265 (1971).

33. F. Delale and F. Erdogan, Bonded orthotropic strips with cracks. *Int. J. Fracture. Mech.* **15**, 343-364 (1979).

34. A. Hoenig, Near-tip behavior of a crack in a plane anisotropic elastic body. *Eng. Fracture. Mech.* **16**,393-403 (1982).

35. S. S. Wang and I. Choi, Boundary-layer effects in composite laminates: Part I— Free-edge stress singularities. *J. Appl. Mech.* **49**, 541-548 (1982).

36. S. S. Wang and I. Choi, Boundary-layer effects in composite laminates: Part II— Free-edge stress solution and basic characteristics. *J. Appl. Mech.* **49**, 549-560 (1982).

37. A. N. Stroh, Dislocations and cracks in anisotropic elasticity. *Philos. Mag.* **7**, 625-646 (1958).

38. T. C. T. Ting and S. C. Chou, Edge singularities in anisotropic composites. *Int. J. Solids. Struct.* **17**, 1057-1068 (1981).

39. T. C. T. Ting, Effects of change of reference coordinates on the stress analyses of anisotropic elastic materials. *Int. J. Solids. Struct.* **18**, 139-152 (1982).

40. T. C. T. Ting and P. H. Hoang, Singularities at the tip of a crack normal to the interface of an anisotropic layered composite. *Int. J. Solids. Struct.* **20**, 439 454 (1984).

41. T. C.T. Ting, Explicit solution and invariance of the singularities at an interface crack in ansotropic composites. *Int. J. Solids. Struct.* **22**, 965-983 (1986).

42. J. L. Bassani and J. Qu, Finite cracks on bimatererial and bicrystal interfaces. *J. Mech. Phys. Solids.* **37**, 435-453 (1989).

43. J. Qu and J. L. Bassani, Cracks on bimatererial and bicrystal interfaces. *J. Mech. Phys. Solids.* **37**, 417-433 (1989).

44. V. K. Tewary, R. H. Wagoner, and J. P. Hirth, Elastic Green's function for a composite solid with a planar crack in interface. *J. Mater. Res.* **4**, 124-136 (1989).

45. Z. Suo, Singularity interfaces and cracks in dissimilar anisotropic media. *Pro R. Soc. Lond.* **A427**, 331-358 (1990).

46. L. Ni and S.Nemat-Nasser, Interface cracks in anisotropic dissimilar materials: an analytic solution. *J. Mech. Phys. Solids.* **39**,113-144 (1990).

47. R.J. Hartranft, and G.C. Sih, TheUse of eigenfunction expansions in the general solution of the three dimensional crack problems. *J. Math. Mech.* **19**, 123-138 (1969).

48. J.P. Benthem, State of stress at the vertex of a quarter-infinite crack in a half-space. *Int. J. of Solids and Struct.* **13**, 479-492 (1977).

49. E.S. Folias, On the three dimensional theory of cracked plates. *J. Appl. Mec.* **42**,, 663-674 (1975).

50. E.S. Folias, Method of solution of a class of three-dimensional elastostatic problems under mode I loading. *Int. J.Solids Struct.* **16**, 335-348 (1980).

51. E. S. Folias, On the three-dimensional bending theory of cracked plates. *Int. J. Solids Struct.* **25**, 497-513 (1989).

52. A. I. Lure, *Three dimension problems of the theory of elasticity*. Interscience, New York (1964).

53. M. N. Bapu Rao, Three-dimensional analysis of a finite thick plate with a through crack. *Int. J. Fracture Mech.* **17**, R43-46 (1981).

54. M. N. Bapu Rao, Three-dimensional stress problem of a finite thick plate with a through crack under tension. *Proc. Int. Conf. Frac.* (ICF6), New Delhi, Vol. 2, (1984) 963-970.

55. K. T. Sundara Raja Iyengar, M.V.V. Murthy, and M.N. Bapu Rao, Three-dimensional elastic analysis of cracked thick plates under bending fields. *Int. J. Solid Structures* **24**, 683-703 (1988).

56. G. C. Sih, A review of the three-dimensional stress problem for a cracked plate. *Int. J. Fracture Mech.* **7**, 39-61 (1971).

57. S. P. Timoshenko, and J. N. Goodier, *Theory of elasticity*. 3rd Edn. McGraw-Hill, New York.

58. T. S. Cook and F. Erdogan, Stresses in bonded matenals with a crack perpendicular to the interface. *Int. J. Eng. SCi.* **10**, 677-697 (1972).

59. D. B. Bogy, On the prohlem of edge-honded elastic quarter plane loaded at the boundary. *Int. J. Solids. Struct.* **6**, 1287-1313 (1970).

60. D. B. Bogv and K. C. Wang, Stress singularities at interface corners in honded dissimilar isotropic elastic materials. *Int. J. Solids. Struct.* **7**, 993-1005 (1971).

61. F. Erdogan and G. D. Gupta, Stresses near a flat inclusion in bonded dissimilar materials. Int. J. Solids. Struct. 8, 533-547 (1972).

62. G. C. Sih and H. Liebowitz, *Mathematical theories of brittle fracture*. In Fracture (Edited hy H. Liehowitz), Vol. 11, pp. 115-125. Academic, New York (1968).

63. D. B. Bogy, Plane solutions for traction problems on orthotropic unsymmetrical wedges and symmetrically twinned wedges. *J. Appl. Mech.* **41**, 203-208 (1974).

64. G. C. Sih and E. P. Chen, *Cracks in composite metierials*. Martinus Nijhoff, The Hague (1981).

65. R. 1. Zwiers, T. C. T. Ting and R. L. Spilker. On the logarithmic singularity of free-edge stress in laminated composites under uniform extension. *J. Appl. Mech.* **49**,, 561-569 (1982).

66. K. Y. Lin and J. W. Mar, Finite element analysis of stress intensity factors for cracks at a bi-matenal interface. *Int. J. Fracture. Mech.* **12**, 521-531 (1976).

67. A. N. Stroh, Steady state problems in anisotropic elasticity. *J. Math. Phys.* **41**, 77-103 (1962).

68. A. E. Green and W. Zerna, *Theoretical elasticity*. Clarendon, Oxford (1954).

69. S. G. Lekhnitskii, *Theory of elasticity of an anisotropic body*. MIR, Moscow (1981).

70. D. M. Barnett and J. Lothe, Synthesis of the sextic and the integral formalism for dislocation, Greens functions and surface waves in anisotropic elastic solids. *Phys. Norv.*. **7**,13-19 (1973).

71. D. M. Barnett and J. Lothe, Line force loadings on anisotropic half-space and wedge. *Phys. Norv.* **8**, 13-22 (1975).

72. P. Chadwick and G. D. Smith, Foundations of the theory of surface waves in anisotropic elastic materials. *J. Appl. Mech.* **17**, 303-376 (1977).

73. M. Comninou, The interface crack. *J. Appl. Mech.* **44**, 631-636 (1977).

74. M. Comninou, The interface crack in a shear field.*J. Appl. Mech.* **45**, 287-290 (1978).

75. G. C. Sih, *Experimental evaluation of stress concentration and intensity factors*. Martinus Nijhoff, (1981).

76. L. Rongved, Force interior to one of two joined semiinfinite solids. *Second Midwestern Conference on Solid Mech.* 1-13 (1955).

77. J. T. Frasier, and L. Rongved, Force in the plane of two joined semiinfinite plates. *Journal of Applied Mechanics*, **24**, 582-602 (1957).

78. E. E. Gdoutos, *Fracture mechanics criteria and applications*. Kluwer Academic Publishers, (1990).

79. W. Rudin, *Real and complex analysis*. 3rd Edn. McGraw-Hill, New York (1987).